

DESIGN AND EVALUATION OF HIV MICROBICIDES LOADED
MUCOADHESIVE NANOFORMULATION

A DISSERTATION IN
Pharmaceutical Sciences
and
Chemistry

Presented to the Faculty of the University
of Missouri-Kansas City in partial fulfillment of
The requirements for the degree of
DOCTOR OF PHILOSOPHY

by
Jianing Meng
B. S., China Pharmaceutical University, 2008

Kansas City, Missouri

2015

© 2015

JIANING MENG

ALL RIGHTS RESERVED

DESIGN AND EVALUATION OF HIV MUCOADHESIVE MICROBICIDES LOADED NANOFORMULATION

Jianing Meng, Candidate for the Doctor of Philosophy Degree

University of Missouri-Kansas City, 2015

ABSTRACT

HIV/AIDS had caused more than 25 million deaths since it was first recognized. Women are more susceptible to HIV infection in comparison with men due to human physiology, social, economic disadvantages. To protect women from HIV transmission, there is an urgent need to develop a formulation with proper vaginal retention time for the topical application of anti-HIV microbicides. The aim of this dissertation is to test the hypothesis that a mucoadhesive polymer based nanomedicine can prolong the contact time with the vaginal tissue, provide the controlled release of the drug, and is safe *in vivo*. Various formulation and are investigated, their physicochemical properties, mucoadhesive properties, and safety are evaluated.

In Chapter 3, a chitosan (CS) based nanoparticle (NP) delivery system suitable for the encapsulation of tenofovir (TFV) is designed and optimized. The physicochemical characteristics of the NPs including encapsulation efficiency (EE%), diameter, morphology, *in vitro* drug release as well as *in vitro* cytotoxicity are evaluated. the size of CS NPs ranged from 168 nm to 277 nm. It is shown that NPs are safe to both vaginal epithelial cell line and Lactobacillus over 48 h. The mucoadhesion is about 12%. The CS NPs are mucoadhesive and safe as a microbicide carrier, the drawback of the CS NPs is

the low EE%.

In Chapter 4, the hypothesis that TFV loaded thiolated chitosan (TCS) NPs exhibit superior biophysical properties for mucoadhesion compared to those of native chitosan NPs is tested. The NPs are prepared by ionic gelation. The particle mean diameter, EE%, release profile, in vitro cytotoxicity, cellular uptake, uptake mechanism, and percent mucoadhesion are assessed. The particles are spherical with diameters ranged from 148 nm to 255 nm. The EE% and drug loading is 25% and 1.62% (w/w), respectively. The NPs provide a controlled release over of the drug following Higuchi model. The TCS NPs are not cytotoxic to both vaginal epithelial cell line and *Lactobacillus* over 48 h. The cellular uptake is time dependent. It is mainly occurred via caveolin mediated endocytosis. The mucoadhesive properties of TCS NPs is 5-fold higher than that of CS NPs. Compare to the CS NPs, the TCS NPs exhibit relatively higher EE%, drug loading, and mucoadhesion.

In Chapter 5, we develop a TCS coated multilayer microparticles (MPs). Sodium alginate MPs are prepared by spray drying. The multilayer MPs are developed by coating the optimal alginate MPs with the TCS solution using a layer-by-layer method. The morphological analysis, drug loading, in vitro drug release, cytotoxicity, mucoadhesion and *in vivo* toxicity are evaluated. The MPs diameter ranges from 2 μ m to 3 μ m with a drug loading of 7-12% (w/w). The MPs show a controlled drug release. The MPs are found to have a high mucoadhesion (~50 folds at a higher ratio, and ~20 folds at a lower ratio of mucin: MPs) compare to non-layered sodium alginate MPs in both vaginal fluid and semen fluid simulant buffers. The multilayer MPs are non-cytotoxic to vaginal and endocervical epithelial cells. Histological analysis of the female C57BL/6 mice genital tract and other organs shows no damage upon once-daily administration of MPs up to 24 h and 7 days. The drug loading of the TCS MPs is significantly enhanced (from 1.62% to

12.73%) compare to that of the TCS NPs. However, the mucoadhesion of the MPs is slightly lower than that of the NPs due to the larger particle size.

In chapter 6, the TCS core/shell nanofibers (NFs) are fabricated by a coaxial electrospinning technique. The drug loading is 13%-25% (w/w), the EE% is about 100% because no loss of material during the electrospinning process. The NFs exhibit smooth surface with average diameters in the range of 50 to 100 nm. The NFs are non-cytotoxic at the concentration of 1 mg/ml. The core-shell NFs exhibit a release kinetic following Weibull model, and are 40-60 fold more bioadhesive than NFs made solely with PEO. H&E and immunohistochemical (CD45) staining analysis of genital tract indicates non-toxicity and non-inflammatory effects of the NFs daily treatment for up to 7 days. The TCS NFs exhibit both high drug loading and high mucoadhesion; these data highlight the potential of TCS NFs templates for the topical vaginal delivery of anti-HIV/AIDS microbicides.

Overall, the present work demonstrates TFV loaded NF can be considered as a good candidate for the delivery of water-soluble small-molecule drugs, and a promising vaginal delivery system for the prevention of HIV transmission.

APPROVAL PAGE

The faculty listed below, appointed by the Dean of the School of Graduate Studies, have examined the dissertation titled “Design and Evaluation of HIV Microbicides Loaded Nanoformulation”, presented by Jianing Meng, candidate for the Doctor of Philosophy Degree, and certify that in their opinion it is worthy of acceptance.

Supervisory Committee

Bi-Botti C. Youan, Ph.D., Committee Chair

Division of Pharmaceutical Sciences

William G. Gutheil, Ph.D.

Division of Pharmaceutical Sciences

Nathan A. Oyler, Ph.D.

Division of Chemistry

Zhonghua Peng, Ph.D.

Department of Chemistry

James B. Murowchick, Ph.D.

Department of Geochemistry

CONTENTS

ABSTRACT	i
LIST OF ILLUSTRATIONS.....	vii
LIST OF TABLES.....	xii
LIST OF ABBREVIATIONS.....	xiv
ACKNOWLEDGEMENTS.....	xv
CHAPTER	1
1. INTRODUCTION	1
1.1 Overview	1
1.2 Research hypothesis.....	2
1.3 Objectives.....	3
2. CURRENT STATE OF THE ART IN HIV MICROBICIDES DELIVERY	5
2.1 Normal vaginal physiology and environment	5
2.2 Vaginal transmission of HIV.....	7
2.4 Topical microbicides for HIV prevention.....	9
2.5 Mucoadhesive drug delivery system	16
3. ENGINEERING TENOFOVIR LOADED CHITOSAN NANOPARTICLES FOR THE PREVENTION OF HIV TRANSMISSION.....	22
3.1 Rationale	22
3.2 Materials and Methods.....	23
3.3 Result and Discussion	29
3.4 Conclusion.....	48
4. COMPARATIVE BIOPHYSICAL PROPERTIES OF TENOFOVIR LOADED THIOLATED AND NON-THIOLATED CHITOSAN NANOPARTICLES INTENDED FOR HIV PREVENTION.....	50

4.1 Rationale	50
4.2 Materials and Methods.....	51
4.3 Result and Discussion	62
4.4 Conclusion.....	87
5. THIOLATED CHITOSAN COATED SODIUM ALGINATE MULTILAYER	
MICROPARTICLES FOR ENHANCED DRUG LOADING AND	
MUCOADHESION.....	88
5.1 Rationale	88
5.2 Materials and Methods.....	89
5.3 Result and Discussion	97
5.4 Conclusion.....	116
6. TENOFOVIR CONTAINING THIOLATED CHITOSAN CORE/SHELL	
NANOFIBERS: IN VITRO AND IN VIVO EVALUATIONS.....	117
6.1 Rationale	117
6.2 Materials and Methods.....	118
6.3 Result and Discussion	126
6.4 Conclusion.....	146
6. SUMMARY AND CONCLUSIONS	147
6.1 Summary	147
6.2 Future perspective.....	149
REFERENCES	150
VITA	R

LIST OF ILLUSTRATIONS

Figure	Page
1-1 Mucoadhesive nano-formulation for vaginal delivery of microbicide.....	2
2-1 Structure of the human vaginal epithelium.....	6
2-2 Life cycle of HIV.....	8
2-3 Formation of the disulfide bond between mucin and thiomers by thiol/disulfide exchange reactions, and oxidation process.....	21
3-1 Standardized pareto chart for Y_1 (A) and Y_2 (B).	31
3-2 Prediction profiler and desirability plot showing the effect of formulation variables on EE% (Y_1) and size (Y_2).	34
3-3 EE% (A) and size (B) of NPs that are formed in water and in 50% (v/v) ethanol....	36
3-4 Particle size distributions by intensity of chitosan NPs.....	39
3-5 Transmission electron microscopy (TEM) of chitosan NPs prepared using water (A) and 50% (v/v) ethanol (B) as the preparation media.	40
3-6 <i>In vitro</i> release profiles of chitosan NPs with small, medium and large size.....	41
3-7 LDH release of vaginal epithelial cells treated by chitosan NPs with different sizes for 4 hours (A) and 48 hours (B)	43
3-8 Percent viability of vaginal epithelial cells treated by chitosan NPs with different sizes for 4 hours (A) and 48 hours (B)	44
3-9 Percent viability of <i>Lactobacillus crispatus</i> treated by chitosan NPs with different sizes for 4 hours (A) and 48 hours (B)	46
3-10 Percent mucoadhesion of chitosan particles with different sizes on porcine vaginal tissue.....	47
4-1. ^1H Nuclear Magnetic Resonance (NMR) spectrum of the synthesized TCS conjugate and starting materials.....	63

4-2 A: Curve fitting of Y_1 (EE%), where $R^2=0.98$; B: Standardized Pareto chart showing the standardized effect of the formulation variables and their interaction on Y_1 . X axis indicates the t ratio of the variables. Bars extending pass the vertical line indicate values reach statistical significance ($\alpha=0.05$). C: Prediction profiler showing the effect of the formulation variables on EE% (Y_1).	64
4-3 Scanning electron microscopy (SEM) of CS NPs (A) and CS-TGA NPs (B), and transmission electron microscopy (TEM) of CS NPs (C) and CS-TGA NPs (D).....	65
4-4 <i>In vitro</i> drug release profiles from CS and CS-TGA NPs, in VFS (pH = 4.2).....	71
4-5 Cytotoxicity study of CS and CS-TGA NPs. Top panel: percent LDH release of VK2/E6E7 cell line (A) and End/E6E7 cell line (B), percent viability of VK2/E6E7 cell line (C) and End/E6E7 cell line (D) and percent viability of <i>L. cripatus</i> (E). Bottom panel: <i>L. cripatus</i> under microscopy after incubation with blank CS NPs, TNF loaded CS NPs, Blank CS-TGA NPs, TNF loaded CS-TGA NPs, free TNF, Media and Triton-X (F).	74
4-6 Top panel: the particle uptake efficiency of FITC labeled CS and CS-TGA NPs on VK2/E6E7 cell line (A) and End/E6E7 cell line (B). Bottom panel: NPs cellular uptake assessed by flow cytometry (Count. vs FITC fluorescence intensity); VK/E6E7 cell line treated with media (C), FITC labeled CS NPs (D), FITC labeled CS-TGA NPs (E); End/E6E7 cell line treated with media (F), FITC labeled CS NPs (G), FITC labeled CS-TGA NPs (H) for 48 h.	77
4-7 <i>In vitro</i> localization of FITC-labeled CS and CS-TGA NPs in VK2/E6E7 and End/E6E7 cell lines by fluorescence microscopy.	79
4-8 Effects of inhibitors on uptake of FITC-labeled NPs on VK2/E6E7 cell line (A) and	

End/E6E7 cell line (B).	80
4-9 Percent viability of VK2/E6E7 and End/E6E7 cell lines after treated with inhibitors.	81
4-10 Top panel: concentration dependent percent mucoadhesion by infusion method (A); and time dependent percent mucoadhesion by immersion method (B). Bottom panel: fluorescence microcopy of FITC-CS NPs suspension (3 mg/ml) (C), FITC-CS-TGA NPs suspension (3 mg/ml) (D), thin sections of porcine vaginal tissue treated with suspension A (E), suspension B (F) and media (G). H: H&E staining of porcine vaginal tissue.	85
5-1 Schematic preparation scheme of the TCS coated multilayer MPs.....	91
5-2 Standardized effect of variables and their interaction on yield.....	99
5-3 prediction profiler and desirability plot showing the effect of independent variables on yield.....	100
5-4 ¹ H Nuclear Magnetic Resonance (NMR) spectrum of the synthesized TCS conjugate and starting materials.....	103
5-5 Change in zeta potential values (A) and FTIR (B) after coating with oppositely charged TCS and sodium alginate.....	105
5-6 SEM image (left) and size distribution (right) of A: alginate MPs, B: TCS coated single layer MPs, C: TCS coated double layer MPs, D: TCS coated triple layer MPs...107	
5-7 <i>In vitro</i> release profile of drug from alginate MPs, SLMPs, DLMPs and TLMPs in VFS (A) and SFS (B)	109
5-8 LDH release of cells treated by alginate MPs, SLMPs, DLMPs and TLMPs for 24 and 48 h. A: VK2/E6E7 cell line 24h; B: VK2/E6E7 cell line 48 h; C: End1/E6E7 cell line 24 h; D: End1/E6E7 cell line 48 h.....	111

5-9 Viability of cells treated by alginate MPs, SLMPs, DLMPs and TLMPs for 24 and 48 h. A: VK2/E6E7 cell line 24h; B: VK2/E6E7 cell line 48 h; C: End1/E6E7 cell line 24 h; D: End1/E6E7 cell line 48 h.....	112
5-10 Mucin adsorption in VFS (A) and SFS (B)	114
5-11 H&E stain <i>in vivo</i> safety evaluation in C57BL/6 mice after 24 h (top row) and 7 days (bottom row) exposure with PBS, PEO/TCS-PLA nanofibers (NFs), and Benzalkonium chloride (BZK).	115
5-12 Immunohistochemical stain <i>in vivo</i> safety evaluation in C57BL/6 mice after 24 h (top row) and 7 days (bottom row) exposure with PBS, PEO/TCS-PLA nanofibers (NFs), and Benzalkonium chloride (BZK).....	116
6-1 Ionization of chitosan and TPP blend from formic acid to water.....	129
6-2 Morphology of the nanofibers (NFs). Scanning electron microscopy (SEM) image of PEO NFs (A), PEO/TCS NFs (B), PEO/TCS-PLA NFs (C), Transmission electron microscopy (TEM) image of PEO/TCS NFs before PEO core extraction (D), PEO/TCS-PLA NFs before PEO core extraction (E), PEO/TCS NFs after PEO core extraction (F), PEO/TCS-PLA NFs after extraction (G).....	132
6-3 Schematic description of PEO/TCS nanofibers (NFs) (A) and PEO/TCS-PLA NFs (B).....	134
6-4 The FT-IR reflectance spectra of neat PEO, TCS, PLA powder, PEO/TCS and PEO/TCS-PLA nanofibers (NFs).....	136
6-5 <i>In vitro</i> drug release profiles from PEO nanofibers (NFs), PEO/TCS NFs, and PEO/TCS-PLA NFs in vaginal fluid simulant buffer	138
6-6 Cytotoxicity study of PEO nanofibers (NFs), PEO/TCS NFs, and PEO/TCS-PLA NFs. CS and CS-TGA NPs. LDH release of VK2/E6E7 cell line (A) and End1/E6E7 cell line (B), percent viability of VK2/E6E7 cell line (C) and End1/E6E7 cell line (D),	

percent viability of <i>L.cripatus</i> after incubated with the NFs for 24 h (E) and 48 h (F).....	140
6-7 Adsorption of mucin on PEO, PEO/TCS and PEO/TCS-PLA nanofibers (NFs)....	142
6-8 Fluorescence microcopy of thin sections of porcine vaginal tissue treated with PEO/TCS nanofibers (NFs), PEO/TCS-PLA NFs, and VFS without NFs before (top row) and after (bottom row) rinsing by vaginal fluid simulant buffer.....	143
6-9 H&E stain <i>in vivo</i> safety evaluation in C57BL/6 mice after 24 h (top row) and 7 days (bottom row) exposure with PBS, PEO/TCS-PLA nanofibers (NFs), and Benzalkonium chloride (BZK).....	144
6-10 Immunohistochemical stain <i>in vivo</i> safety evaluation in C57BL/6 mice after 24 h (top row) and 7 days (bottom row) exposure with PBS, PEO/TCS-PLA nanofibers (NFs), and Benzalkonium chloride (BZK).....	145

LIST OF TABLES

Table	Page
2-1 Classification of Anti-HIV Microbicide and their formulations.....	10
2-2 Critical characteristics of ideal vaginal microbicide formulations.....	14
2-3 Marketed mucoadhesive vaginal products.....	16
2-4 Commonly used anionic and cationic polymers.....	18
3-1 Independent variables and their levels in Box-Behnken design.....	24
3-2 Box-Behnken experimental design of independent variables with measure responses.....	29
3-3 ANOVA analysis for both responses.....	32
3-4. Checkpoint experiments comparing measured predicted value.....	34
3-5 Physical-chemical properties of NPs used in drug release and cytotoxicity studies...	40
4-1 Independent Variables and their levels in Box-Behnken Design	53
4-2 ANOVA for Encapsulation Efficiency (Y_1).....	66
4-3 Checkpoint Experiments Comparing Measured and Predicted EE% ($n=3$).....	67
4-4 Effect of DL-dithiothreitol (DDT) on Size, Zeta potential and EE% of CS and CS-TGA NPs	68
4-5 Curve Fitting of the Release Kinetics of Tenofovir from CS and CS-TGA nanoparticles.....	71
5-1 Independent and dependent variables and their levels in custom design.....	90
5-2 Different release models for model fit analysis of the <i>in vitro</i> data.....	93
5-3 responses obtained by the custom design.....	97
5-4 ANOVA analysis for measured responses.....	98
5-5 Checkpoint experiments comparing measured and predicted responses ($n = 3$).....	102
5-6 Drug loading in the multilayer MPs, pure TFV is considered as 100 %.....	104

5-7 Mathematical modeling for drug release from different MPs in VFS and SFS.....	110
6-1 Composition, drug loading, yield and mean diameter of the NFs. Data are given as mean \pm SEM for n=3.....	130

LIST OF ABBREVIATIONS

BBD:	Box-Behnken Design
CS:	Chitosan
DDT:	DL-dithiothreitol
DLS:	Dynamic light scattering
DOE:	Design of experiments
EE:	Encapsulation efficiency
ESP:	Electrospinning
FITC:	Fluorescein-5-isothiocyanate
HEC:	Hydroxyethyl cellulose
MA:	Mucoadhesion
MP:	Microparticles
NP:	Nanoparticles
PDI:	polydispersity index
PLA:	Poly (lactic acid)
SEM:	Scanning electronic microscope
SFS:	Semen fluid simulant
TCS:	Chitosan thioglycolic acid conjugation
TEM:	Transmission electronic microscope
TFV:	Tenofovir
TGA:	Thioglycolic acid
TPP:	Sodium tripolyphosphate
VFS:	Vaginal fluid simulant

ACKNOWLEDGEMENTS

Though the following dissertation is an individual work, I would like to express my deepest appreciation and thanks to my advisor and the committee chair, Dr. Bi-Botti C. Youan, for giving me a great opportunity to work in his laboratory. I would like to thank him for his constant guidance, persistent encouragement, and continuous support in not only research but also in the daily life. He has always been the most valuable part of my experience and my life.

I am also grateful to my committee members, Dr. William G. Gutheil of the Division of Pharmaceutical Sciences, Dr. Nathan A. Oyler and Dr. Zhonghua Peng of the Department of Chemistry, Dr. James B. Murowchick of Department of Mineralogy and Geochemistry, for both kindly serving in my committee and all their help and guidance throughout my graduate work. Special thanks to Dr. Nathan Oyler, who has been an insightful collaborator as well as a supportive mentor. I would like to acknowledge Dr. James Murowchick in the department of geological sciences for his support in XRD analysis.

Over the years I am fortunate to work with a team of brilliant scientists in my lab. I would like to express thanks to my senior and current lab mates, Dr. Tao Zhang, Vivek Agrahari, Fohona Coulibaly, Albert Ngo, Alex Owiti, Dr. Ibrahima Youm, and Dr. Miezan Ezoulin for their time, support, and friendship.

I would like to give my deep thanks to Joyce Johnson and Sharon Self for their help through the years. I would also like to express my gratitude towards all the other professors, staff members, and graduate students in the Division of Pharmaceutical Sciences for their help and friendship.

I would like to acknowledge National Institute of Health (NIH) for funding my research.

CHAPTER 1

INTRODUCTION

1.1 Overview

HIV/AIDS had caused more than 25 million deaths since it was first recognized. Nowadays, HIV/AIDS is one of the most destructive epidemics recorded in history¹. HIV infection rates have reached pandemic levels worldwide with the number of people living with HIV estimated more than 35 million². Among these people, women represent a growing proportion, and the ratio of infected men to women is particularly skewed among young people³. Women are more susceptible to infection in comparison with men due to not only the human physiology, but also social, economic, and legal disadvantages, which limit their ability to protect themselves, especially in Asia and Africa³. In sub-Saharan Africa, for every HIV-infected young man (15–24 years old) there are nearly three infected young women⁴. Therefore, this is an urgent and critical need to identify effective strategies that can reduce women's risk of HIV/AIDS and other sexually transmitted infections.

More than 80% of HIV infections of women occur through heterosexual contact with an infected partner⁵. While unprotected heterosexual vaginal intercourse has become a predominant route of infection for this disease, a lot of studies have shown that the vagina is also a suitable site for the delivery of drugs⁶. The large surface area, permeability, and the rich blood supply of the mucous membrane of the vagina provide significant potential for the delivery of drugs⁷. Polymer-based nano- or micro-medicine has been considered in the intra vaginal delivery of microbicides as they could avoid the degradation, improve the uptake and allow sustained release of drugs⁸. Various formulations of this type have been developed. Recent advances have been made in the area of bioadhesive nanomedicine. Thiolated

polymer, so-called thiomers is a new generation of mucoadhesive polymers that can form covalent mucus bridging between thiomers and mucosa, leading to improved mucoadhesion. Thiomers based nanomedicines show great promise for use as controlled intra vaginal delivery systems. By prolonging the contact time of the microbicide with the vaginal tissue, the effect of the microbicide could be significantly improved. These improvements range from better treatment of local pathologies, to superior drug bioavailability, and controlled release to enhance patient compliance⁹.

1.2 Research hypothesis

The research hypothesis of this study is that a thiolated chitosan based mucoadhesive anti-HIV nanomicrobicide delivery system is effective, safe and for HIV prevention in women (Fig. 1-1).

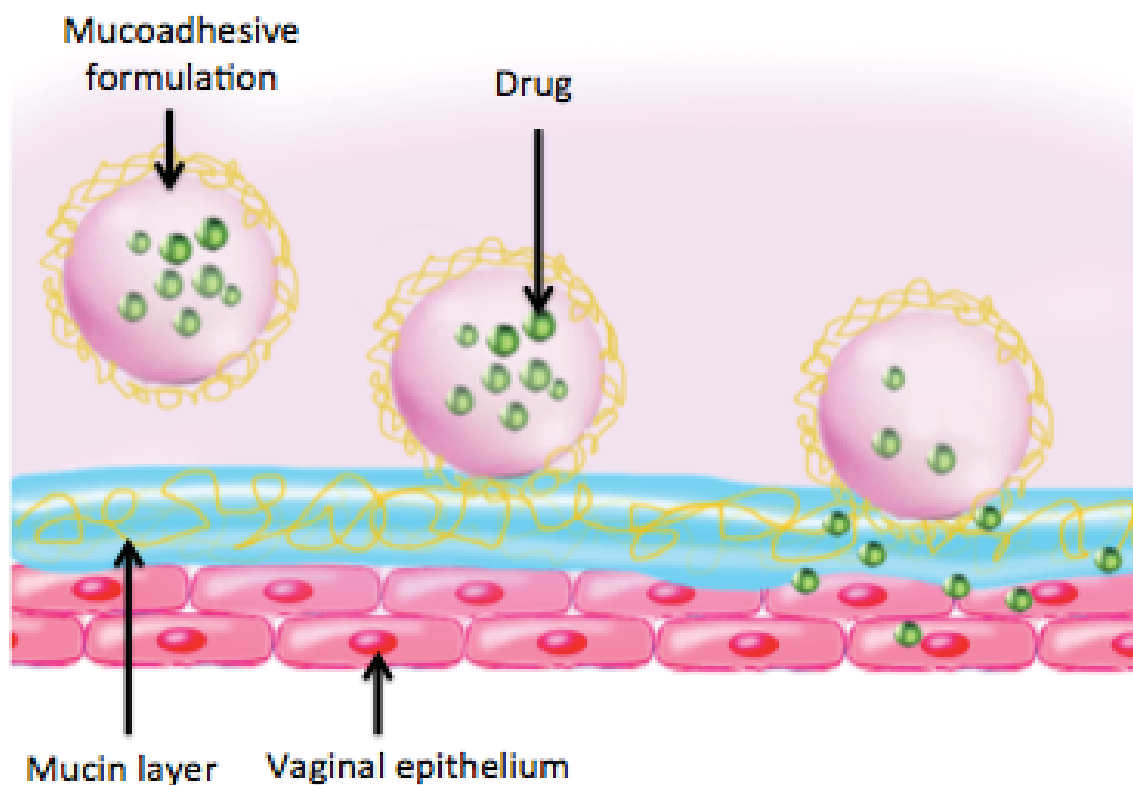


Fig. 1-1 Mucoadhesive nano-formulation for vaginal delivery of microbicide.

1.3 Objectives~The objectives of the dissertation are:

(1) To design a chitosan (CS) based nanoparticle (NP) delivery system suitable for the encapsulation of tenofovir (TFV). To optimize the preparation process and understand which variables can affect the NP mean diameter as well as drug encapsulation, Design of Experiment is used. The physicochemical characteristics of the NPs including encapsulation efficiency (EE%), diameter, morphology, *in vitro* drug release as well as *in vitro* cytotoxicity are evaluated.

(2) To test the hypothesis that TFV loaded thiolated chitosan (TCS) NPs exhibit superior biophysical properties for mucoadhesion compared to those of native chitosan NPs. The NPs are prepared by ionic gelation. The particle mean diameter, EE%, release profile, *in vitro* cytotoxicity, cellular uptake, uptake mechanism, and percent mucoadhesion are assessed.

(3) To develop the thiolated chitosan coated multilayer microparticles (MPs) with enhanced drug loading. Sodium alginate MPs are prepared by spray drying. Formulation optimization is achieved through a custom experimental design. The yield of the MPs is evaluated as the dependent variables. The multilayer MPs are developed by coating the optimal alginate MPs with the TCS solution using a layer-by-layer method. The morphological analysis, drug loading, *in vitro* drug release, cytotoxicity, mucoadhesion and *in vivo* toxicity are evaluated.

(4) To prepare the TCS core/shell nanofibers (NFs) that can enhance the loading of TFV and improve the mucoadhesivity, Core/shell NFs are fabricated by a coaxial

electrospinning technique. The morphology, drug loading, drug release profiles, cytotoxicity and mucoadhesion of the NFs *in vitro* cytotoxicity and *In vivo* safety studies are carried out.

Overall, the present work aims to solve the following problems in the vaginal delivery of HIV microbicides, namely the lack of EE% and drug loading, the lack of retention time, and the lack of assurance in biosafety.

CHAPTER 2

LITERATURE REVIEW

2.1 Normal vaginal physiology and environment

In order to develop an appropriate drug delivery system for the prevention of HIV transmission through heterosexual route, an understanding about the vaginal physiology environment is necessary. The vagina is an 8-10 cm long fibromuscular canal, leading from the cervix to the outside of the body. From the lumen outwards, the first layer is a mucosa of the epithelium that lines the inner surface of the vagina. The vaginal fluid secreted by the epithelium lubricates the mucosa and provides moisture to the vaginal environment. For healthy women, the pH of the vaginal fluid is normally 3.5-5.0. The acidic pH is attributed to the *Lactobacillus*, a predominant normal vaginal flora species, which is able to produce *lactic acid* and hydrogen peroxide (H_2O_2)¹⁰. The acidic pH can prevent the growth of yeast and bacteria; it is a natural barrier for HIV transmission. The epithelium is responsible for protecting from friction to the underlying layers, and therefore is multilayered, durable and relatively strong. The non-keratinized epithelium divides into columnar ecto- and endocervical epithelium gradually near the cervix, and keratinized epithelium resembling skin and covers the introitus when it is close to the opening. Beneath the epithelial layer is the lamina propria, a layer of connective tissue with a lot of fibers allowing the stretch of the vagina; several classes of lymphoid cells are within it, including Langerhans cells, dendritic cells, T lymphocytes and macrophages. Most of these cells are potential target cells for HIV (Fig. 2-1). Deep to the lamina propria is a layer of smooth muscle tissue, surrounded by the outermost layer known as the tunica externa of the vagina¹¹.

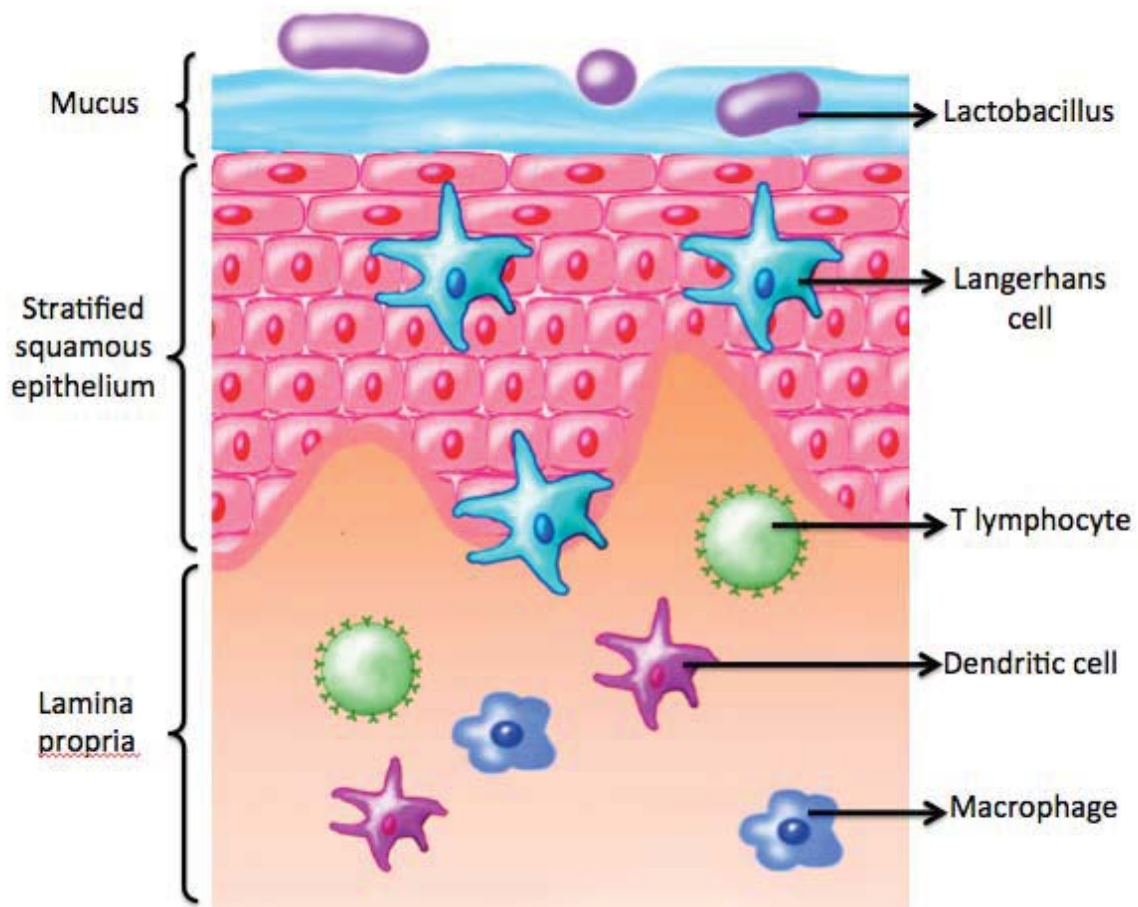


Fig. 2-1 Structure of the human vaginal epithelium.

The integrity of vaginal epithelium is highly associated with the risk of vaginal acquisition of HIV. In case of an intact vaginal environment, the epithelium is responsible maintaining a functional immune response that against any genital pathogens. However, when the epithelium is damaged, HIV can penetrate the mucosa rapidly, transmit and infect the dendritic projection of Langerhans cells, followed by reaching the other target cells.

There are several other factors that may significantly increase the likelihood of HIV transmission, including the bacterial vaginosis¹², dry or traumatic sex¹³, and vaginal inflammatory diseases¹⁴. These factors enhance the HIV vaginal transmission through disrupting the integrity of vaginal mucosal, alteration of normal vaginal pH or vaginal

microbiota, increasing the amount of HIV target cells, disrupting the H₂O₂ producing *Lactobacillus* bacteria, and thinning the cellular liningb[17]. After local infection, HIV can disseminate throughout the lymph nodes and secondary lymphoid organs to generate a systemic infection.

2.2 Vaginal transmission of HIV

Multiple type of cells in human body HIV can be infected by HIV, CD4 lymphocyte is the main target. CD4 lymphocytes are infection-fighting cells made in spleen and lymph nodes. They can identify and destroy foreign particles such as viruses and bacteria, therefore is an essential part of the immune system. HIV goes through several steps to bind and then infect the CD4 cells. Once a CD4 cell is infected with HIV, the virus reproduces itself in the host cell, create and release more virus particles. The life cycle (Fig. 2-2) is broken up into the following steps¹⁵:

(1) Binding: CD4 receptors express on the surface of CD4⁺ cells including macrophages, monocytes, T lymphocytes, and dendritic cells, it is an essential for the membrane fusion and entry of HIV. When HIV attacks a CD4⁺ cell, HIV gp120 binds to the CD4 receptor, and then binds to CCR5/CXCR4.

(2) Fusion: The binding of gp120 to CCR5/CXCR4 coreceptor induces conformational changes in the viral gp120-gp41 glycoprotein complex, the N-terminal domain of gp41 is exposed so that the fusion peptide sequence can insert into the host cell membrane of the host cell. The N-terminal heptad repeat region and C-terminal heptad repeat region of the intra-gp41 protein folds together to form a hairpin structure, which allows the viral envelope to fuse with the CD4 cell membrane, which further enables the virus to enter the cell.. Once inside the cell, the HIV releases HIV RNA and enzymes, such as reverse

transcriptase and integrase.

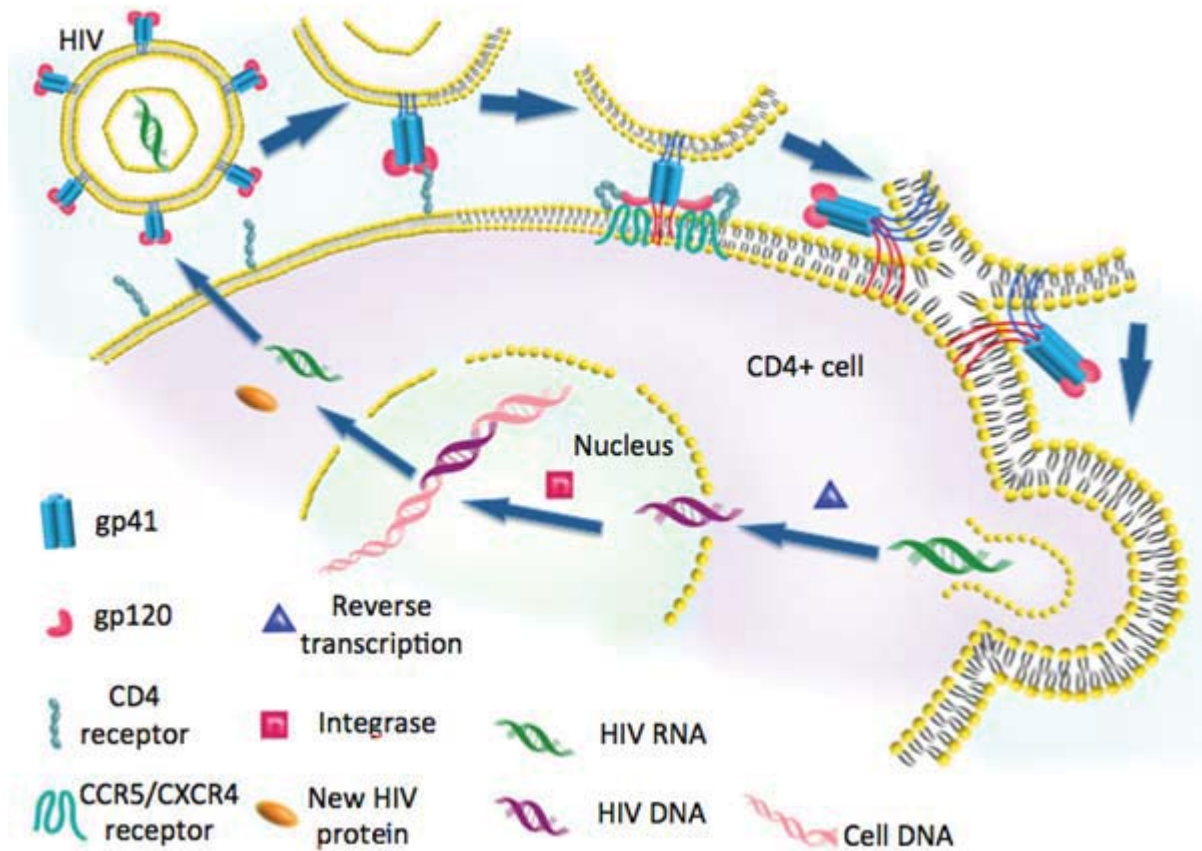


Fig. 2-2 Life cycle of HIV

(3) Reverse Transcription and integration: The reverse transcriptase converts single-stranded HIV RNA into double-stranded HIV DNA. This is called reverse transcription. Integrase is another enzyme released from HIV. With the help of integrase, HIV DNA enters the CD4 cell nucleus, and inserts itself into the host cell DNA.

(4) Replication: Once HIV genetic material is integrated into the host cell DNA, the virus begins to create new viral RNA using the machinery of the host cell. The newly formed multiple copies of HIV RNA move out of the nucleus, and produce viral proteins and enzymes, such as the viral envelope, reverse transcriptase and integrase, through the translation process. The new proteins and enzymes are the building blocks for more HIV.

(5) Assembly and budding: New HIV RNA proteins formed by the host cell move to the cell surface and assemble into immature HIV, which then pushes itself out of the CD4 cell, taking part of the cell membrane to covers it, and forms mature, infectious HIV. A single HIV infected cell can release a lot of new virus, which repeat the same life cycle and infect more cells. Eventually, the host cells are destroyed.

2.3 Topical microbicides for HIV prevention

Microbicide can kill or neutralize viruses by blocking the attachment of HIV to immune cells, inactivating or killing the virus, preventing the spreading infection to other cells, and strengthening normal defenses of the body. A great number of HIV microbicides candidates have been studied and tested¹⁶, more than 30 of them have been approved by the U.S. Food and Drug Administration (FDA). Due to the different viral cycle steps they target, these microbicides can be classified into several categories as follow¹⁷ (Tab. 2-1)¹⁸.

(1) Entry Inhibitors: Interfere with the virus ability to bind to gp120 receptors on the outer surface of the CD4+ cell it tries to enter[49]. There are several subcategories such as gp120 inhibitors, gp41 inhibitors, CD4 inhibitors, CCR5 inhibitors, CXCR4 inhibitors.

(2) Fusion Inhibitors: Binds to the HIV-1 membrane glycoprotein gp41 and prevents the conformational changes required for viral membrane fusion with the cells. This prevents HIV from entering a cell.

(3) Reverse-transcriptase inhibitors (RTs), NRTIs act by blocking the RT enzyme. RTs have two subcategories: Nucleoside/nucleotide reverse transcriptase inhibitors (NRTIs) and Non-nucleoside reverse transcriptase inhibitors (NNRTIs). NRTIs are preferentially incorporated into HIV DNA, leading to termination of DNA synthesis; NNRTIs bind to a pocket near the active site, which causes a conformational change of the enzyme and

inhibition of reverse transcription¹⁹.

(4) Protease Inhibitors: Inhibits virus-specific processing of viral Gag and Gag-Pol polyproteins in HIV infected cells by inhibiting viral protease.

(5) Integrase Inhibitors: Block the action of HIV enzyme integrase, which the virus uses to integrate its genetic material into the DNA of the host cell.

(6) Capsid Inhibitors: Inhibitors of HIV-gag polypeptide assembly. Dismantles assembled HIV-1 capsid assembly tubes.

Tab. 2-1 Classification of Anti-HIV Microbicide and their formulations.

Category		Microbicide	Nature of the molecules	Formulation
RT	NRTI	Zidovudine*	Small molecule	Tablet
		Emtricitabine*	Small molecule	Capsule, Tablet
		Lamivudine*	Small molecule	Tablet
		Abacavir*	Small molecule	Tablet
		Zidovudine*	Small molecule	Tablet, oral solution, capsule
		Tenofovir (TFV)*	Small molecule	Tablet
		Didanosine*	Small molecule	Capsule
		Tenofovir DF*	Small molecule	Tablet
		Stavudine*	Small molecule	Capsule
	NNRTI	Rilpivirine*	Small molecule	Tablet
		Etravirine*	Small molecule	Tablet
		Delavirdine*	Small molecule	Tablet
		Efavirenz*	Small molecule	Tablet

		Nevirapine*	Small molecule	Tablet
Integrase Inhibitor		Raltegravir*	Small molecule	Tablet
		Dolutegravir*	Small molecule	Tablet
Protease Inhibitor		Tipranavir*	Small molecule	Capsule
		Indinavir*	Small molecule	Capsule
		Cobicistat*	Small molecule	Tablet
		Saquinavir*	Small molecule	Tablet
		Lopinavir*	Small molecule	Tablet
		Fosamprenavir*	Small molecule	Tablet
		Ritonavir*	Small molecule	Tablet
		Darunavir*	Small molecule	Tablet
		Atazanavir*	Small molecule	Tablet, capsule
		Nelfinavir*	Small molecule	Tablet
Entry	gp120	b12	Monoclonal antibody	Injection, gel
Inhibitor	inhibitor	2F5	Monoclonal antibody	Injection
		4E10 ²	Monoclonal antibody	Injection
		P2G12 ¹	Monoclonal antibody	intravaginal administration
		F105 ¹	Monoclonal antibody	Injection
		VRC01 ¹	Monoclonal antibody	Injection, gel
		Pro-542 ²	Protein	Injection
		M48UI	Peptide	Gel

gp120 and gp41 inhibitor	Cyanobacterial Griffithsin 2G12, F105, 2F5 CCR5 inhibitor PSC-RANTES, 5P12-RANTES PRO140 ³ HGS004 ¹ CXCR4 inhibitor AMD11070 ² CD4 inhibitor	Cyanobacterial protein Cyanobacterial protein Monoclonal antibody Small molecule Peptide Monoclonal antibody Antibody Small molecule Antibody	Gel, Live bacteria Purified protein Injection Tablet Purified peptide Injection Injection Tablet Injection
Fusion Inhibitor	T-20* T-1249 ² Sifuvirtide ²	Peptide Peptide Peptide	Injections Injection Injection
Capsid Inhibitor			

* FDA approved, ¹ Clinical trial Phase 1, ² Clinical trial Phase 2, ³ Clinical trial Phase 3.

Among the above microbicides, TFV is selected as a model drug in this study. TFV is classified as NRTIs, in order for HIV to be incorporated into the host's genomic DNA, a copy of viral RNA must be made, which is facilitated by reverse transcriptase. TFV inhibits enzyme activity by attaching to its active site, subsequently disabling the binding of the natural substrate deoxyadenosine 5'-triphosphate. Once TFV is inserted into the viral DNA,

the normal 5' to 3' links are prevented from occurring, resulting in HIV DNA chain termination²⁰. The FDA approves TFV for the treatment of HIV infections in October 2001. Numerous formulations of tenofovir have been prepared to prevent the male to female sexual transmission of HIV, such as gel and the intravaginal ring²¹.

Although the oral drug delivery route is the most preferred and convenient route of administration, it has limitations such as:

- (1) Hepatic first-pass metabolism and enzymatic degradation within the gastrointestinal (GI) tract.
- (2) Absorption limitation of drugs due to their physico-chemical characteristics
- (3) Possible of gastrointestinal mucosa irritation⁵.
- (4) Ciliary clearance and transit of food can limit the retention of drug in the GI track.

More than 80% of HIV infections of women occur through sexual contact with an infected partner⁵. While unprotected heterosexual vaginal intercourse has become a predominant route of infection for this disease, a lot of studies have shown that the vagina is also a suitable site for the delivery of drugs⁶. The large surface area, permeability, and the rich blood supply of the mucous membrane of the vagina provide significant potential for the delivery of drugs⁷. For the delivery of a female controlled anti-HIV microbicide, vaginal administration offers many advantages over systemic delivery such as the oral and injection route:

- (1) Potential for non-invasive, controlled delivery of drugs.
- (2) Vaginal route prolonged the contact of the drug delivery system with the mucosa

may be achieved more easily than that of the GI tract.

- (3) The possibility of maintaining the drug delivery system in the site of application for extended periods of time, thereby reducing the dosing frequencies.
- (4) Vaginal route provides higher local concentration of drug, and thereby reduces the systemic side effect.
- (5) Good permeability to a wide range of compounds including both small molecules and large molecules.
- (6) Avoidance of the caused by pain, tissue damage and other inconvenience associated with parenteral routes.

To achieve a significant effect, the ideal vaginal microbicide formulation should have high vaginal retention time, high drug loading and be able to release a high dose of microbicides in a short period of time when required. Several important properties for vaginal microbicide formulation products with regard to their safety and efficacy have been established as shown in Tab.2-2^{17, 18b, 22}.

Tab. 2-2 Critical characteristics of ideal vaginal microbicide formulations

Properties	Acceptable	Unacceptable
Safety	<ul style="list-style-type: none"> • Lack of localized/systemic toxicity. • inertness towards the normal vaginal microbiota. • Have no-effect on fertility and/or fetal abnormalities. 	<ul style="list-style-type: none"> • Induce epithelial disruption • Cause inflammation • Absorbed systemically
Activity	<ul style="list-style-type: none"> • Efficient in preventing HIV 	<ul style="list-style-type: none"> • Affect normal vaginal (rectal)

	transmission.	microbial ecology
	<ul style="list-style-type: none"> • Active against a range of sexually transmitted pathogens. 	<ul style="list-style-type: none"> • Enhance growth of secondary pathogens or sexually transmitted infections or • Induce drug resistance.
Effective	<ul style="list-style-type: none"> • Fast • long-term efficacy • Irreversible 	<ul style="list-style-type: none"> • Interval of efficacy between application and intercourse
Stability	<ul style="list-style-type: none"> • stable under diverse environmental conditions. 	<ul style="list-style-type: none"> • Requires special storage/transport • Short half-life <i>in vivo</i>
Acceptability	<ul style="list-style-type: none"> • Acceptable to the user and user's sex partner • Less administration times daily • Extended periods of use • Affordable by high-risk populations 	<ul style="list-style-type: none"> • Leaky, Messy, • Burning, itching • Interfere with sexual pleasure • Cumbersome Delivery vehicle • Taste / odor / texture / color • Costly for use and/or manufacturing
Uses	<ul style="list-style-type: none"> • Vaginal and/or rectal • Unlimited use • Compatible with condoms and other STI prevention methods 	<ul style="list-style-type: none"> • Complicated use

2.4 Mucoadhesive drug delivery system

Mucoadhesion can be defined as the interfacial forces by which a biological material and mucus layer are held together. When this concept is applied to pharmaceutical formulation, the mucoadhesive molecules is incorporated into drug delivery systems, so that it intends to maintain together with mucosa for a prolonged time period, and release the drug near the site of action. Some of the market available mucoadhesive vaginal formulations are summarized in Tab. 2-3.

Tab. 2-3 Marketed mucoadhesive vaginal products.

Brand name	Active pharmaceutical ingredient	Formulation
Prochieve [®]	Progesterone	Gel
Aci-Jel [®]	Acid-buffering	Gel
Buffer Gel [®]	Acid-buffering	Gel
Metrogel Vaginal [®]	Metronidazole	Gel
PRO 2000/5 [®]	2-Naphthalene sulfonic acid	Gel
K-Y Jelly [®]	Glycerin and Hydroxyethyl cellulose	Gel
Clomirex [®]	Chlorhexidine	Gel
Mifluor [®]	Fluor	Gel
Advantage S [®]	Nonoxynol-9	Gel
Conceptrol [®]	Nonoxynol-9	Gel
Gynol II [®]	Nonoxynol-9	Gel
Gynazole [®]	Butoconazole	Cream
Replens [®]	Glycerin	Moisturizer
Prostin E2 [®]	Dinoprostone	Suppository

Currently, most commercially available formulations conventional drug delivery system. However, they all suffer from several limitations. A lot of the emphasis has been put on the gel and cream formulation²³. Although they are female controlled and easy to formulate, the trouble includes: messy and leakage out of the vaginal cavity, limitation of encapsulating hydrophobic drugs; the low retention time requires a high dosing frequency, which leads to significant patient compliance issues²⁴; Non-uniform distribution; poor acceptability and adherence. In the case of solid dose, such as tablets and suppositories, the advantages are no leakage, and no applicator required, however, they may leave a grainy residue after application in the vaginal cavity; contact of solids can result in vaginal epithelium irritation; disintegration of the product depends on local hydration.

These limitations can be solved by novel nano-formulations, which is the medical application of biological materials and nanotechnology. Nanomedicines can provide sustained drug release, which is necessary for maintaining effective concentration of drug between the time of application and intercourse and therefore reducing the dosing frequency. Nanomedicines are nanoscopic or microscopic drug carriers, patients feel neither leakage nor residue due to their tiny size, as a result, the patient compliance can be improved. Moreover, nano-formulations have the ability to encapsulate both hydrophilic and hydrophobic drugs. Due to the above properties, nanomedicine is a promising vehicle for vaginal delivery of microbicides.

Most nanomedicines are polymer based. To select a proper mucoadhesive polymer, it is necessary to understand the mucoadhesion theory. After the initial contact between the two surfaces, the surface force between the chemical structures, due to one or more

secondary forces such as hydrophobic bonding, hydrogen bonding, and van der Waal's forces²⁵. A system for mucoadhesive polymers can be categorized due to the mechanism of mucoadhesion. Their principles of mucoadhesion include:

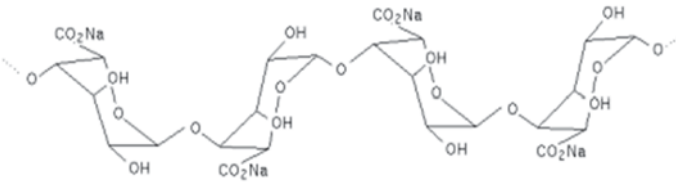
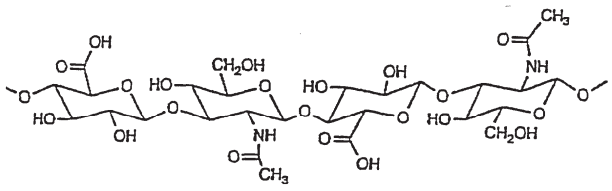
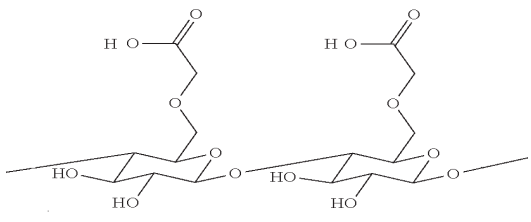
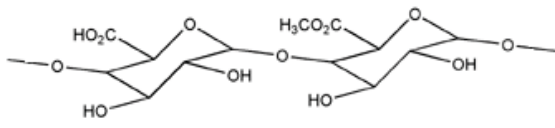
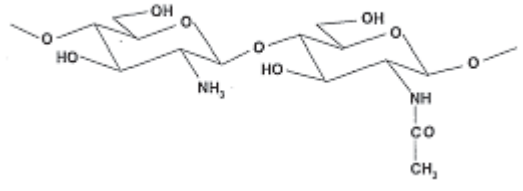
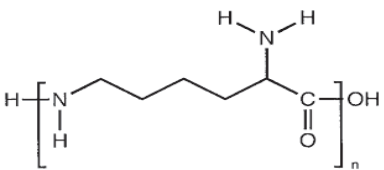
Diffusion theory of mucoadhesion: In the case of diffusion theory, the driving force of penetration is the concentration gradient. The polymer chains form the semi-permanent bond chain with glycoprotein mucin chains. After an intimate contact is established, chains move into the opposite phases along the concentration gradients. A depth of 0.2–0.5 mm is needed for effective bioadhesive bonds. The depth of diffusion is dependent on the molecular weight, which can influence the diffusion coefficient²⁶.

Wetting theory of mucoadhesion: The key element of the Wetting theory is the embedding process. Polymers penetrate into surface irregularities of the mucin and then produce adhesive anchors. The adhesive force is related to the surface tension of both phases²⁷.

Electrostatic theory of mucoadhesion: Following the electrostatic theory, the adhesive force is generated by transferring of electrons along the adhering surface and the adhesive interface. The contact between the two layers is maintained by a series of attractive forces²⁶.

Based on their surface charge surface, which plays a key role in the binding mechanism. Mucoadhesive polymers can be classified into two major types: anionic polymers and cationic polymers, some important anionic polymer and cationic polymers are shown in Tab. 2-4.

Tab. 2-4 Commonly used anionic and cationic polymers

Category	Polymer	Structural formula
Anionic mucoadhesive polymer	Alginate	
	Hyaluronic acid	
	Carboxymethylcellulose	
	Pectin	
	Chitosan	
Cationic mucoadhesive polymer	Polylysine	

The carboxylic moiety ($-\text{COOH}$) of anionic polymers is mainly responsible for mucoadhesion²⁸. The carboxyl groups can form hydrogen bonds with the hydroxyl groups, which presents on the side chains of the oligosaccharide on mucus proteins. For cationic polymers, their mucoadhesive properties are due to ionic interactions between cationic polymers and anionic sialic acid groups of the mucus gel layer. Among all cationic polymers, chitosan is a potential representative, it is most commonly used polymer with high mucoadhesive properties.

Thiolated polymer, so-called thiomers is a new generation of mucoadhesive polymers. Thiomers form covalent mucus bridging between thiomers and mucosa, leading to improved mucoadhesion. Nowadays, thiomers have been widely used in vaginal delivery with enhanced mucoadhesion.

As shown in Fig. 2-3, thiomers display thiol bearing side chains that mimic the natural mechanism of secreted mucus glycoproteins²⁹. Based on thiol/disulfide exchange reactions, and/or a simple oxidation process, disulfide bonds are formed between polymers and cysteine-rich subdomains of mucus glycoproteins so that the polymers can covalently anchor in the mucus layer³⁰. In this study, thiolated chitosan is used as a mucoadhesive material in the nanomedicines for the vaginal delivery of anti-HIV microbicide.

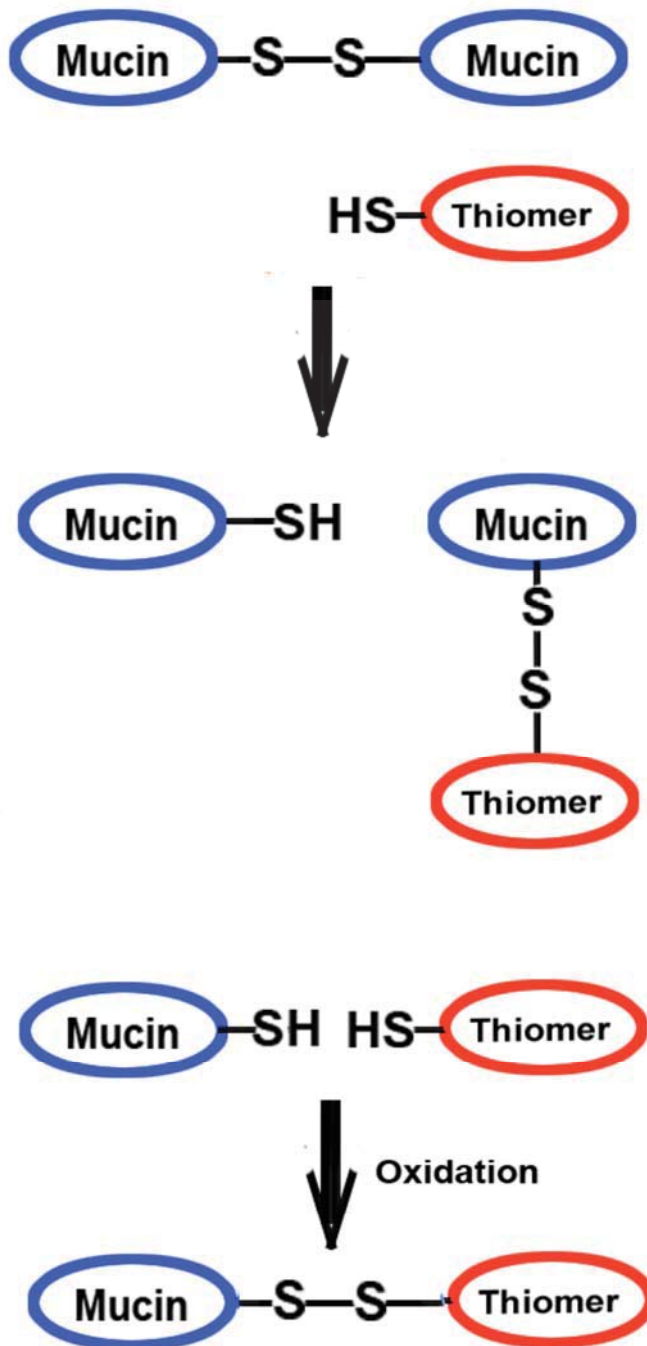


Fig. 2-3 Formation of the disulfide bond between mucin and thiomers by thiol/disulfide exchange reactions, and oxidation process.

CHAPTER 3

ENGINEERING TENOFOVIR LOADED CHITOSAN NANOPARTICLES FOR THE PREVENTION OF HIV TRANSMISSION

3.1 Rationale

As one of the most promising drug delivery systems, polymeric nanoparticles (NPs) have been studied extensively and intensively in recent years³¹. Several polymeric nanoparticulate systems have been prepared and characterized based on both natural and synthetic polymers. Among these polymers, chitosan attracts considerable attention because of its applicable physicochemical and biological properties³².

Chitosan is a water-soluble, linear amino polysaccharide, which is composed of 2-amino-2-deoxy- β -D-glucan combined with glycosidic linkages³³. It can be obtained by the deacetylation of chitin, which is one of the most abundant natural polysaccharides found in the exoskeletons of crustaceans, such as shrimp and lobster³⁴.

Chitosan exhibits many advantages in developing NPs, including biocompatibility, biodegradability, and low-immunogenicity³⁵. The high positive charge density also confers its mucoadhesive properties³⁶, and make it an ideal candidate for the delivery of drugs to mucosal tissues³⁷. Chitosan also has a very low toxicity. Its LD₅₀ in laboratory mice is 16 g/kg body weight, which is close to sugar and salt^{35a}.

In comparison with many other polymers, the chitosan backbone contains a number of free amine groups, which makes it used extensively in drug delivery applications. In an acidic environment, the amino groups could be positively charged after protonation. Therefore, chitosan is able to interact with negatively charged molecules³⁸. Sodium tripolyphosphate (TPP) is a polyvalent anion with three negatively charged phosphate groups.

This property enables it to work as a cross linking agent of chitosan. NPs could form spontaneously in mixed TPP and chitosan solutions through inter and intra molecular linkages created between TPP phosphates and chitosan amino groups³⁸. These types of nanoparticulate systems have shown a high affinity for the association of negatively charged macromolecules³⁹, such as the mucin that are present on the mucosal surface.

Tenofovir (TFV) is a water-soluble, small-molecule drug, which contains a phosphate group and is negatively charged in a NaOH solution. It can also interact with chitosan through electrostatic forces. The use of complexation between oppositely charged macromolecules to prepare chitosan NPs has attracted much attention. This technique has been previously adapted for the encapsulation of peptides and proteins³⁸. This study aims for the preparation of TFV loaded NPs through the ionic cross-linking of chitosan, which is a kind of physical cross-linking induced by electrostatic interaction. In comparison with chemical cross-linking, it is advantageous because the process is simple and carried out under mild conditions without using hazardous organic solvents⁴⁰. Thus, it has better biocompatibility than covalently cross-linked chitosan, and it is possible to reduce the potential toxicity^{35a, 41}.

3.2 Materials and methods

3.2.1 Materials

The chitosan (deacetylation degree of 0.92 and molecular weight of 50,000-190,000 Da) and sodium triphosphate pentabasic (TPP) are purchased from Sigma Aldrich (St. Louis, MO, USA). TFV (99% purity) is purchased from Zhongshuo Pharmaceutical Co. Ltd. (Beijing, China). Acetic acid is supplied by Fisher Scientific (Pittsburgh, PA, USA). CytoTox-ONE™ reagent and CellTiter 96® Aqueous One Solution Reagent is purchased

from Promega (Madison, WI, USA). All chemicals used in the study are of analytical grade and used as received without further purification.

3.2.2 Method

3.2.2.1 Box–Behnken experimental design

A Box–Behnken statistical design with three levels, three factors, and 15 runs is used to design the experiment to optimize the preparation conditions. Some of the polynomial Equations relating factors and responses are obtained by Box–Behnken design software (JMP 8, SAS Institute, Cary, North Carolina, USA).

As shows in Tab. 3-1, the three key formulation variables (concentration of chitosan, weight ratio of TPP and chitosan, weight ratio of drug and TPP) are represented by X_1 , X_2 , and X_3 , respectively. The evaluated responses (encapsulation efficiency and particle size) are represented by Y_1 and Y_2 , respectively⁴².

Tab. 3-1 Independent variables and their levels in Box-Behnken design

Independent variables	Low	Medium	High
X_1 = concentration of chitosan (w/v %)*	0.1	0.2	0.3
X_2 =TPP/chitosan (w/w)	0.1	0.2	0.3
X_3 =drug/chitosan (w/w)	0.1	0.2	0.3
Coded values	-1	0	1
Dependent values			
Y_1 = encapsulation efficiency (EE, %)			
Y_2 = size (nm)			

* The volume of chitosan is 10 ml

3.2.2.2 Preparation of CS Based NPs

The preparation of CS NPs is adapted from a previously described method⁴³. Briefly, chitosan is dissolved in 10 ml of acetic acid (1% v/v) at different concentrations. TPP is dissolved in 1 ml of purified water at various concentrations in order to obtain the final ratio shown in Tab. 3-1. The TPP solution is added to a chitosan solution during magnetic stirring at room temperature, spontaneously forming an opalescent suspension.

For the preparation of TFV loaded NPs, TFV is dissolved in 2 ml of 0.5 M NaOH. Then the drug solution is dropped into the chitosan solution during magnetic stirring, followed by the addition of the TPP solution. The pH of the mixture is adjusted between 5 to 6.5 under continuous stirring for 10 min at room temperature.

Chitosan can dissolve in a mixture of acetic acid (1% v/v) and ethanol⁴⁴. Therefore, in this experiment, beside 1% v/v acetic acid used alone, the solvent mixtures are made of ethanol in 1% acetic acid solution in various ratios (25 and 50%v/v).

NPs are recovered by centrifugation at 20,000 rpm and 20 °C for 60 min (Beckman L8-70 M Ultracentrifuge, Brea, CA, USA). The supernatant is used to determine the drug EE%. The deposited NPs are washed three times by deionized water, and are freeze-dried (Labconco Corporation, Kansas City, MO, USA) and stored at 4 °C–8 °C.

3.2.2.3 Particle size determination

Different NPs samples are resuspended by sonication (Qsonica LLC, Newtown, CT, USA) in distilled water, and the particle size and polydispersity index is determined through dynamic light scattering (Zetasizer Nano ZS, Malvern Instruments Ltd, Worcestershire, UK) at the temperature of 25°C. Samples with PI < 0.05 are considered monodispersed according to the National Institute Standard⁴⁵.

3.2.2.4 Encapsulation efficiency (EE%)

The content of TFV is calculated from the difference between the total amount of drug added in the NP preparation and the amount of free drug in the supernatants. The amount of unencapsulated drug is measured by UV spectrophotometer (Spectronic Genesys 10 Bio, Thermo Electron Corporation, WI, USA) at a wavelength of 259 nm. The drug EE% is calculated as follows:

$$EE\% = \frac{\text{Total amount of tenofovir-Free tenofovir}}{\text{Total amount of tenofovir}} \times 100 \quad (3-1)$$

3.2.2.5 Morphological analysis

The transmission electron microscopy (TEM) is used to assess the morphology of NPs. To obtain the specimens, drops of NP suspension are placed on a copper grid with a carbon support film and air dried. The NPs are viewed under a Scanning Transmission Electron Microscope CM12 (FEI, Hillsboro, OR, USA) at 80 kV accelerating voltage. Digital images are acquired with an ORIUSTM SC 1000 11 Megapixel CCD camera (Gatan, Pleasanton, CA, USA).

3.2.2.6 *In vitro* release study

Two milliliters of the NP suspension is put into a Spectra/Por cellulose ester membrane dialysis bag (Spectra/Por Float-A-Lyzer G2, MWCO 3.5-5 KD, Spectrum Laboratories Inc. Rancho Dominguez, CA, USA), and immersed into 20 ml of vaginal fluid stimulant (VFS) that is prepared according to previous reports⁴⁵⁻⁴⁶. The media is incubated in a thermostatically controlled shaking (60 rpm) water bath (BS-06, Lab Companion, Seoul, Korea) at 37 °C. At predetermined time intervals, all the buffer solution outside the dialysis bag is removed and replaced by fresh buffer solution to maintain a sink condition. The concentration of the drug in the solution is determined by a UV spectrometer at 260 nm. Each

experiment is run in triplicate together with a blank.

3.2.2.7 Cell culture

3.2.2.7.1 Lactate dehydrogenase (LDH) assay

The vaginal epithelial cells are seeded in a 96-well plate. The medium is changed with 100 μ l medium with chitosan NPs of different sizes. The concentration of NPs is 1 mg/ml. A medium without NPs is used as negative control, and 1% Triton X is used as positive control. A row of wells without cells is used to determine the background fluorescent that might be present due to media only. The plate is incubated at 37 °C for 4 and 48 h, and then equilibrated to 22 °C.

One hundred microliters (100 μ l) of CytoTox-ONE™ reagent (Promega, Madison, WI, USA) is added to each well and shaken for 30 seconds. The plate is incubated under 22 °C for 10 min, and then 50 μ l of stop solution is added to each well. The fluorescence is determined by a DTX 800 multimode microplate reader (Beckman Coulter, Brea, CA, USA) at an excitation wavelength of 560 nm and an emission wavelength of 590 nm. The percent cytotoxicity of can be expressed as:

$$Cytotoxicity(\%) = \frac{Experimental - Background}{Positive - background} \times 100 \quad (3-2)$$

Where Experimental is the absorbance of NP-treated wells, Background is the absorbance of background wells (wells without cells), and Positive is absorbance of positive control wells (cells treated with 1% Triton X).

3.2.2.7.2 MTS assay

Cell viability is determined by adding MTS and then checking the amount of the colored formazan product that is bio-reduced from the MTS by the cells. Cells are seeded and

incubated with NPs under the same condition as above following the manufacturing protocol. At different intervals, NP suspension is removed and substituted with fresh medium. Twenty microliters of CellTiter 96[®] Aqueous One Solution Reagent (Promega, Madison, WI, USA) is added to each well and incubated at 37 °C for 4 h. The absorbance is recorded at a wavelength of 490 nm.

$$Viability(\%) = \frac{ABS_{Test}}{ABS_{Control}} \times 100 \quad (3-3)$$

where ABS_{Test} and ABS_{Control} represent the amount of formazan detected in viable cells.

3.2.2.7.3 *Lactobacillus* viability assay

The *Lactobacillus* viability assay is performed to assess the effect of chitosan NPs on *L. crispatus* growth using the established method⁴⁷. Briefly, the bacteria density is adjusted to an OD₆₇₀ of 0.06, corresponding to a 0.5 McFarland Standard or 10⁸ CFU/ml⁴⁸. *L. crispatus* is plated in a 96-well plate at a volume of 100 µl, and then incubated with 100 µl of 1 mg/ml NP suspension under 37 °C. Commercially available 10 µg/ml of Penicillin-Streptomycin solution (Invitrogen, Carlsbad, CA, USA) is used as positive control. After 4 and 48 h, 20 µl of MTS reagent is added to each well and the bacterial viability is determined by a microplate reader by measurement of the absorbance at a wavelength of 490 nm. The percent viability can be calculated using the above Equ. 3-3.

3.2.2.8 Bioadhesion test

Fluorescein isothiocyanate (FITC)-labeled chitosan is synthesized based on the reaction between the isothiocyanate group of FITC and amino group of chitosan⁴⁹, using the method previously described⁵⁰. Porcine tissue is freshly obtained from the local abattoir (Fairview Farm Meat Co., Topeka, KS, USA) within 2 h of the death of the animal⁵¹. The

tissue is washed with normal saline, snap-frozen in liquid nitrogen, and kept at -80 °C. When required, the tissue is thawed at 4 °C then brought to room temperature gradually⁵² and cut into pieces of 8 cm length and 1 cm width. The outside of the vaginal tissue is stuck to a plastic strip by cyanoacrylate glue, which is resistant to water and harmless to the tissue as previously reported⁵³. Then, the tissue-containing strip is immersed into a tube containing FITC labeled NPs (10 mg/ml) in 10 ml of VFS. The tube is put into a shaking water bath for 30 min at 100 rpm, and then removed for analysis of the remaining fluorescence in the VFS⁵⁴. The fluorescence of the VFS before and after the treatment is analyzed by a microplate reader at λ_{ex} 490 nm and λ_{em} 520 nm. The percent mucoadhesion is calculated as follows:

$$Mucoadhesion(\%) = \frac{F_i - F}{F_i} \times 100 \quad (3-4)$$

Where F_i is the initial fluorescence and F is the remaining fluorescence of the VFS after the treatment⁵⁴.

3.2.2.9 Statistics analysis data

All experiments are performed in at least three independent assays. The results are given as mean \pm standard error of the mean (SEM). Statistical comparisons of the results to control are made with independent sample t-tests or ANOVA. The level of significance is taken as p value < 0.05.

3.3 Results and discussions

3.3.1 Formation and physicochemical characterization of CS NPs

Upon addition of TPP, the NPs are formed through the gelation process. The results of the Box-Behnken design for EE% (Y_1), average particle size (Y_2), and polydispersity index (PI) are shown in Tab. 3-2.

Tab. 3-2 Box-Behenken experimental design of independent variables with measure responses

Model	X ₁	X ₂	X ₃	Y ₁	PI	Y ₂
—0	-1	-1	0	4.47	0.307	174.1
-0—	-1	0	-1	2.07	0.316	183
-0+	-1	0	1	1.23	0.436	209.1
—+0	-1	1	0	3.11	0.227	168.5
0—	0	-1	-1	4.25	0.284	238
0—+	0	-1	1	0	0.272	228.2
000	0	0	0	4.57	0.411	196
000	0	0	0	5.09	0.226	188.2
000	0	0	0	4.33	0.236	176.8
0+—	0	1	-1	6.04	0.272	179.1
0++	0	1	1	2.98	0.319	277
+—0	1	-1	0	2.42	0.248	231.3
+0—	1	0	-1	6.07	0.249	204.5
+0+	1	0	1	3.98	0.306	217.8
++0	1	1	0	7.33	0.428	250.1

The polynomial Equations for both response values are:

$$Y_1=4.66+1.12X_1+1.04X_2-1.28X_3+1.58X_1X_2-0.31X_1X_3+0.30X_2X_3-0.16X_1^2-0.18X_2^2-1.17X_3^2$$

(3-5)

$$Y_2=187+21.13X_1+0.37X_2+15.94X_3+6.1X_1X_2-3.2X_1X_3+26.93X_2X_3-3.99X_1^2+22.99X_2^2+20.59$$

$$X_3^2 \quad (3-6)$$

Equ. 3-5 and 3-6 show the effect of the independent variables and their influences on the EE% and particle size. The coefficient of interaction terms show how the Y_1 and Y_2 changed when the two independent variables changed simultaneously. The significance of these variables and their interactions are shown in Fig. 3-1.

A

Sorted Parameter Estimates

Term	Estimate	Std Error	t Ratio		Prob> t
X3	-1.28	0.37108	-3.45		0.0182*
X1	1.115	0.37108	3.00		0.0299*
X1*X2	1.5675	0.524786	2.99		0.0306*
X2	1.04	0.37108	2.80		0.0379*
X3*X3	-1.170417	0.546215	-2.14		0.0850
X1*X3	-0.3125	0.524786	-0.60		0.5774
X2*X3	0.2975	0.524786	0.57		0.5953
X2*X2	-0.175417	0.546215	-0.32		0.7611
X1*X1	-0.155417	0.546215	-0.28		0.7874

B

Sorted Parameter Estimates

Term	Estimate	Std Error	t Ratio		Prob> t
X1	21.125	7.115208	2.97		0.0312*
X2*X3	26.925	10.06242	2.68		0.0440*
X3	15.9375	7.115208	2.24		0.0752
X2*X2	22.9875	10.4733	2.19		0.0796
X3*X3	20.5875	10.4733	1.97		0.1065
X1*X2	6.1	10.06242	0.61		0.5708
X1*X1	-3.9875	10.4733	-0.38		0.7190
X1*X3	-3.2	10.06242	-0.32		0.7633
X2	0.3875	7.115208	0.05		0.9587

Fig. 3-1 Standardized pareto chart for Y_1 (A) and Y_2 (B). Pareto chart showing the

standardized effect of formulation variables and their interaction on Y_1 and Y_2 . The X-axis shows the t ratio of the variables; bars extending pass the vertical line indicate values reaching statistical significance ($\alpha=0.05$).

The values on the x-axis of the Pareto charts represent the standardized effects, which are in fact the ratio of estimate and the standard error of the factor effect (t value)⁵⁵. The obtained t value is compared to a tabulated critical t value, which is determined at $\alpha=0.05$ for residual degrees of freedom (df), where df=5 from ANOVA (Tab. 3-3)⁵⁶.

Tab. 3-3 ANOVA analysis for both responses.

Response	Source	DF	SS	MS	F ratio	P value
Y_1	Model	9	47.376	5.26	4.77	0.049
	Error	5	5.50	1.10		
	Total	14	52.88			
Y_2	Model	9	12147.75	1349.75	3.33	0.099
	Error	5	2025.05	405.01		
	Total	14	14172.80			

DF: degree of freedom, SS: sum of square, MS: mean sum of square, F ratio: Model MS/error MS

The factors whose length passed the vertical line ($t_{critical}=2.571$ at $P<0.05$) indicates significance on the response value⁵⁷. According to Fig. 3-1, X_3 , X_1 , X_1X_2 , and X_2 contributed substantially to EE% (Fig. 3-1 A), while X_1 and X_2X_3 contributed to size (Fig. 3-1 B). Chitosan is used in these nano-formulations as polymeric matrix required to entrap the drug and to allow controlled drug release. The concentration of chitosan (X_1) is found to increase the EE%. By increasing the amount of polymeric matrix (chitosan), more TFV could interact

with the chitosan through electrostatic forces. TPP is the cross-linking agent. By increasing the weight ratio of TPP/chitosan (X_2), more chitosan molecules, which contain several drug molecules, can participate in the gelation process and form NPs so that more drug can be entrapped into the particles. The interaction factor X_1X_2 is also positively related to the EE% as a result of the above phenomena. The ratio of TPP/chitosan and TFV/chitosan is chosen according to the Nitrogen to Phosphate or N/P ratio previously described⁵⁸. Briefly, the molar ratio of the amino/phosphate group (N/P ratio) in the solution should be larger than 1:1. A high EE% occurred when the molar ratio of the amino group of chitosan to the phosphate group of drug is 8:1. These values agrees with the results obtained from the BBD design where the ratio of drug/chitosan (X_3) shows a negative effect on the EE%, which meant that the higher the relative amount of drug to polymer in the solution, the lower the percentage of the total drug that can be entrapped in the NPs.

According to Fig. 3-1 B, the concentration of polymer (X_1) in this study has a positive effect on the NP size, which agrees with published results⁵⁹ that larger sized NPs are obtained with higher concentrations of chitosan. However, the mechanism by which X_2X_3 contributed to size increase is not clear, perhaps because TPP and TFV (both with phosphate groups) competitively interacted with the same chemical group of chitosan. Therefore, X_2X_3 interaction might affect the cross-linking efficiency leading loosely packed polymeric chain inside the NPs with increased particle size.

At a medium amount of chitosan the TPP and drug mixture is required to achieve a higher EE% and lower size. Base on the interaction plot shows in Fig. 3-2 and Equ. 3-5 and 3-6, the optimal formulation, which exhibited the highest EE% ($5.83\% \pm 0.88\%$) and lowest particle size (207.97 ± 19.07 nm), is selected through the mathematical optimization process,

where X_1 , X_2 , and X_3 are 0.66, 0.67, and -0.69.

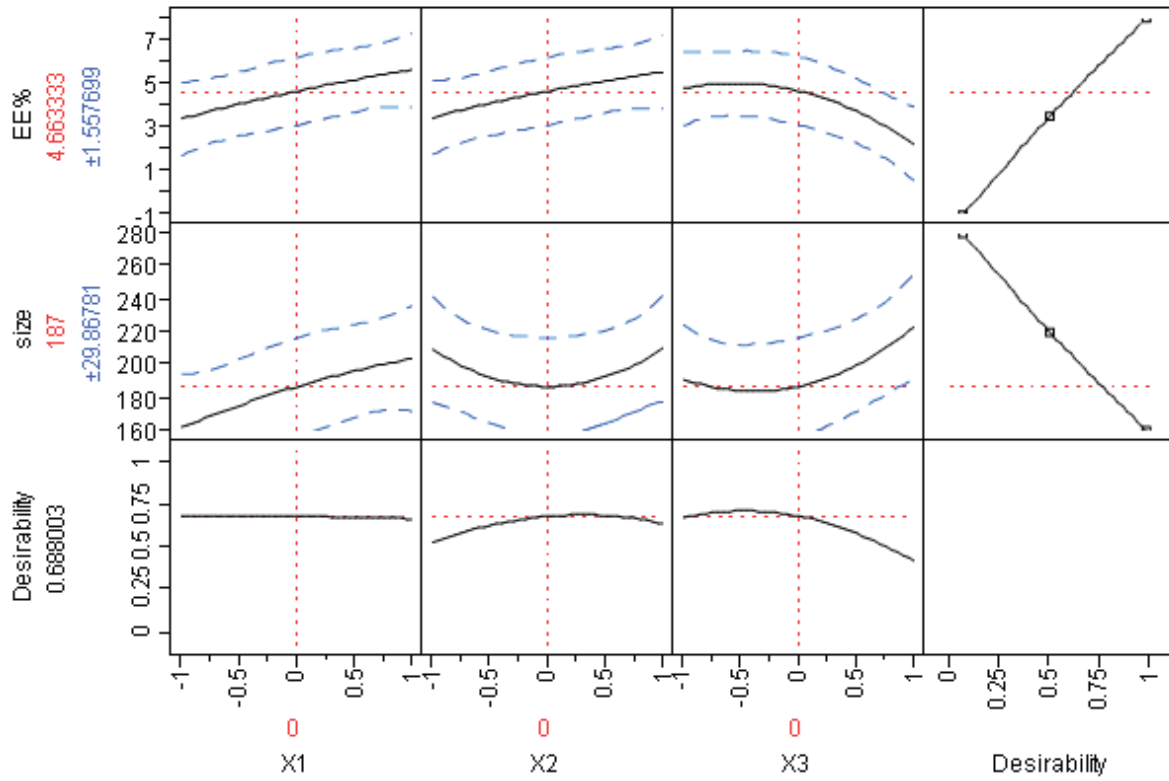


Fig. 3-2 Prediction profiler and desirability plot showing the effect of formulation variables on EE% (Y_1) and size (Y_2).

A check point analysis base on Equ. 3-5 and 3-6 is performed to confirm; the analysis is shown in Tab. 3-4.

Tab. 3-4. Checkpoint experiments comparing measured predicted value (n=3)

Ru n no.	X_1	X_2	X_3	Measur ed Y_1	Pre dic ted Y_1	Error % of Y_1	P valu e of Y_1	Measure d Y_2	Predic ted Y_2	Error % of Y_2	P Valu e of Y_2
C1	-0.5	-0.	-0	5.55	4.2	30.9	0.34	166.23	185.6	-10.4	0.17
		5	.5	(±1.82)				(±16.05)			
C2	0.5	0.5	0.	3.18	5.1	-42.7	0.15	266.33	223.0	20.7	0.47
			5	(±1.44)				(±85.84)			

		0.6	-0	5.83			207.97				
C3	0.66				6.9	-16.4	0.15		200.3	3.8	0.56
		7	.7	(±0.88)			(±19.07)				

Three points are selected: two random points out of the 15 runs of the experiment, and the above theoretical and optimal point. Though the Error % on the EE% is large (which might result from the variability in the UV spectroscopy absorbance reader), the differences between measured and predicted values are not found to be statistically significant ($p > 0.05$); thus, it can be concluded that these Equations fit the data satisfactorily and are valid for 3.3.2 predicting the EE% and the particle size.

At a higher pH, more particles are formed compared to a lower pH because the proportion of the protonated amino groups in chitosan is pH dependent. Chitosan has weak basic amino groups that are protonated in acidic medium. TPP with a negative charge could interact strongly with positively charged chitosan in such a low pH environment⁶⁰.

However, in optimal conditions of the BBD design, the EE% of TFV is quite low (5.83%), although the preparation is performed at a pH 6.5. To improve the EE%, a mixture of ethanol and water is used as a solvent for chitosan. The effects of ethanol concentration on the EE% and the size of NPs are shown in Fig. 3-3.

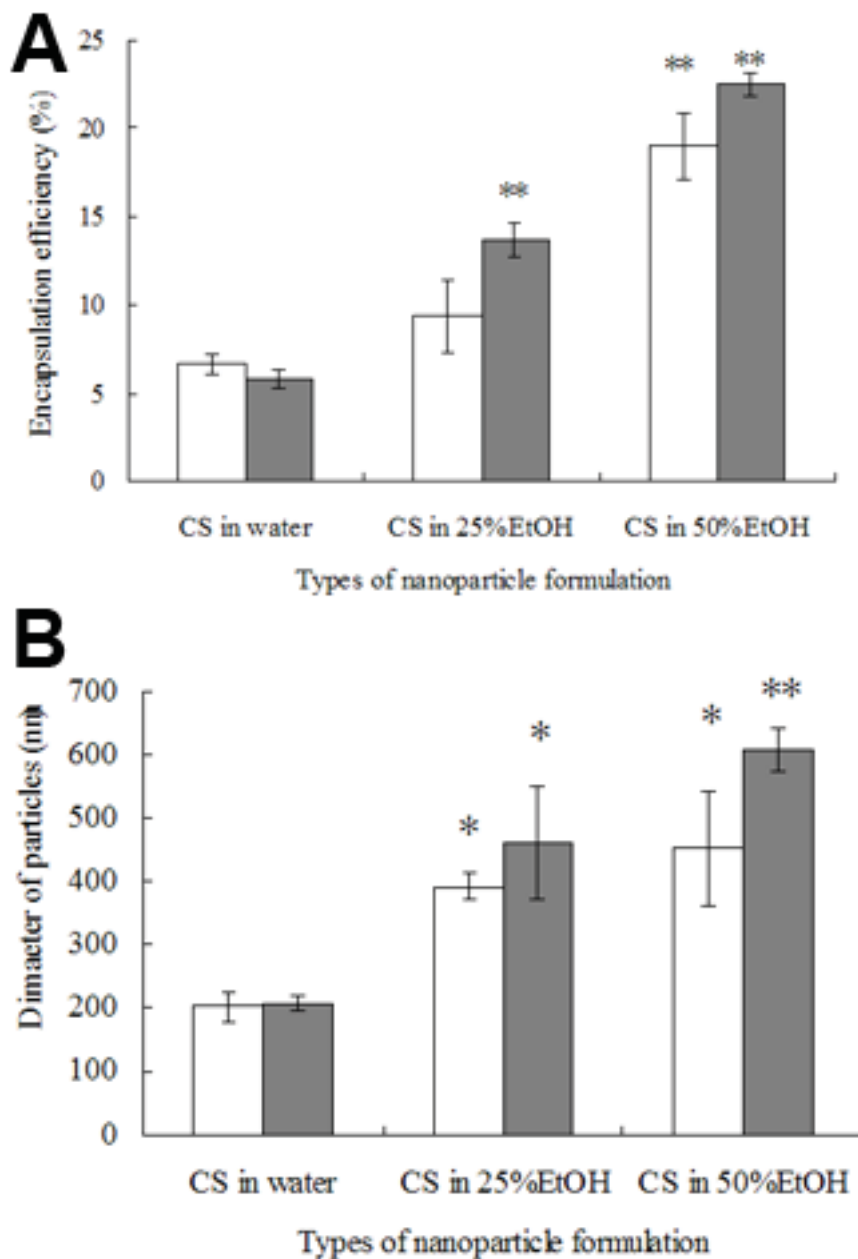


Fig. 3-3 EE% (A) and size (B) of NPs that are formed in water and in 50% (v/v) ethanol.

□ : NPs formed under the conditions from exhibiting the highest EE% among the 15 run ($X_1=1$, $X_2=1$, $X_3=0$); ■ : NPs formed under the optimal condition ($X_1=0.66$, $X_2=0.67$, $X_3=-0.69$) ($n=3$). * $P<0.05$ vs Water, ** $P<0.01$ vs Water

The predicted water solubility of TFV is 1.87 mg/ml and Log P is -1.6⁶¹; thus, the

observed low EE% may be explained by the relatively high hydrophilicity of the drug. It has been reported that polysaccharide-based drug-delivery systems usually have a low EE% and drug loading for water-soluble drugs with low molecular weight⁶². TFV could not dissolve in ethanol, and the addition of ethanol reduced the amount of required water. As a result, the solubility of TFV in ethanol is lower than that in water alone. Therefore, the drug could not diffuse out in massive amounts during the NP preparation, leading to a higher EE%⁶³. Indeed, the EE% with ethanol on the optimal condition is 20.05±3.27% (n=3), which is almost three fold higher than that of water alone.

However, the use of ethanol also increased the particle size from 207.97±19.07 nm to 580.60±98.71 nm. The size increase might be explained by the Kelvin Equation (Equ. 3-7):

$$\ln \frac{p}{p_0} = \frac{2\gamma V_m}{rRT} \quad (3-7)$$

Where p is the actual vapor pressure of the liquid, p_0 is the saturated vapor pressure, γ is the surface tension, V_m is the molar volume, R is the universal gas constant, r is the radius of the droplet, and T is temperature. Rewriting Equ. 3-8 gives:

$$r = \frac{2\gamma V_m}{RT \ln \frac{p}{p_0}} \quad (3-8)$$

The surface tension of ethanol (22.8 mN/m) is less than that of water (72.8 mN/m)⁶⁴; thus, ethanol can significantly decrease the surface tension of the chitosan solution. According to Equ. 3-8, the radiuses of the droplets (r) decrease with the decrease in the surface tension when the other Equation parameters are fixed, which means that ethanol can

lead to smaller droplets.

Even if we assume that γ effect is negligible, another important parameter that describes droplet deformation is the Weber number (We):

$$We = \frac{G\eta R}{2\gamma} \quad (3-9)$$

Where G is the shear stress, η is the viscosity, R is the radius of the droplets, and γ is the interfacial tension⁶⁵. Equ. 3-10 can be rewritten as:

$$R = \frac{2We\gamma}{G\eta} \quad (3-10)$$

The radius of the droplets decreases with the increase of η . At 25 °C, the viscosity of water is 0.894 cP, while the viscosity of ethanol is 1.074 cP⁶⁶, which means that the ethanol addition also leads to smaller droplets.

The initial smaller particles, produced under the influence of either low surface tension or low viscosity induced by ethanol, will undergo Brownian motion and particle collision leading to particle growth. In fact, the growth of aggregates can be simulated by making simple assumptions concerning the transport of particles to the growing agglomerate, and the events that occur when primary particles collide with the growing aggregate. The relationship between mass and final size of the NPs can be defined by a mass-fractal aggregation Equation:

$$R = \alpha N^{1/df} \quad (3-11)$$

Where α is the Lacunarity constant, R is the aggregate overall size, N is the number of primary particles in an aggregate, and df is the mass-fractal dimension which ranges from

1 to 3 in a 3-dimensional space. The colliding particles can probe the surface of the growing aggregate, or become “trapped”, by high coordination number regions of the aggregate. According to Equ. 3-11, the larger number of colliding droplets leads to the growth of larger droplets, which agrees with the result that the size of the final NPs cured in ethanol solution is relatively larger. Fig. 3-4 shows the mean size distribution of particles formed in water (Fig. 3-4. A) and 50% (v/v) ethanol (Fig. 3-4. B). These size analyses data are consistent with the TEM data (Fig. 3-5).

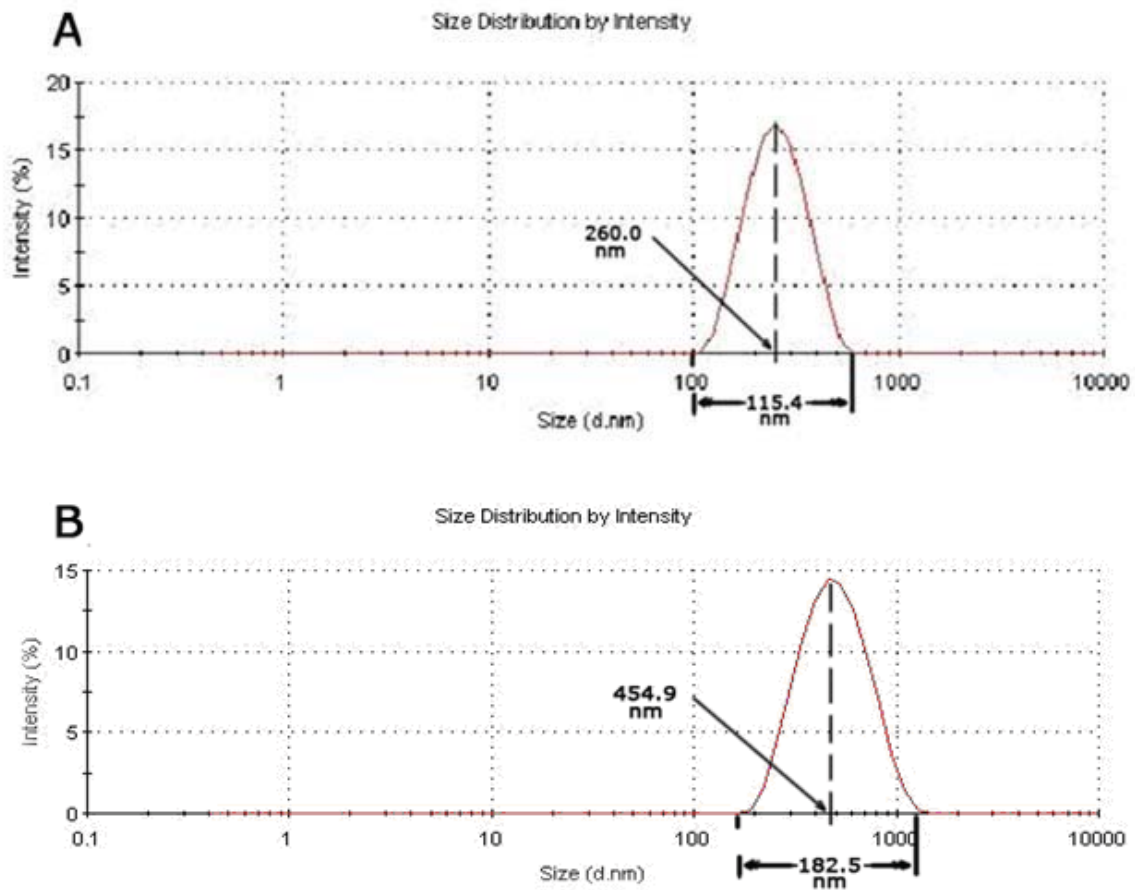


Fig. 3-4. Particle size distributions by intensity of chitosan NPs formed in water (A) and in 50% (v/v) ethanol (B).

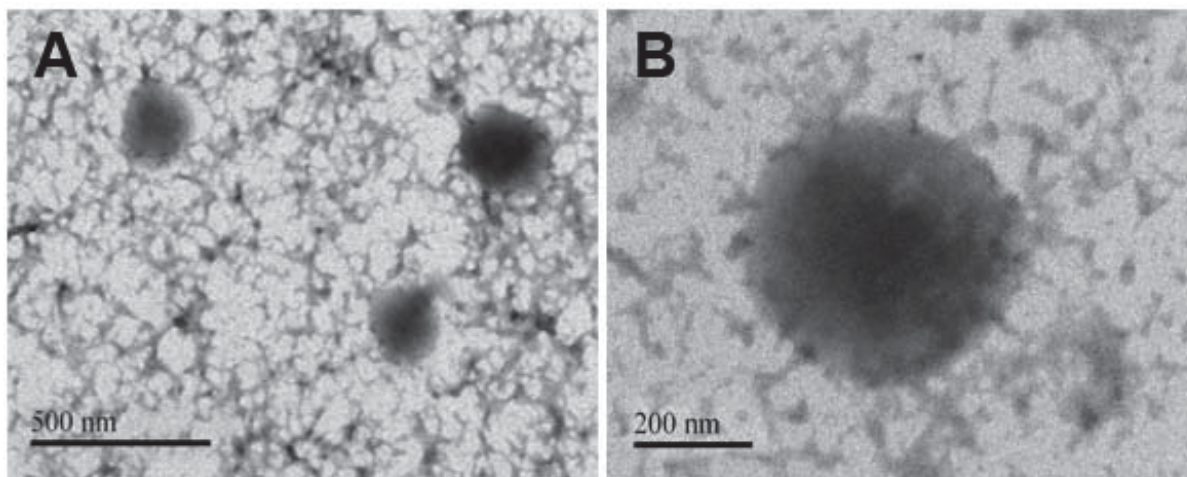


Fig. 3-5 Transmission electron microscopy (TEM) of chitosan NPs prepared using water (A) and 50% (v/v) ethanol (B) as the preparation media.

3.3.3 *In vitro* release study

Drug release from solid dosage form has been described by kinetic models such as zero-order, first order, Higuchi model, Peppas model, and Hixon-Crowell⁶⁷. The release data is fitted to zero-order, first order, and the Higuchi model to propose the release mechanism⁶⁸. Tab. 3-5 shows the formulation and characteristic of NPs used in the release study.

Tab. 3-5 Physical-chemical properties of NPs used in drug release and cytotoxicity studies. (n=6)

Size	Formulation				Average particle size (nm)	Zeta potential (mV)	EE %	Drug loading % (w/w)
	X1	X2	X3	Preparati on media				
Low	-1	0	-1	water	182.36 (±15.83)	46.4 (±1.22)	2.1 (±0.6)	0.21 (±0.06)
Mediu	0.66	0.67	-0.69	water	281.67	53.07	6.9	0.33

m					(±25.62)	(±0.56)	(±0.7)	(±0.05)
High	0.66	0.67	-0.69	ethanol/	602.43	55.23	23.5	1.14
				water 1/1	(±48.96)	(±2.29)	(±1.2)	(±0.06)
				(v/v)				

The suspensions are stable, with zeta potential being as high as 45-55mV, which is also close to the results reported in the previous published literature^{34, 69}. The positive charge of NPs is due to the amino groups on the surface of the NPs. The drug release profiles of chitosan NPs are shown in Fig. 3-6.

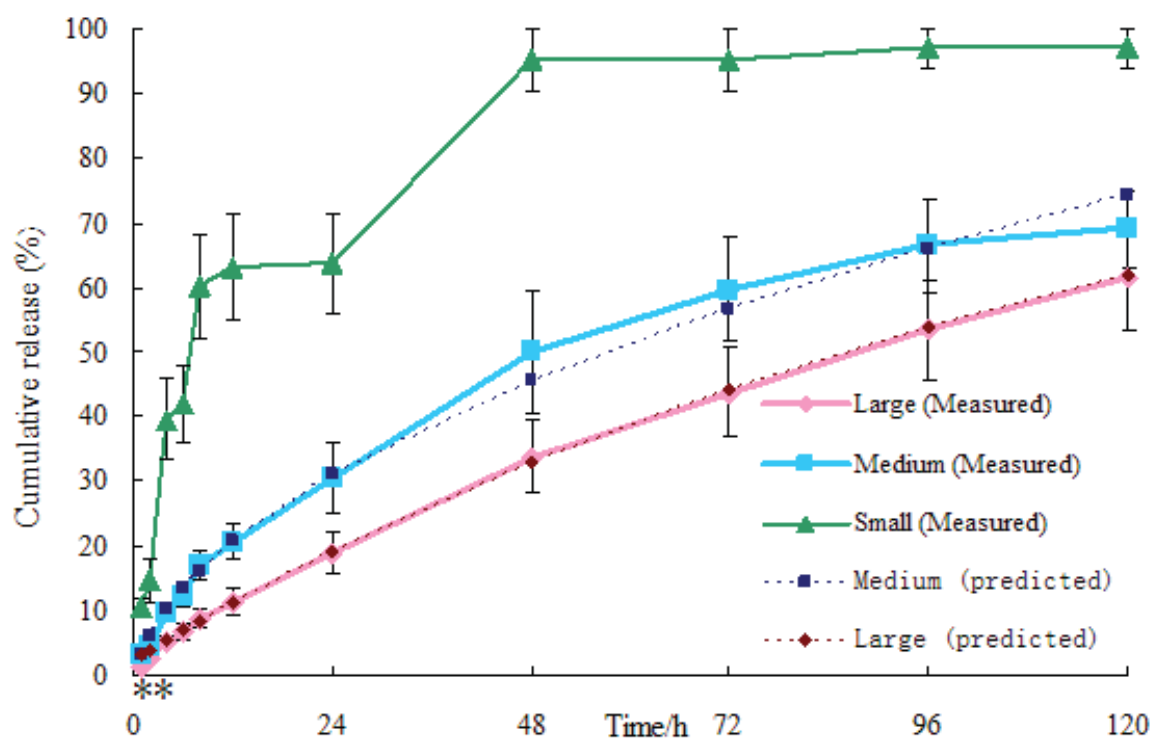


Fig. 3-6. *In vitro* release profiles of chitosan NPs with small, medium and large size (n=3).

It is noteworthy that small-sized NPs shows an initial burst release phase within the first 8 h. Since it is well known that in most of the drug release conditions for the particles, a

higher drug loading level generally leads to a higher drug release rate because of the enhanced diffusion driving force of the concentration gradient⁶³. However, in this study the burst release occurred possibly due to the small size of the NPs. As the particle diameter is reduced, the specific surface area increased, while the path length to the surface of the drug decreased⁷⁰. It is thus more likely for a drug to be released from the NPs. Medium and large-sized NPs provided a controlled drug release without an obvious burst release. Drug release from medium-sized NPs fit well with the Higuchi model⁶⁷:

$$Q=7.15t^{1/2}-4.04 \quad (r^2=0.991) \quad (3-12)$$

Where Q is the percent of drug released in time t. The high-sized NPs fit with the first-order release model⁶⁷:

$$\ln(100-Q)=-0.0078t+4.5 \quad (r^2=0.999): \quad (3-13)$$

Both of medium-sized and large-sized NPs could be considered as promising drug nanocarriers for controlled release of the microbicide. The size of NPs appears to be a major factor affecting the drug release rate.

The average daily release of TFV from chitosan NPs is 14% (medium) and 12% (large). As the drug loading of the two kinds of particles is 0.33% (w/w) and 1.14% (w/w) (Tab. 3-5), 1 mg of NPs could release 0.5×10^{-3} mg and 1.4×10^{-3} mg of drug every 24 h. Women of reproductive age produce fluid at a rate of approximately 6 ml/day⁷¹, while the EC₅₀ of TFV is about 0.5 μ M⁷², which means that about 1.7 g of medium size chitosan NPs, or 0.6 g large-size chitosan NPs, would be able to provide the daily requirement of TFV for an adult woman patient. This is feasible considering that the average vaginal suppository that could be measured as an additional vehicle had a weight of 5 grams.

3.3.4 Cytotoxicity studies

3.3.4.1 LDH release study

Lactate dehydrogenase (LDH) and MTS tests are utilized to evaluate the effect of chitosan NPs on both cellular viability and membrane integrity. The LDH from cells with damaged membranes is determined by measuring the fluorescent signal. NPs used in this study are the same as shown in Tab. 3-5, but without drug loading. After incubation with chitosan NPs for 4 and 48 h, only minimal LDH release from vaginal epithelial cells is observed. As shown in Fig. 3-7, the extent of the release of LDH from the cells incubated with NPs is 10% higher than that of media.

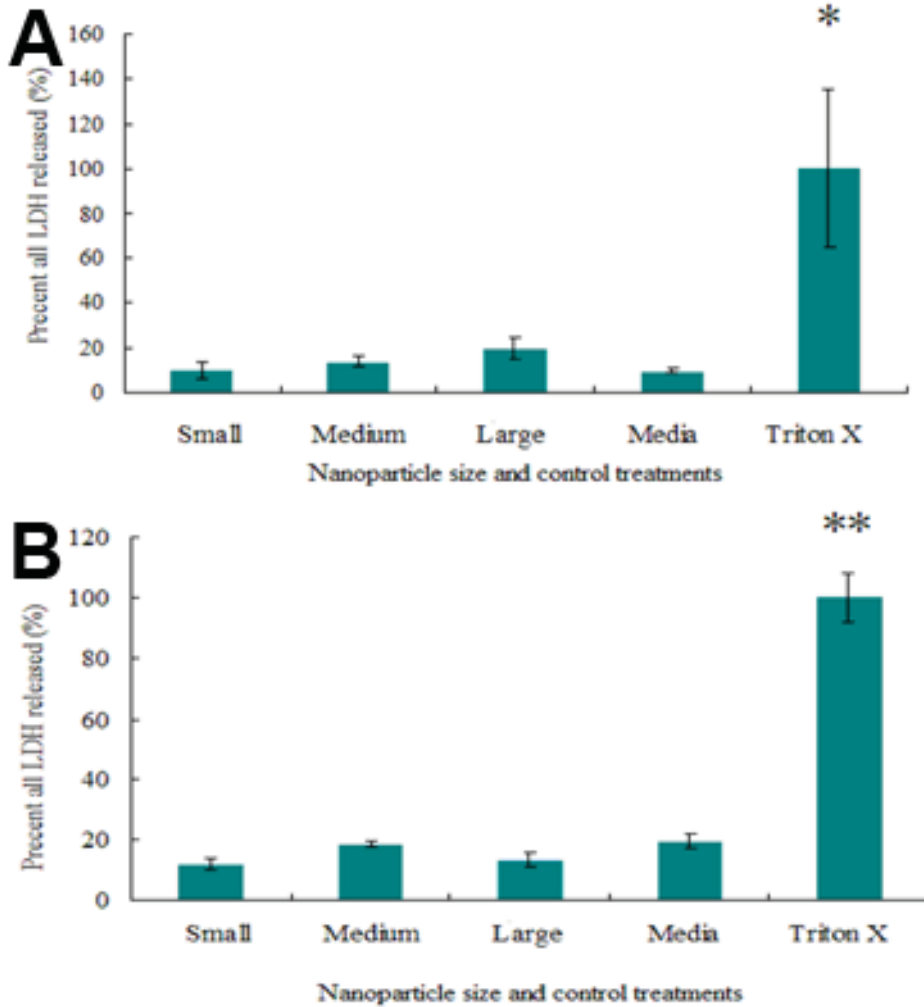


Fig. 3-7. LDH release of vaginal epithelial cells treated by chitosan NPs with different sizes

for 4 h (A) and 48 h (B), (n=3). * $P < 0.05$ vs Media, ** $P < 0.01$ vs Media

3.3.4.2 Cell viability study

The MTS tetrazolium compound is able to be bio-reduced by living cells into a colored formazan product that is soluble in the cell culture media. Thus, after the incubation, the number of living cells could be determined by the absorbance of the formazan product of MTS. The viability of cells, which is higher than 80%, is shown in Fig. 3-8. For some in the sample, the cell viability is even higher than 100% in comparison with the media control, which may be due to the differences of the number of cells in each well.

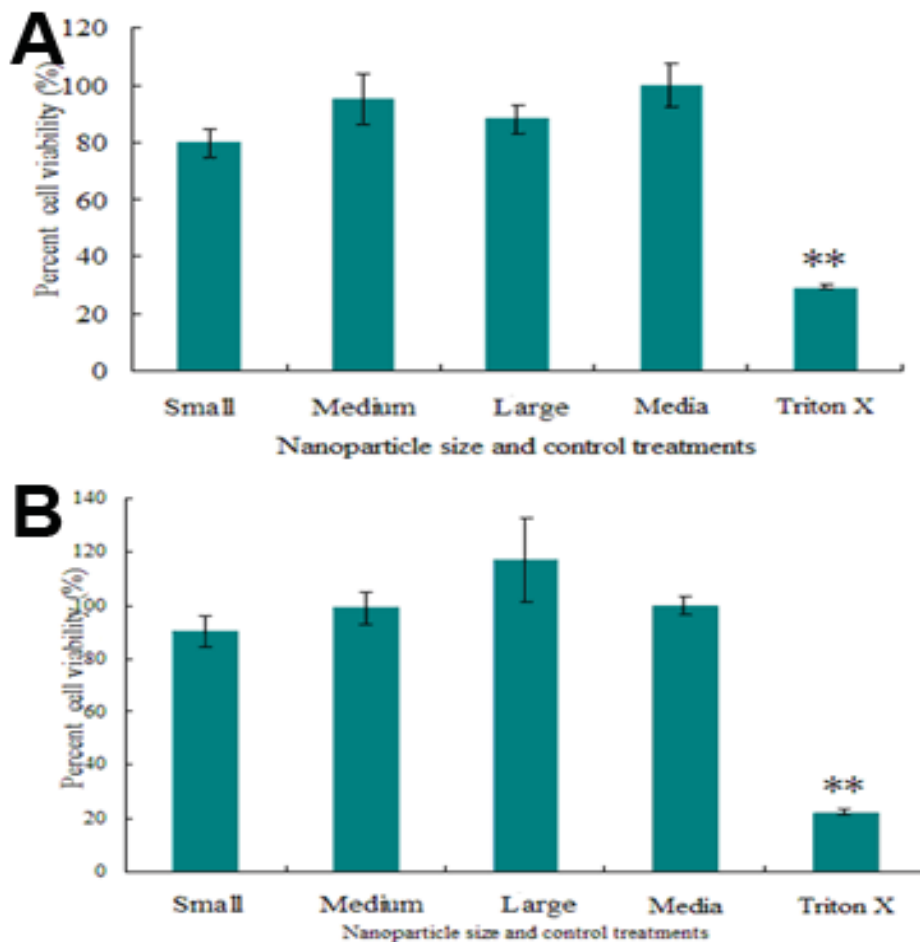


Fig. 3-8. Percent viability of vaginal epithelial cells treated by chitosan NPs with different sizes for 4 h (A) and 48 h (B), (n=3). * $P < 0.05$ vs Media, ** $P < 0.01$ vs Media

In both of the assays, no statistical difference is observed by the t-test between media control and NPs with different sizes, which means that the chitosan NPs are not harmful to the cells and the size has no effect on cytotoxicity.

3.3.4.3 Effects on Viability of *Lactobacillus Crispatus*

Lactobacillus, which is a predominant normal vaginal floral species, is used as model bacteria since it is able to produce hydrogen peroxide (H₂O₂)¹⁰. It is critical that any microbicide formulation won't disturb normal vagina flora so that they can maintain a low pH environment and secrete H₂O₂, which provides a natural barrier for HIV transmission⁴⁸.

As shows in Fig. 3-9, after incubation for 4 and 48 h, there is no statistical difference between the media control and the chitosan NPs, which suggests that these NPs are not harmful to the cells and the size has no effect on cytotoxicity.

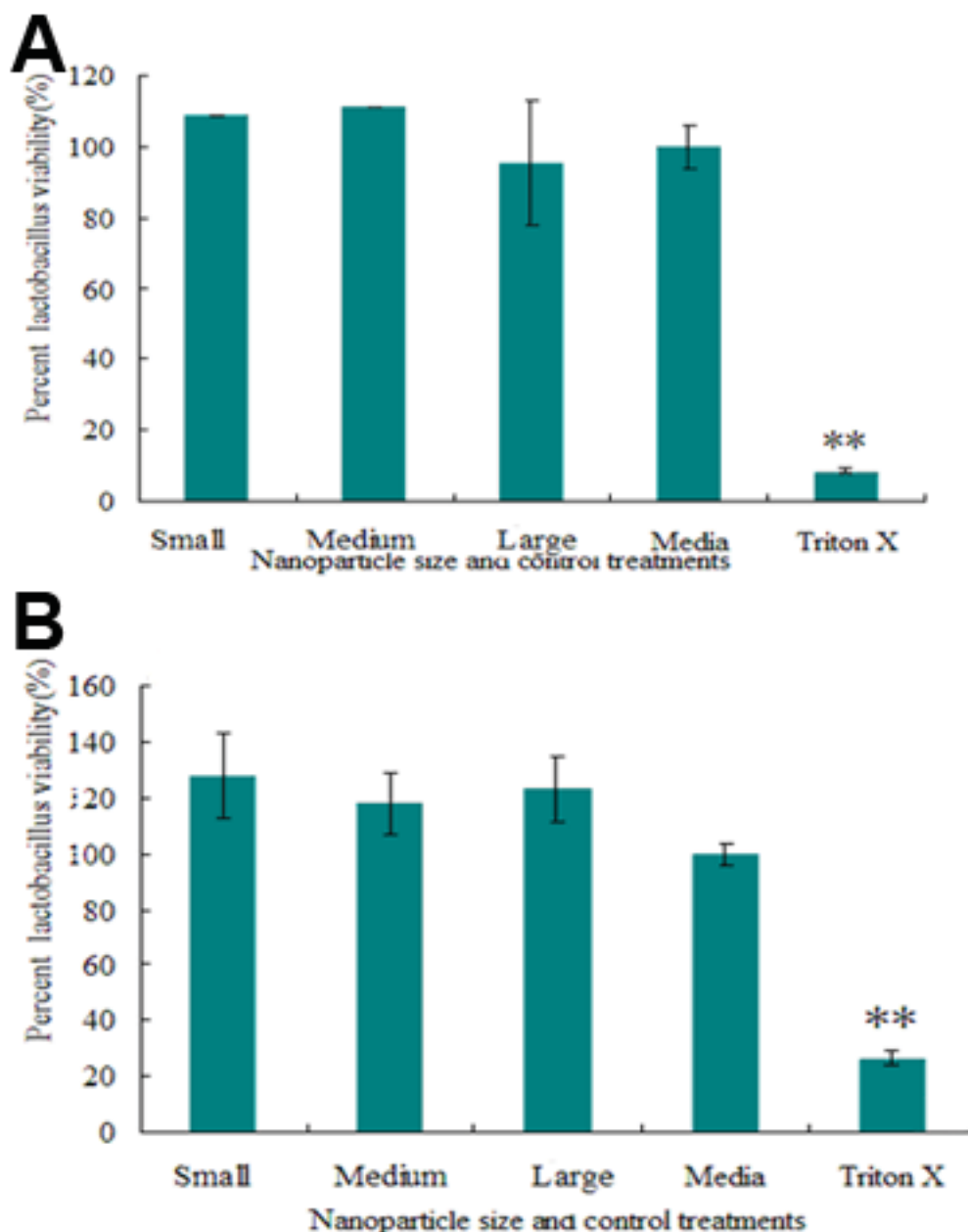


Fig. 3-9. Percent viability of *Lactobacillus crispatus* treated by chitosan NPs with different sizes for 4 h (A) and 48 h (B), (n=3). * $P < 0.05$ vs Media, ** $P < 0.01$ vs Media

3.3.5 Mucoadhesion studies

Porcine vaginal tissue is used for this study because vaginal mucosa is a realistic and reproducible system to assess the therapeutic potential of new agents in humans⁷³. After

fluorescence tagging, the average diameter of small, medium, and large particles is 188.7 ± 43.3 nm, 273.5 ± 53.1 nm, and 900.2 ± 118.4 nm, respectively. For large-sized NPs, the difference in size may be due to the ethanol use. The performance of most drugs could be improved by using bioadhesive carriers, which provide prolonged contact time between the polymeric system and mucous layer surface⁷¹, and a controlled drug release. Chitosan has a well-known bioadhesive property by establishing the electrostatic interactions with sialic groups of mucins in the mucus layer⁷⁴, which is on the surface of the vaginal tissue. Moreover, it is also demonstrated that chitosan can enhance the absorption of hydrophilic molecules by promoting a structural reorganization of the tight junction-associated proteins⁷⁵.

The contribution of particle size to the mucoadhesion % of chitosan NPs is shown in Fig. 3-10. There is no statistical difference between low and medium-sized NPs ($P=0.32$); however, the mucoadhesion % of large-sized NPs is halved (P value between low and large size NPs is 0.003).

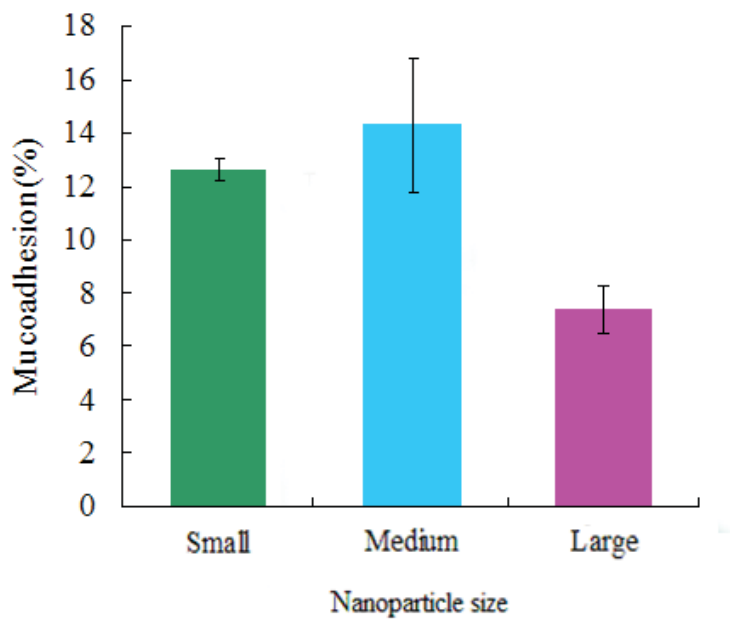


Fig. 3-10. Percent mucoadhesion of chitosan particles with different sizes on porcine vaginal

tissue. After fluorescence labeling, the mean diameters of small, medium, and large particles are 188.7 ± 43.3 nm, 273.5 ± 53.1 nm, and 900.2 ± 118.4 nm, respectively for $n=3$.

Since the mucoadhesive properties of the NPs are due to the electrostatic attraction between chitosan on the surface of the NPs and the sialic acid group of mucin, the total specific surface area is the decisive factor of the mucoadhesion. For small particles, more chitosan molecules have a chance to contact the mucous layer. Thus, the mucoadhesive property of small chitosan NPs is improved. To achieve a desired dosage, both the EE% and mucoadhesion % (MA%) should be considered to efficiently identify the ultimate formulation process. Assuming that for all the three kinds of NPs, drug EE% remains unchanged after fluorescence tagging, the mass fraction of $EE\% \times MA\%$ is found to be 0.26%, 0.99%, and 1.71%, respectively, using the approach in the previous report⁷⁶. Though the percent mucoadhesion of large-sized NPs is lower than that of low and medium-sized particles, the mass fractions are higher than that of the other two kinds of particles, which indicates that large-sized chitosan NPs are ultimately the most promising vehicle for preparing chitosan based vaginal or topical microbicide delivery.

3.4 Conclusion

In this work, reported for the first time, microbicide loaded chitosan NPs are prepared by ionic gelation. The EE% of TFV, which is used as a model microbicide, could be improved significantly by using an ethanol solution as a solvent of chitosan. However the use of ethanol also increases the particle size. The *in vitro* release, cytotoxicity assays, and mucoadhesive studies suggests that relatively large chitosan NPs have the potential to be a controlled release, safe, and bioadhesive microbicide delivery system. These properties make chitosan NPs good candidates for the topical vaginal microbicide delivery system for further

study related to the quest of the prevention of HIV transmission.

CHAPTER 4

COMPARATIVE BIOPHYSICAL PROPERTIES OF TENOFOVIR LOADED THIOLATED AND NON-THIOLATED CHITOSAN NANOPARTICLES INTENDED FOR HIV PREVENTION

4.1 Rationale

Numerous polymers and hydro gel have been used to prolong the residence time at the site of application. Among which, chitosan (CS) is a promising candidate because of its favorable biological properties such as non-toxicity, biocompatibility, and biodegradability⁷⁷. Compared to unmodified CS, it has been shown that the thiolation of CS, by the covalent attachment of thioglycolic acid (TGA), leads to a strongly improved mucoadhesion⁷⁸. Chitosan thioglycolic acid conjugation (TCS) display thiol bearing side chains that mimic the natural mechanism of secreted mucus glycoproteins²⁹. Based on thiol/disulfide exchange reactions, and/or a simple oxidation process, disulfide bonds are formed between polymers and cysteine-rich subdomains of mucus glycoproteins so that the polymers can covalently anchor in the mucus layer³⁰.

We have recently engineered TFV loaded CS NPs⁷⁹ to increase drug retention into the topical route. In order to further maximize the microbicide mucoadhesion, TCS is used here instead of native CS during the preparation of NPs. This study is thus designed to test the hypothesis that anti-HIV microbicide (TFV) loaded TCS NPs exhibit superior biophysical properties for mucoadhesion to the vaginal epithelium compared to those of native CS NPs and gel formulations. TCS is chosen as a matrix of the drug carrier, and sodium tripolyphosphate (TPP) worked as a cross-linking agent. NPs are prepared on the basis of the ionic gelation of TCS with TPP anions⁸⁰.

4.2 Materials and methods

4.2.1 Materials

Chitosan (CS) (molecular weight of 50~190 KDa), sodium triphosphate pentabasic (TPP), DL-dithiothreitol (DDT), and lysozyme (activity: 50 units/mL at 5 µg/mL) from chicken egg white are purchased from Sigma Aldrich (St. Louis, MO, USA). Tenofovir (TFV) is purchased from Zhongshuo Pharmaceutical Co. Ltd. (Beijing, China). Acetic acid and methanol are supplied by Fisher Scientific (Pittsburgh, PA, USA). Fluorescein-5-isothiocyanate (FITC) is purchased from Invitrogen (Carlsbad, CA, USA).

The human vaginal epithelial cell line VK2/E6E7, human endo cervical epithelial cell line End/E6E7 and *Lactobacillus crispatus* (ATCC Number 33197) are purchased from American Type Culture Collection (ATCC, Boston, Massachusetts, USA). The Keratinocytes–SFM serum-free medium is from GIBCO Invitrogen (Carlsbad, California, USA); the medium composition is modified to reach the desired calcium concentration by adding CaCl₂ (0.4 mM) 155 µl/100ml medium, recombinant epidermal growth factor (0.1 ng/ml), (2.69 µl/100 ml), and bovine pituitary extract (400 µL/100 mL). *L. crispatus* is grown in an ATCC medium 416 Lactobacilli MRS broth (BD, Franklin Lakes, NJ, USA). Aqueous nonradioactive cell proliferation assay [3-(4,5-dimethylthiazol-2-yl)-5-(3-carboxymethoxyphenyl)-2-(4-sulfophenyl)-2H-tetrazolium, inner salt; MTS], and lactate dehydrogenase (LDH) cell cytotoxicity kit (CytoTox-ONE™), are purchased from Promega (Madison, WI, USA). All other chemicals used in this study are of analytical grade and used as received without further purification.

4.2.2 Methods

4.2.2.1 Synthesis of chitosan-thioglycolic acid conjugates (TCS)

Chitosan-thioglycolic acid conjugates or thiolated chitosan (TCS) is synthesized using a previously described method⁸¹. Briefly, 100 mg of chitosan is dissolved in 10 ml of 0.1 M HCl to obtain a 1% w/v solution of chitosan hydrochloride. Then 100 mg (1.09 mmol) of TGA is added. After TGA is completely dissolved in the chitosan hydrochloride solution, 10 mg (0.05 mmol) of EDC and 15 mg (0.13 mmol) NHS is added. The pH is adjusted to 5 and the reaction mixture is incubated for 3 h at room temperature under constant stirring. The control samples are without EDC and NHS also prepared and analyzed.

The reaction mixture subsequently, undergoes dialysis for 3 days at 10°C in the dark against 1L of 5 mM HCl to isolate the pure chitosan conjugates and to eliminate unbound TGA, then against the same medium but containing 1% w/v NaCl, in order to reduce the ionic interactions between chitosan and the sulfhydryl compound.

4.2.2.2 Proton nuclear magnetic resonance (¹H-NMR) spectroscopy analysis of TCS

In order to confirm the effective conjugation between CS and TGA, proton (¹H) NMR spectroscopy analysis is performed. The samples are dissolved in deuterium oxide (D₂O). The spectra are observed on a Varian (Palo Alto, CA, USA) 400MHz spectrometer with a Varian two channel probe. V_{nmrj} 2.2 (Palo Alto, CA, USA) is used to process the experimental data. Typically, the spectra are acquired with relaxation delay of 2 sec and the number of scans is 2048. The concentration of each 500 µl sample is 4 mg/ml.

4.2.2.3 Preparation of tenofovir (TFV) loaded TCS based NPs

TCS is hydrated in 2 ml of purified water for 1 h, and then dissolved in 10 ml 1% acetic acid at concentrations of 0.1%, 0.2% and 0.3%(w/v%). The method of preparation is adapted from the method described by Fernandez-Urrusuno et al.⁴³. Briefly, TPP is dissolved in 1 ml purified water. The weight ratio of TPP/TCS is 0.1, 0.2 and 0.3 respectively. The TFV

is dissolved in 0.5 M NaOH solution. The weight ratio of TFV/TCS is 0.1, 0.2 and 0.3 respectively. The concentrations of TCS, TPP, and TFV solution are shown in Tab. 4-1.

Tab. 4-1 Independent Variables and their levels in Box-Behnken Design

Independent variables	Low	Medium	High
X ₁ = concentration of TCS (w/v %)	0.1	0.2	0.3
X ₂ = TPP/TCS weight ratio	0.1	0.2	0.3
X ₃ = drug/TCS weight ratio	0.1	0.2	0.3
Coded values	-1	0	1
Dependent variables			
Y ₁ = encapsulation efficiency (EE %)			
Y ₂ = particle mean diameter (nm)			

The drug solution is added to the CS solution and followed by the addition of the TPP solution under magnetic stirring at room temperature. The system is then stirred for 10 min at room temperature. The NP suspension is formed spontaneously by ionic gelation.

NPs are separated by centrifugation (Beckman L8-70 M Ultracentrifuge, Brea, CA, USA) at 12,000 rpm (g force 19560 xg), 20 °C for 40 min. The supernatant, which is clear and translucent, is used to determine the drug EE%; the cake is washed three times with deionized water, freeze-dried (Labconco Corporation, Kansas City, MO, USA) and stored at 4°C until use.

The preparation of FITC-labeled CS and TCS is based on the reaction between the isothiocyanate groups of FITC and the amino groups of CS⁴⁹, as previously described⁵⁰. The FITC-labeled CS NPs are prepared also by ionic gelation (as described above), characterized,

and used for mucoadhesion and uptake studies as shown below.

4.2.2.4 Determination of drug encapsulation efficiency (EE%)

After centrifugation, the supernatant is used to determine the percent drug EE%. The amount of unencapsulated (or free) drug in the supernatant is measured by UV spectrometer (Spectronic Genesys 10 Bio, Thermo Electron Corporation, WI, USA) at a wavelength of 259 nm. The content of TFV is calculated using the following Equ. 4-1:

$$EE(\%) = \frac{\text{Total amount of TFV} - \text{Free TFV}}{\text{Total amount of TFV}} \times 100 \quad (4 - 1)$$

4.2.2.5 Size and size distribution analysis

The particle mean diameter and polydispersity index (PDI) in water medium are determined by dynamic light scattering (Zetasizer Nano ZS Malvern Instruments Ltd, Worcestershire, UK) base on the intensity of the processed light signal⁸². The particle mean diameter is represented as Z-average diameter following the cumulant model. The PDI is given by the following Equ. 4-2:

$$PDI = \frac{K_2}{K_1^2} \quad (4 - 2)$$

Where K_1 is an effective mean diffusion coefficient and K_2 is the relative width of the size distribution if normalized by K_1 ⁸².

The measurements are taken at the temperature of 25°C. Each measurement is repeated three times and an average value is reported. A sample with a $PDI < 0.05$ is considered monodispersed according to the National Institute Standard¹.

4.2.2.6 Morphological analysis

The morphology of the NPs is examined by the scanning electron microscope (SEM) and transmission electron microscopy (TEM). To obtain the specimens, after freeze-drying, NPs are mounted to aluminum stubs with conductive tape, and sputter coated with 20 nm of

gold–palladium alloy. The NPs are visualized under a Philips SEM 515 microscope (Philips/FEI, Eindhoven, NL). For TEM, 8 μ L of the particle suspension are placed on a copper grid with a carbon support film, allowed to equilibrate for 5 min, and then air dried. The grids are viewed under a transmission electron microscope (Philips CM12 STEM, Philips Electronic Instruments, Inc., Mahwah, NJ). Digital images are acquired with the large format (II Megapixel), retractable, and fiber-optical coupled CCD camera SC100 ORIUS[®] CCD camera.

4.2.2.7 *In vitro* TFV release profile

The *in vitro* release of NPs is compared with hydroxyethyl cellulose (HEC) gel containing TFV, with TFV powder used as a control. Ten milligrams of NPs, HEC gel containing 1% of TFV and 0.2 mg of TFV powder are suspended, respectively, in the Spectra/Por cellulose ester membrane dialysis bag (Spectra/Por Float-A-Lyzer G2, MWCO 3.5-5 KD, Spectrum Laboratories Inc. Rancho Dominguez, CA, USA), and then immersed in a tube containing 20 ml vagina fluid simulant (VFS) at pH 4.2. The VFS is prepared according to previous reports⁴⁵. The tubes are kept in a thermostatically controlled shaking water bath (BS-06, Lab Companion, Seoul, Korea) that is maintained at 37°C and 60 rpm. At predetermined time intervals, all the buffer solution (20 ml) outside the dialysis bag is removed and replaced by fresh buffer solution to maintain a sink condition. The concentration of drug in the buffer solution is determined by a UV spectrometer at 259 nm. Each experiment is run in triplicate together with a blank NP control. One hundred percent drug release is obtained from complete enzymatic digestion of NPs using lysozyme after 120 h using the method of Don et al.⁸³. TCS NPs obtained under the optimal conditions are used in this study compared with CS NPs prepared at the same condition.

The drug release data are fitted to kinetic models below (Equ. 4-3 to 4-5), respectively, related to zero-order, first-order, and Higuchi model to elucidate the release mechanism⁸⁴.

For zero-order kinetics:

$$Q=k_0t, \quad (4-3)$$

Where Q represents the percent of drug released in time t , and k_0 is the apparent release rate constant or zero-order release constant.

For first-order kinetics:

$$\ln(1-Q)=-k_1t \quad (4-4)$$

Where Q represents the percent of drug released in time t , and k_1 is the first-order release constant.

For Higuchi model:

$$Q=k_Ht^{1/2} \quad (4-5)$$

Where Q represents the percent of drug released in time t , and k_H is the Higuchi dissolution constant.

4.2.2.8 Cell cultures

Two cell lines are used in this study: human vaginal keratinocyte cell line VK2/E6E7 and human endocervical epithelial cell line End/E6E7. Both cell lines are grown in the Keratinocytes-SFM medium, which is with 10% (v/v) fetal bovine serum (FBS) and 1% penicillin/streptomycin. Cells are cultured at 37°C in a humidified 5% CO₂ atmosphere and sub-cultured prior to confluence using trypsin.

4.2.2.8.1 LDH release studies

To measure the lactate dehydrogenase (LDH) release, cells are seeded in 96-well

plate. After 80% confluence is reached the cells are incubated with 100 μ l media containing 1 mg/ml blank or TFV loaded CS or TCS NPs, or 200 μ g/ml TFV in each well. A media without NPs is used as a negative control, and 1% Triton-100 X is used as a positive control. The background fluorescence that might be present due to the media only, is kept by adding NP suspension to the cell-free wells. The plate is incubated at 37°C for 4, 24, and 48 h and then equilibrated to 22 °C. At different time intervals, 100 μ l of CytoTox-ONE™ Reagent (Promega, Madison, WI, USA) is added to each well and shaken for 30 s. The plate is incubated at 22 °C for 10 min and then 50 μ l of stop solution is added. The fluorescence is determined by a microplate reader at λ_{ex} 560 nm and λ_{em} 590. The percent LDH released by the cell membrane is calculated using Equ. 4-6:

$$\text{LDH release (\%)} = \frac{F_{\text{Experimental}} - F_{\text{Background}}}{F_{\text{Positive}} - F_{\text{Background}}} \times 100 \quad (4 - 6)$$

Where $F_{\text{Experimental}}$, $F_{\text{Background}}$ and F_{Positive} represent the fluorescence intensity of NPs-treated, background (without cells), and positive control (cells treated with 1% Triton-100 X) wells, respectively.

4.2.2.8.2 Cell viability assays

The cell viability is determined by adding MTS and then checking the amount of a colored formazan product that is bio-reduced from MTS by cells. Cells are seeded and incubated with 1 mg/ml blank or TFV loaded CS or TCS NPs, or 200 μ g/ml TFV under the same condition as above and by following the manufacturing protocol. At different intervals (4, 24, and 48 h), the particle suspension is removed and substituted with fresh medium. Twenty microliters of CellTiter 96® Aqueous One Solution Reagent (Promega, Madison, WI, USA) is added to each well and incubated at 37°C for 4h. The absorbance is recorded at a wavelength of 490 nm. The cell viability is expressed using Equ. 4-7:

$$\text{Viability(\%)} = \frac{A_{\text{Test}}}{A_{\text{Control}}} \times 100 \quad (4 - 7)$$

Where A_{Test} and A_{Control} represent the absorbance related to the amount of formazan detected in viable cells in wells treated with NPs and not treated with NPs, respectively.

The *Lactobacillus* viability assay is performed in order to assess the effect of CS NPs on *L. crispatus* growth using the established method⁴⁷. Briefly, the bacteria density is adjusted to an OD₆₇₀ of 0.06, corresponding to a 0.5 McFarland Standard or 10⁸ CFU/ml^{48a}. *L. crispatus* is plated in a 96-well plate at a volume of 100 µl and then incubated with 100 µl of medium containing 1 mg/ml blank or TFV loaded CS or TCS NPs, or 200 µg/ml TFV at 37 °C. A commercially available 10 µg/ml of Penicillin-Streptomycin solution (Invitrogen, Carlsbad, CA, USA) is used as a positive control. After 4, 24, and 48 h, 20 µl of MTS reagent are added to each well, and the bacterial viability is determined by measurement of the absorbance at a wavelength of 490 nm by a microplate reader. The percent viability can be calculated using the above Equ. 4-7. After 48 h, the bacterial is imaged with a microscope (Nikon Instruments, Inc. Melville, NY) at a magnification of 1000.

4.2.2.8.3 Cellular uptake studies

Cellular uptake studies are performed using a microplate reader and a confocal microscope as previously described⁸⁵. The cells (1 x 10⁴) are seeded in 96-well plates. After 80% confluence is reached, the cells are incubated with FITC labeled CS and TCS NPs suspension (500 µg/ml in the media). Cells treated with media only are used as background. The control is determined by adding NP suspension in a row of wells without cells. After 4, 24, and 48 h, the suspension in the test wells is removed and the cells are washed three times using a phosphate buffer saline (PBS, pH = 7.4) solution. One percent of Triton-100 X is added for cells lysis, the fluorescence is measured using a microplate reader. The cellular

uptake efficiency is calculated using Equ. 4-8:

$$\text{cellular uptake(\%)} = \frac{F_{\text{Cell}}}{F_{\text{Control}}} \times 100 \quad (4 - 8)$$

Where F_{cell} and F_{control} represent the fluorescence intensity related to the amount of particles up taken in the cells in test wells and in the control wells, respectively.

4.2.2.8.4 Flow cytometry analysis

Both VK2/E6E7 and End/E6E7 cell lines are cultured in the T-25 culture flask till 80% confluence. FITC labeled CS and TCS NPs (500 $\mu\text{g/ml}$) are incubated with cells for 48 h. Cells treated with media only are used as a negative control. The cells are washed three times with PBS and harvested using 5 ml of trypsin for 5 min, then diluted with an equal volume of FBS. Finally, the number of cells containing FITC labeled NPs is measured using the BD LSR II Flow Cytometer (BD Biosciences 2350, Qume Drive San Jose, CA).

4.2.2.8.5 Assessment of uptake using fluorescence microscopy

Both VK2/E6E7 and End/E6E7 cells are seeded on the 96-well plate at a concentration of 2×10^5 cells/ml. After 48h incubation at 37°C , the cells are treated with FITC labeled CS and TCS NPs suspension (1 mg/ml in the media) and incubated for another 48 h. Then the suspension in the test wells is removed and the cells are washed twice using a PBS solution ($\text{pH} = 7.4$). Cells treated with media are used as control. Subsequently, 100 μl of Hoechst 33342, a permeable DNA dye, prepared in PBS solution (10 $\mu\text{g/ml}$) are added and the cells are incubated at room temperature for 20 min⁸⁶. Then the cells are imaged with a fluorescence microscope (Nikon Instruments, Inc. Melville, NY) at a magnification of 400. DAPI and FITC filters are used to observe the nucleus (blue) and the NPs (green), respectively. The images processing is performed with Adobe Photoshop CS software (Adobe Systems, San Jose, CA, USA)

4.2.2.8.6 Cellular uptake inhibition study

Cytoskeleton reorganization is prevented by incubating the cells with cytochalasin D (10µg/mL) for 30 min followed by application of NP complexes. Macropinocytosis is promoted through treatment with phorbolmyristate acetate (PMA, 1 µM) for 30 min prior to addition of the complexes. Clathrin dependent endocytosis is disturbed by co-treatment with chlorpromazine (10µg/mL), following a 30 min pre-incubation at the same concentration. To perturb caveolin-mediated pathways, cells are pre-treated with genistein (100 µg/mL) for 30 min. In all cases, the treatment of the cells with CS and TCS NPs is done in the presence of the respective NPs at the same concentration as used for the pre-treatment. Following treatment under these various conditions, cells are harvested after 24 h and analyzed as described above⁸⁷.

4.2.2.9 Mucoadhesion study

Fresh porcine vaginal tissues are obtained from the local abattoir (Fairview Farm Meat Co., Topeka, KS, USA). These tissues are washed using normal saline, snap frozen in liquid nitrogen, and then stored at -80°C. Before the experiment, the frozen tissue is thawed in normal saline at 37°C for 3 min.

The bioadhesive property of the NPs is determined, as described by RangaRao and Albrecht⁸⁸, for the comparison of CS and TCS NPs using the infusion and immersion method. Porcine vaginal tissues are cut into strips of 8 cm long and 1 cm wide and then mounted on plastic strips of the same width using cyanoacrylate glue⁵³. In the infusion method, each strip is put into a tube that is placed in a water bath of 37°C at an angle of 45°. An equilibration period of 5 min with VFS is allowed before administering the particles to humidify the mucosa. The mucosa are then continuously rinsed with 10 ml VFS, which contained 10, 20,

and 30 mg of FITC labeled NPs. A constant flow rate of 1 ml/min is provided by using an infusion set. The fluid is collected, and the fluorescence of each fluid, before and after the treatment, is analyzed by a DTX 800 multimode microplate reader (Beckman Coulter, Brea, CA, USA) at λ_{ex} 490 nm and λ_{em} 520 nm. The percent mucoadhesion (MA%) is calculated with Equ. 4-9:

$$MA(\%) = \frac{F_{Initial} - F}{F_{Initial}} \quad (4 - 9)$$

Where $F_{Initial}$ represents the initial fluorescence, and F represents the fluorescence after the treatment⁵⁴.

The surface of the tissue is cleaned carefully, the tissue is cut into small cubes, embedded into Histoprep, frozen by using liquid nitrogen, and then sectioned vertically using a cryostat microtome. The skin sections (5 mm) are mounted on glass slides and visualized through a fluorescence microscopy without any additional staining or treatment⁸⁹.

Using the immersion method, the effects of time on bioadhesion are determined as follows: predetermined FITC labeled TCS NPs are suspended in VFS; the plastic strips with tissue are immersed into tubes containing 10 ml of VFS suspension; the tubes are put into a shaking water bath for 30 min, 1 h, and 2 h at 100 rpm; the tissues are then removed⁵⁴; and the fluorescence of each sample before and after the treatment is analyzed as described above.

4.2.2.10 Statistical data analysis

The study is designed according to the Box–Behnken experimental design method⁹⁰. The polynomial Equations relating the independent variables to dependent variables are obtained by Box–Behnken design software (JMP8, SAS Institute), which is used for response optimization.

The results are expressed as the mean of at least 3 experiments \pm the standard error

of the mean (SEM). Statistical data analysis is performed using the student t-test; two tails with 95% confident interval ($p < 0.05$) as the minimal level of significance.

4.3 Results and discussions

4.3.1 Synthesis and characterization of chitosan-TGA conjugates (TCS)

TGA is covalently attached to chitosan by the formation of amide bonds between the carboxylic acid groups of the TGA and the primary amino groups of the chitosan. To achieve this, the carboxylic acid moieties of the TGA are activated by the EDC. The addition of NHS stabilizes the amine-reactive intermediate and increase the efficiency of the EDC-mediated coupling reactions. The synthesis is performed at a $pH < 5$ to avoid the formation of the disulfide bonds by air oxidation since, at $pH < 5$, the formation of disulfide bonds can be excluded due to the low concentration of the thiolate anions⁸¹.

4.3.2 Proton nuclear magnetic resonance (1H -NMR) spectroscopy analysis of TCS

Based on the results of the NMR spectroscopy (Fig. 4-1), amide bond with chemical shift $\delta = 8.22$ is indeed formed and identified in chitosan-TGA conjugate when EDC and NHS are used. The control, which is prepared by the same method as of the conjugates but omitting EDC and NHS, exhibits no peak of the amide bond (Fig. 4-1).

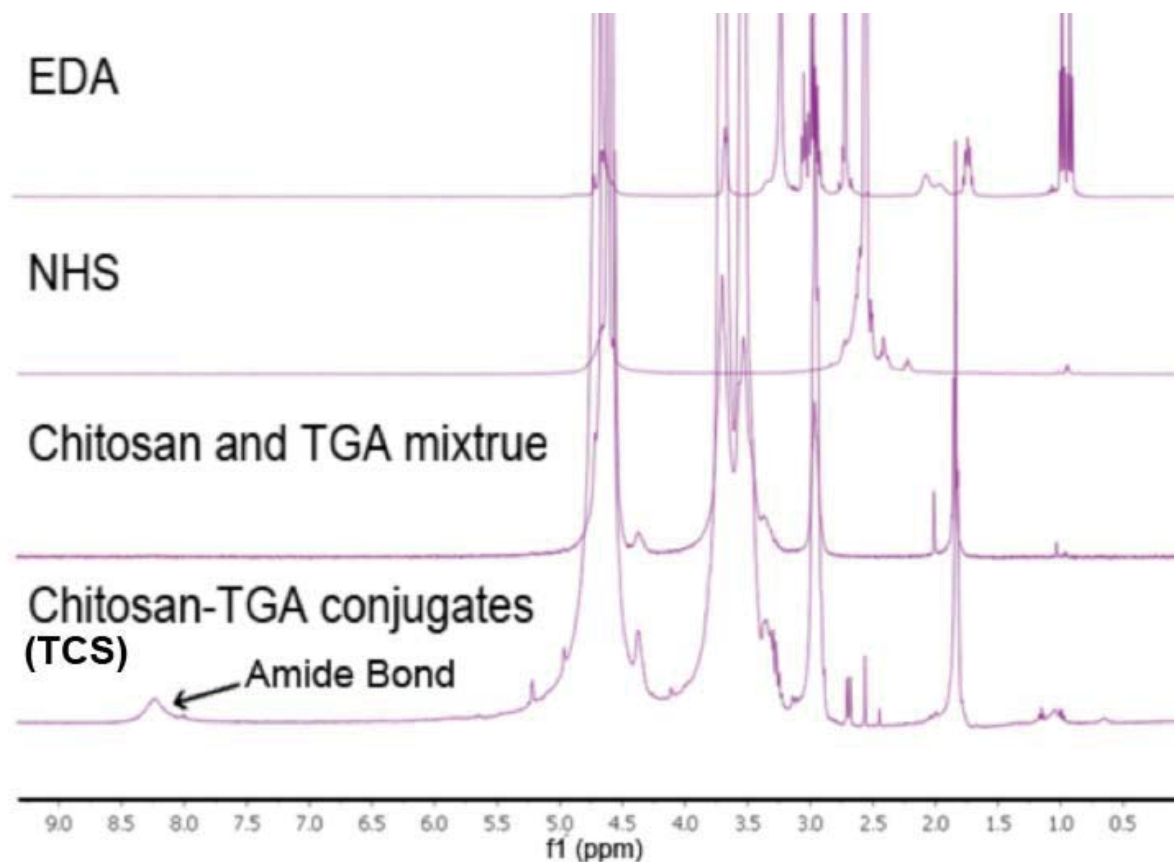


Fig. 4-1. ^1H Nuclear Magnetic Resonance (NMR) spectrum of the synthesized TCS conjugate and starting materials.

4.3.3 Formulation and characterization of TCS NPs

The Box-Behnken design utilized in this study has several advantages. It requires fewer runs in comparison with other experimental designs. Three factors are chosen as independent variables: X_1 = concentration of TCS (w/v %), X_2 = TPP/TCS weight ratio, X_3 = drug/TCS weight ratio. Each factor is studied at three levels, represent with -1, 0 and 1. Two dependent variables: Y_1 = EE%, Y_2 = particle mean diameter (nm) are chosen as response. It is also able to avoid the extreme conditions as it does not contain combinations where all the factors are at their highest or lowest levels⁹¹. According to the acceptability criteria for nano encapsulation process, a p-value of less than 0.1, and a R^2 value of more than 0.9, is required. Since the polynomial Equations for Y_1 fit well ($p = 0.0012$, $r^2=0.98 > 0.90$) (Fig. 4-2 A)⁸⁴, it

can be used for Y_1 response optimization purposes. The polynomial Equ. 4-10 below expresses the influence of the independent variables on Y_1 (EE%):

$$Y_1 = 5.14 + 2.87X_1 + 3.10X_2 - 3.40X_3 + 2.80X_1X_2 - 1.97X_1X_3 - 1.88X_2X_3 + 3.10X_1^2 - 1.03X_2^2 - 2.78X_3^2 \quad (4-10)$$

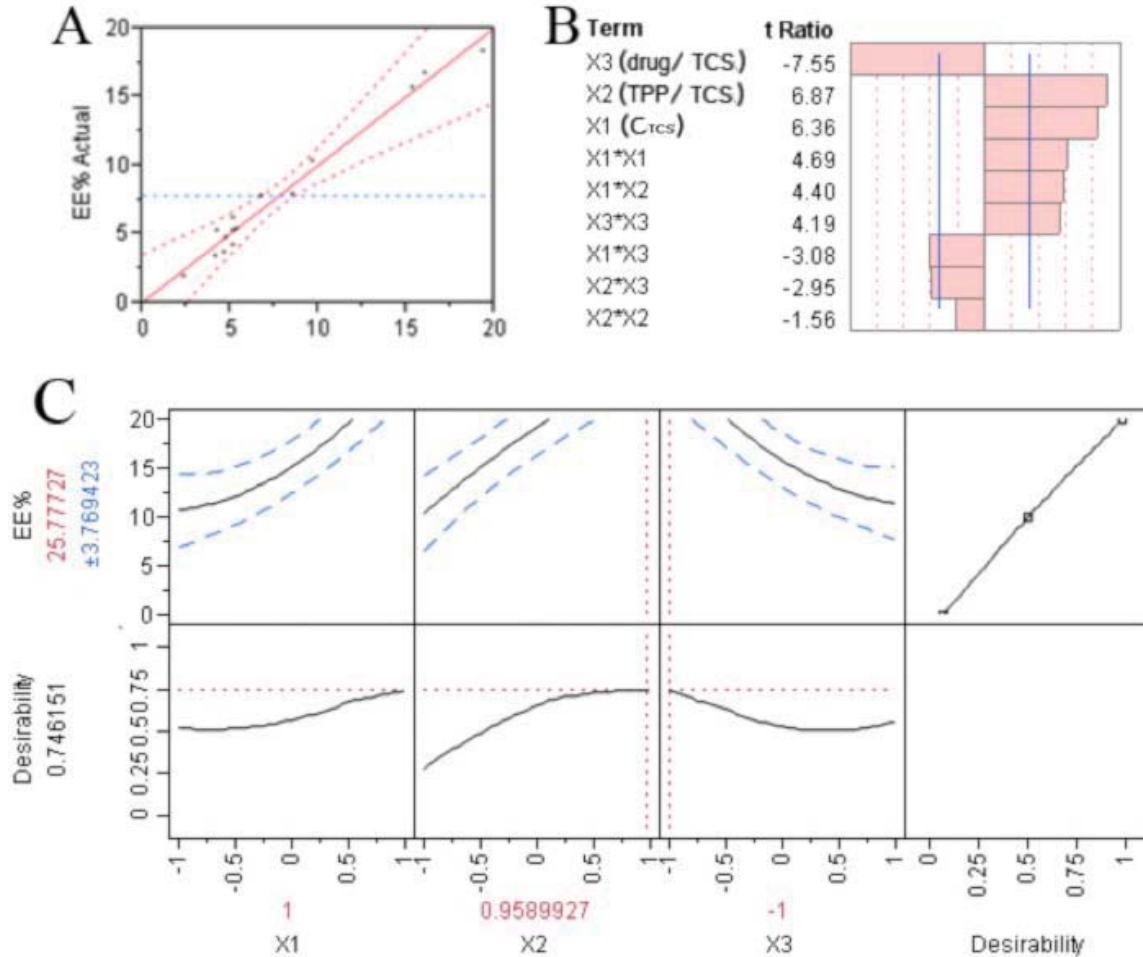


Fig. 4-2 A: Curve fitting of Y_1 (EE%), where $R^2=0.98$; B: Standardized Pareto chart showing the standardized effect of the formulation variables and their interaction on Y_1 . X axis indicates the t ratio of the variables. Bars extending pass the vertical line indicate values reach statistical significance ($\alpha=0.05$). C: Prediction profiler showing the effect of the formulation variables on EE% (Y_1).

A Pareto chart is constructed in Fig. 4-2 B to visualize the significance of the variables in Equ. 4-10. The values on the X-axis of the Pareto charts represent the standardized effects, which are the t values calculated base on the following Equ. 4-11:

$$t = \frac{|E_x|}{SE_e} \quad (4 - 11)$$

E_x is the estimate of factor effect, which is the coefficient in Equ. 4-10, SE_e is the standard error of the factor effect⁵⁵. The obtained t, which indicates the main effect of the independent variables and interactions on Y_1 value, compare to a tabulated critical t value ($t_{critical} = 2.571$ at $p < 0.05$), which is determined at $\alpha=0.05$ for residual degrees of freedom (df), where $df = 5$ ⁵⁶; $t_{critical}$ is shown in the vertical line in the Pareto chart. The factors whose length passed the vertical line indicate significance on the response value⁵⁷. The positive sign of the coefficient shows a positive effect on the responses size, while the negative signs indicate a negative effect.

According to Fig. 4-2 B, X_1 , X_2 , X_3 , $X_1 \times X_1$, $X_1 \times X_2$, $X_3 \times X_3$, $X_1 \times X_3$ and $X_2 \times X_3$ all contribute substantially to the EE%. TCS is used in this study as a polymeric matrix; the encapsulation of drug is based on the interaction between amino groups of TCS and phosphate groups of drug. Higher CS concentration (X_1) means more total available amino groups in CS molecules, and more drug molecules could interact with TCS through electrostatic forces. Thus the EE% increases with the increasing of X_1 , and $X_1 \times X_1$ effect the EE% positively based on the same reason. From Fig. 4-2 B and C, the concentration of CS (X_1) has a curvilinear effect on the EE%. Below the coded value of -1, the EE% begins to increase. It may be due to the decreased viscosity effect at a lower concentration. It has already been reported that low viscosity associated with decreased CS concentration allows the drug to move around the polymer chain, and consequently improves entrapment of the

drug⁹². TPP works as the cross linking agent; many more polymer molecules could be linked together and form NPs while increasing the ratio of TPP/CS (X_2). The EE% increased with the TPP/TCS (w/w) (X_2) linearly. Since both CS and TPP strengthen the mass and cross link density of the polymeric matrix, the combination of $X_1 \times X_1$ and $X_1 \times X_2$ also show a positive effect on EE%. An increase of drug/TCS (w/w) X_3 has a decreasing effect on the EE%. The higher the relative amount of drug to polymer in the solution (X_3), the lower the EE%, because fewer polymers would be available for drug encapsulation. Therefore, the combination of $X_1 \times X_3$ and $X_2 \times X_3$ show a negative effect on the EE% (Y_1). It also appears that the EE% (Y_1) correlated curvilinearly with X_3 . The drug/TCS ratio (X_3) appears to increase the EE%. A possible reason is that the aqueous solution of TFV is weak acid with two pK_a values at 3.8 and 6.7⁹³. At high concentration, TFV possibly affected the pH of the solvent, which is conducive to the ionization of CS or TCS. The subsequent water solubilization is needed for effective cross linking with TPP⁹². However, this effect is limited by the TFV water solubility (1.87 mg/ml in water)⁶¹. In Fig. 4-2.C, it is evident that a higher level of X_1 , X_2 and a lower level of X_3 favored the higher EE% (Y_1). Tab. 4-2 shows the results from the ANOVA.

Tab. 4-2. ANOVA for EE% (Y_1).

Response	Source	DF	SS	MS	F ratio	P value
Y_1	Model	9	363.72	40.41	24.88	0.0012
	Error	5	8.12	1.62		
	Total	14	371.84			

Note: DF: degree of freedom, SS: sum of square, MS: mean sum of square, F ratio: Model MS/error MS

Based on Equ. 4-10 and the interaction plot shown in Fig. 4-2, the optimal formulation, which exhibited the highest EE% ($25.78\% \pm 3.80\%$) is selected, X_1 , X_2 , and X_3 are 1, 0.96, and -1.

To confirm the analysis, a check point analysis is performed. Two random points out of the 15 runs of the experiment $(-0.5, -0.5, -0.5)$ and $(0.5, 0.5, 0.5)$ and the theoretically optimum point resulting from the statistical model (with the three factors set at $X_1 = 1$, $X_2 = 0.96$ and $X_3 = -1$) is selected. As shown in Tab. 4-3, the EE% of the tested points are close to the predicted values.

Tab. 4-3 Checkpoint Experiments Comparing Measured and Predicted EE% (n=3)

Run no.	X_1	X_2	X_3	Measured Y_1 \pm SEM	Predicted Y_1 d Y_1	Error% of Y_1	p value (Y_1)	t value (Y_1)
C1	- 0.5	- 0.5	- 0.5	3.90 ± 1.01	4.81	-18.09	0.46	0.90
C2	0.5	0.5	0.5	6.79 ± 0.80	7.37	-7.87	0.54	0.72
C3	1	0.96	- 1	22.60 ± 1.06	25.78	-12.34	0.10	3.00

The differences between the measured and predicted values are not found to be statistically significant ($p > 0.05$). According to Student's t test, the t value of the optimal point (C_3) is 3.00 ($df = 2$, $\alpha = 0.05$, $t_{critical} = 4.30$), which indicates that the optimal EE% (22.60%) obtained from the experiment appeared to be close to the prediction (25.78%) derived from the model. The other two checkpoints (C_1 and C_2) led to similar responses (t value is 0.90 and 0.72). Thus, it can be reasonably concluded that under these checkpoint conditions, the model fits the data satisfactorily and are valid for predicting the EE%. The model prediction Equation is an acceptable tool to predict the EE% of NPs in this study. The

NP samples used for all the assays below are prepared with the optimal condition.

However, the R^2 of the polynomial Equation for particle mean diameter Y_2 (0.67) is below the threshold for acceptability (0.70)⁸⁴. The possible reason for this is the presence of the thiol groups on TCS chains. It is noteworthy that the molecular weight of TCS (10-150 kDa) is relatively lower than that of CS (50-190 kDa). The size of CS based particles is found to be the proportion to the macromolecules' molecular weight (data not shown). In contrast, there is no apparent difference in particle mean diameters of CS NPs (240.1 nm) and TCS NPs (252.3 nm) (Tab. 4-4).

Tab. 4-4. Effect of DL-dithiothreitol (DDT) on Size, Zeta potential and EE% of CS and TCS NPs (*: $p < 0.05$; **: $p < 0.01$). Data are given as mean \pm SEM for $n=3$.

NPs	Mean	PDI	Zeta	EE (%)	Drug
	diameter (nm)		potential		Loading
			(mV)		(w/w %)
CS	240.1 \pm 3.3	0.298 \pm 0.002	43.9 \pm 0.6	5.4 \pm 1.0	0.51 \pm 0.09
CS+DDT	245.9 \pm 28.1	0.212 \pm 0.029	44.4 \pm 5.4	6.5 \pm 0.6	0.61 \pm 0.06
TCS	252.3 \pm 16.3	0.317 \pm 0.052	21.4 \pm 2.4	19.4 \pm 1.1	1.62 \pm 0.11
TCS+ DDT	113.0 \pm 7.5**	0.305 \pm 0.020	20.2 \pm 3.2	6.5 \pm 1.4**	0.61 \pm 0.13

Thus it is reasonable to infer that initially, the TCS tends to form small NPs. However, the superfluous thiol groups have strong tendency to form inter- and intra-molecular disulfide bonds with each other. These thiol groups provide a cohesive force to link the small fragments to form larger particles, and lead to unpredictable particle

aggregation following the formation of disulfide bonds as a result. This hypothesis is confirmed by the dramatic effect of DDT on the particle mean diameter (Tab. 4-4). DTT is an agent that can reduce the typical disulfide bond via two sequential thiol-disulfide exchange reactions⁹⁴. After adding DDT, the mean diameter of TCS NPs is significantly reduced from 252.3 nm to 113.0 nm, while that of the CS NPs remained constant (from 240.1 nm to 245.9 nm). The EE% also decreased with DDT, which indicates that the formation of the disulfide bond favored drug entrapment by thiolated NPs. The surface charge of the NPs is (as expected) positive under these experimental conditions. The zeta potential of the TCS NPs is 2-fold lower than that of the CS NPs due to the presence of thiol groups. The positive surface charge of the CS based NPs is due to the amino groups⁹⁵. Since the thiol bearing side chains are covalently attached to this primary amino group, it appeared that the existence of bearing chains in the TCS reduced the charge density by half. It is unaffected by DTT.

SEM and TEM image confirmed the morphology and size data of the CS and TCS NPs (Fig. 4-3)³⁴. These NPs exhibit a spherical shape with a diameter ranging from 100 to 500 nm.

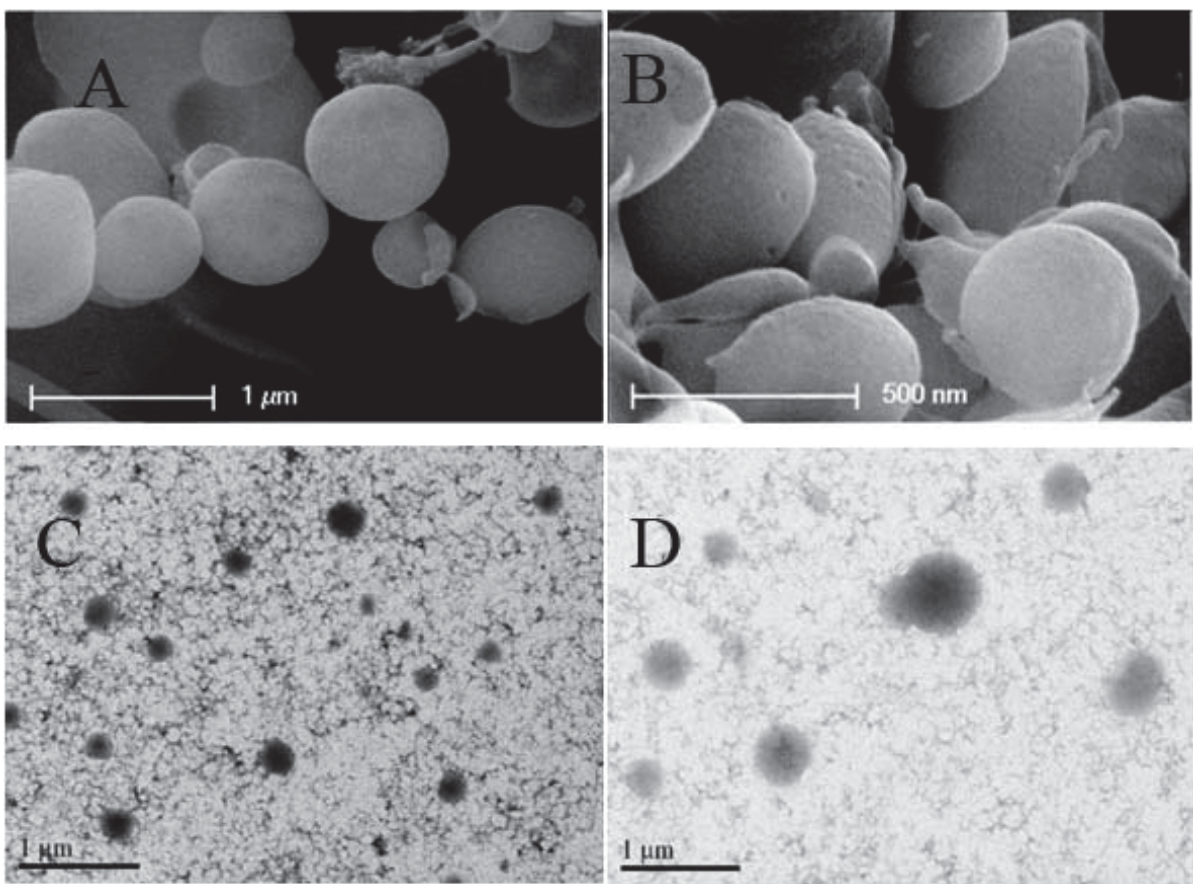


Fig. 4-3 Scanning electron microscopy (SEM) of CS NPs (A) and TCS NPs (B), and transmission electron microscopy (TEM) of CS NPs (C) and TCS NPs (D). All of the four images are obtained with samples prepared with $X_1 = 1$, $X_2 = 0.96$ and $X_3 = -1$, respectively.

4.3.4 *In vitro* Release study

Recently, TFV containing hydroxyethyl cellulose (HEC) gel is developed as a bioadhesive vaginal drug delivery system that appears safe and effective in preventing HIV infection^{21a}. In this study, TFV loaded HEC gel is used for comparison with the CS and TCS NPs with respect to the drug release profiles. The drug release profiles are shown in Fig. 4-4. Approximately, 84% and 95% of cumulative amounts of TFV are released from HEC gel within 24 and 48 h respectively. In the case of the CS and TCS NPs, the percent cumulative

amount release of TFV is 13% and 31% in 24 h, 19% and 39% within 48 h, respectively, and remained constant up to 198 h. These results indicates that the drug release rate is much faster from the HEC gel. The controlled release of TFV is clearly observed in the case of both the CS and TCS NPs.

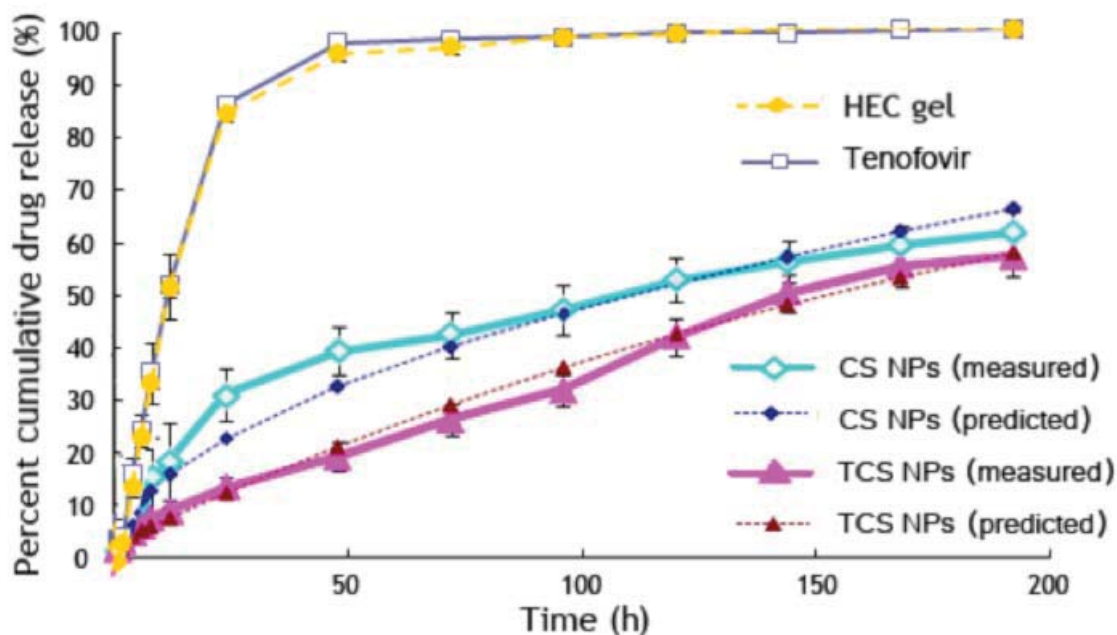


Fig. 4-4 *In vitro* drug release profiles from CS and TCS NPs, in VFS (pH = 4.2), (n = 3). Both samples are prepared with $X_1 = 1$, $X_2 = 0.96$ and $X_3 = -1$, data are shown as mean \pm SEM (n=3).

In order to predict and correlate the release behavior of the CS and TCS NPs, it is necessary to fit the release data into a suitable mathematical model. The results of curve fitting of drug release kinetics into different mathematical models are given in Tab. 4-5.

Tab. 4-5 Curve Fitting of the Release Kinetics of TFV from CS and TCS NPs

CS NPs		TCS NPs	
k	r ²	k	r ²

Zero-order model	0.300	0.987	0.312	0.870
First-order model	0.004	0.990	0.005	0.936
Higuchi model	4.376	0.973	4.848	0.967

The zero-order rate describes the systems where the drug release rate is independent of its concentration. In the first-order release systems, drug release rate is concentration dependent. Higuchi's model describes the release of drugs from an insoluble matrix as a square root of a time-dependent process based on Fickian diffusion⁶⁷. The release constant is calculated from the slope of the appropriate plots, and the regression coefficient (r^2) is determined. It is found that the *in vitro* drug release of the CS NPs is best explained by first-order model, which is the dominant extended release profile found in hydrophilic matrix systems, as the plots shows the highest linearity ($r^2 = 0.990$). The release rate is drug concentration gradient driven. This result is consistent with a previous report related to the tea catechins release for CS NPs⁹⁵. The drug release from TCS NPs fit well the Higuchi's Equation, as the plots shows the highest correlation coefficient($r^2 = 0.967$)⁹⁶. The insoluble matrix is generated by the disulfide bonds that exist only in TCS NPs in this study. The inter disulfide matrix could prevent the TFV molecules from escaping out of the particles and further decrease the release rate of TFV.

The average daily release of TFV is 12% from the CS NPs and 14% from the TCS NPs. As the drug loading of the two kinds of particles are 0.51% (w/w) and 1.62% (w/w) (Tab. 4-4), about 0.6×10^{-3} mg and 2.6×10^{-3} mg drug could be released from 1 mg of CS and TCS NPs every day. Women of reproductive age produce fluid at a rate of approximately 6 ml/day⁷¹;the EC₅₀ value for TFV is about 5 μ M⁹⁷.Therefore, about 14.6 mg of the CS NPs,

or 3.9 mg the TCS NPs, would be able to provide the daily requirement of TFV for an adult woman patient, which is feasible considering that the average vaginal suppository that could be measured as an additional vehicle had a weight of five grams.

4.3.5 Cell culture

4.3.5.1 Cytotoxicity studies

An ideal vaginal drug delivery system has no impact on the viability, function, and structural integrity of the vaginal epithelium. The selected vaginal epithelial cell line VK2/E6E7 and human endocervical epithelial cell line End/E6E7 are used to test the effects of NPs on cell membrane integrity and cell viability. The LDH membrane integrity assay is a fluorometric assay that is used to measure the release of LDH from cells with a disrupted membrane⁹⁸. After 4 h, 24 h, and 48 h, the extent of release of LDH from the cells incubated with NPs is no more than 10% higher than that of media (Fig. 4-5). The CS and TCS NPs and free TFV caused a non-significant release of LDH. MTS is a tetrazolium compound that is bio-reduced by viable cells into formazan. The amount of formazan produced is proportional with the number of living cells⁹⁹. The viability test provided the results that are consistent with the LDH assay, except the TFV led to 17% reduced cell viability of VK2/E6E7 cell line after 48 h incubation. But the reduction didn't appear in cells treated by TFV loaded NP, which indicates the NPs may even decrease the cytotoxicity induced by drug.

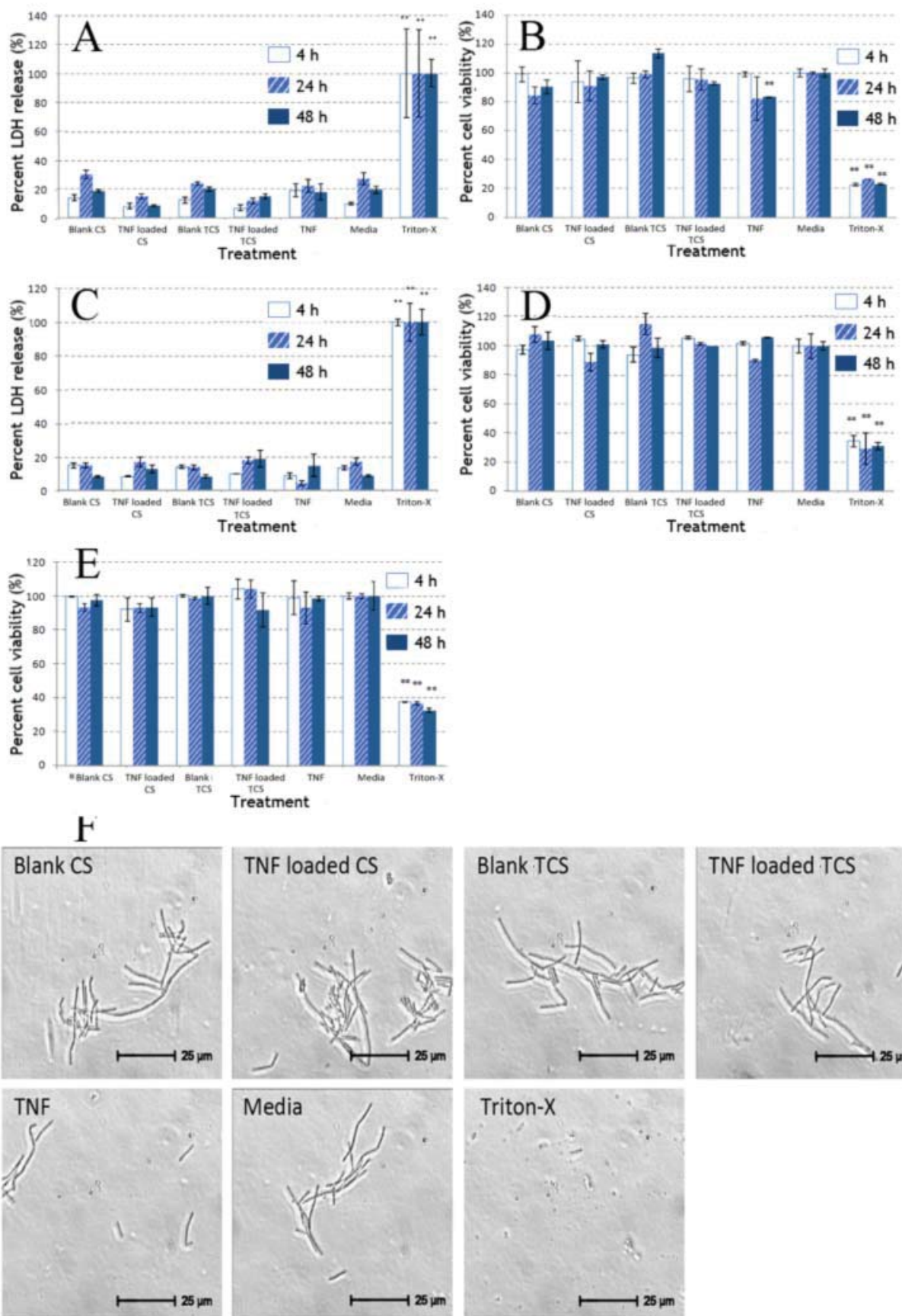


Fig. 4-5 Cytotoxicity study of CS and TCS NPs. Top panel: percent LDH release of VK2/E6E7 cell line (A) and End/E6E7 cell line (B), percent viability of VK2/E6E7 cell line (C) and End/E6E7 cell line (D) and percent viability of *L. crispatus* (E). Bottom panel: *L. crispatus* under microscopy after incubation with blank CS NPs, TFV loaded CS NPs, Blank TCS NPs, TFV loaded TCS NPs, free TFV, Media and Triton-X (from left to right) (F). NPs are prepared with $X_1 = 1$, $X_2 = 0.96$ and $X_3 = -1$, data are shown as mean \pm SEM (n = 3). *: $p < 0.05$ vs media, **: $p < 0.01$ vs media.

In both assays, no statistical difference is observed by t-test between the media control and NPs, which indicates a likely non-cytotoxic nature of the CS and TCS NPs. Therefore, both the CS and TCS NPs can be regarded as non cytotoxic for vaginal cell lines after 48 h. However, these assays are short term studies. The long term effect of the NPs to the vaginal cell lines and vaginal tissue remains to be seen in the future work.

The vagina has natural flora, the natural flora protects other microorganisms from growing in the vagina and cause infections. When the natural flora is disturbed, infection can set it and cause an unpleasant odor. The microbicide formulations should not disturb the normal vagina flora. *L. crispatus*, a predominant normal vaginal floral species¹⁰. It is used here as model bacteria since it can produce hydrogen peroxide (H_2O_2) and lactic acid, which could maintain the low pH environment and provide a natural barrier for HIV transmission^{48a}. No statistical difference is observed between either the media control and the NPs after incubation for 4, 24, and 48 h (Fig. 4-5). These results suggest that neither the CS NPs, nor the TCS NPs are harmful to the *L. crispatus* within 48 h.

Triton X-100 could dissolve the lipid on the cell membrane and increase the membrane permeability leading to cell death. After the treatment for 48 h, the bacteria

incubated with the NPs, free TFV and media appeared to be intact and rod-like structures as previously reported morphology of *L. crispatus*¹⁰⁰. While the integrity of bacteria incubated with Triton X-100 is destroyed, this result indicates that both the CS and the TCS NPs are harmless to the *L. crispatus* within 48 h.

4.3.5.2 Cellular uptake study

Particles labeled with fluorescent dyes are frequently used to study cellular uptake quantitatively by a microplate reader and flow cytometry. Based on an earlier study, the reaction between the isothiocyanate groups of FITC and the amino groups of CS is a stable covalent bond⁴⁹. Little FITC could leach out from the NPs over 48 h under *in vitro* conditions. Thus, the intracellular fluorescence cannot be due to the uptake of dye released or dissociated from the NPs. Fig. 4-6 shows the percentage of the CS and TCS NPs taken by VK2/E6E7 (A) and End/E6E7 (B) cell lines. It is evident that more particles are engulfed by cells with longer incubation period, due to extended exposure. The CS NPs show similar properties and behavior as the TCS NPs in both cell lines.

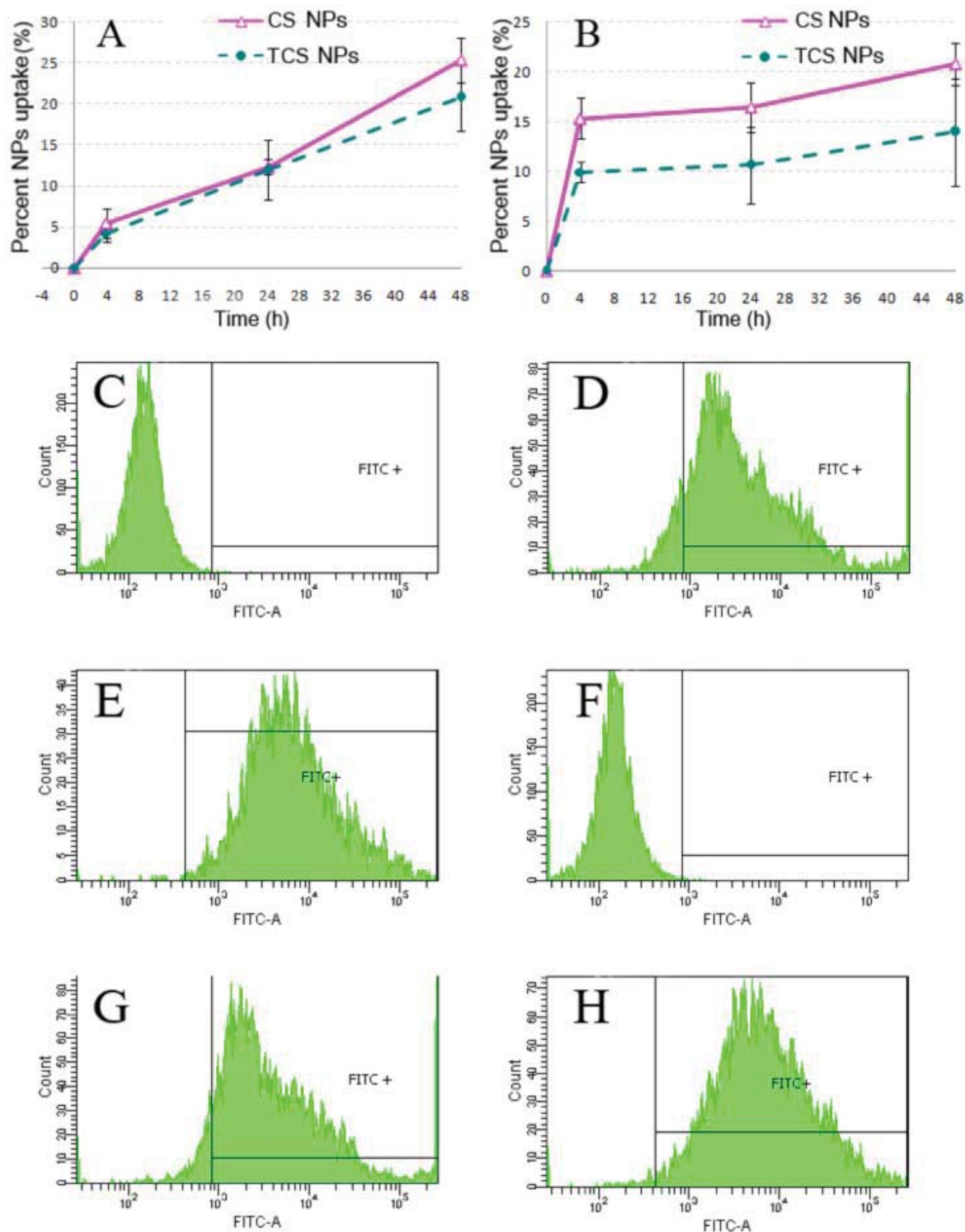


Fig. 4-6 Top panel: the particle uptake efficiency of FITC labeled CS and TCS NPs on VK2/E6E7 cell line (A) and End/E6E7 cell line (B). Cells are incubated with NPs for 4, 24

and 48 h, data are shown as mean \pm SEM ($n = 3$). Bottom panel: NPs cellular uptake assessed by flow cytometry (Count. vs FITC fluorescence intensity); VK/E6E7 cell line treated with media (C), FITC labeled CS NPs (D), FITC labeled TCS NPs (E); End/E6E7 cell line treated with media (F), FITC labeled CS NPs (G), FITC labeled TCS NPs (H) for 48 h. NPs are prepared with $X_1 = 1$, $X_2 = 0.96$ and $X_3 = -1$.

The quantification of the percent of cell uptaking FITC-loaded NPs is investigated by using flow cytometry. The fluorescence intensity curves of the cells treated by FITC-loaded NPs are shown in Fig. 4-6 (Bottom panel). The cell number is on the Y-axis, while the X-axis is fluorescence intensity which indicates the number of particles internalized by the cells. The shifting of the peak to the right along the X-axis means an intensity increase with increasing concentration of FITC labeled NPs. In VK/E6E7 cell line, the percentage FITC-positive cells are 90.1% for the CS NPs and 99.3% for the TCS NPs. In End/E6E7 the values are 92.6% and 98.6% for the CS and TCS NPs, respectively. A significant uptake of NPs is observed in both cell line treated with different NPs compared to the control. The results confirmed that these NPs are successfully internalized into the vaginal cells.

The uptake is confirmed by fluorescence microscopy. Fig. 4-7 shows the localization of NPs in cells. Cell membrane is observed by phase contrast microscopy. A blue fluorescence dye, Hoechst 33342, is used to stain the nucleus. It can bind to the minor groove of DNA and impart a blue color to identify the nucleus. The fluorescence signal of FITC labeled NPs in the cells is detected by the FITC filter. At 48 h after incubation a high level of uptake of FITC-labeled NPs by both VK2/E6E7 and End/E6E7 cells is observed by fluorescence microscopy.

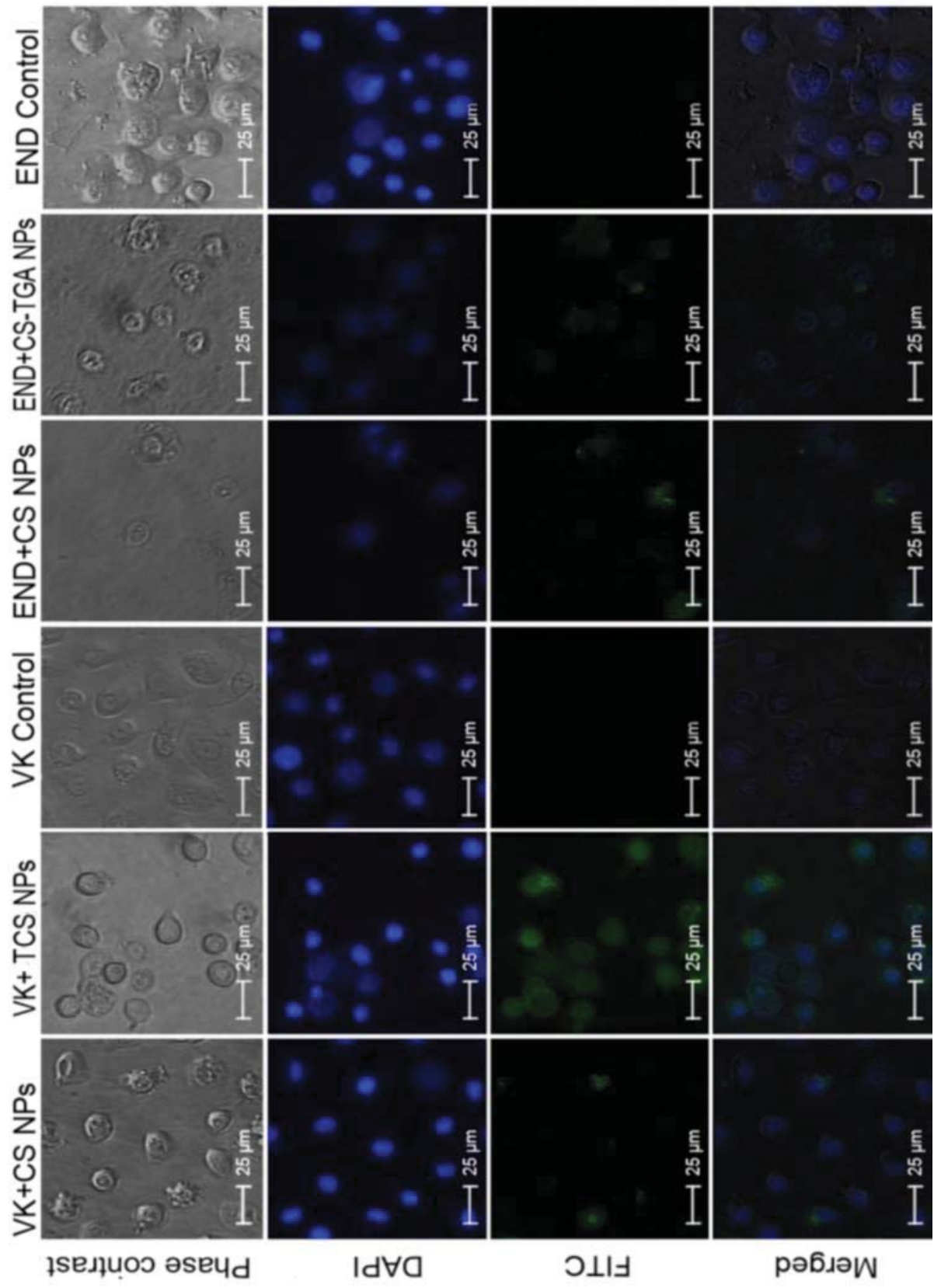


Fig. 4-7 *In vitro* localization of FITC-labeled CS and TCS NPs in VK2/E6E7 and End/E6E7 cell lines by fluorescence microscopy. Cells are observed under phase contrast microscopy, DAPI and FITC filters are used to observe the nucleus (blue) and the NPs (green), respectively. Then the three images are merged.

Inhibition of cellular uptake study

The result of uptake inhibition is shown in Fig. 4-8.

Fig. 4-8 Effects of inhibitors on uptake of FITC-labeled NPs on VK2/E6E7 cell line (A) and End/E6E7 cell line (B). ■: CS NPs; ■: TCS NPs. Cells are incubated with NPs for 24h and lysed by 1% Triton X. NPs are prepared with $X_1 = 1$, $X_2 = 0.96$ and $X_3 = -1$, data are shown as mean \pm SEM (n=3).

The cell viability after treated with the inhibitors is shown in Fig. 4-9.

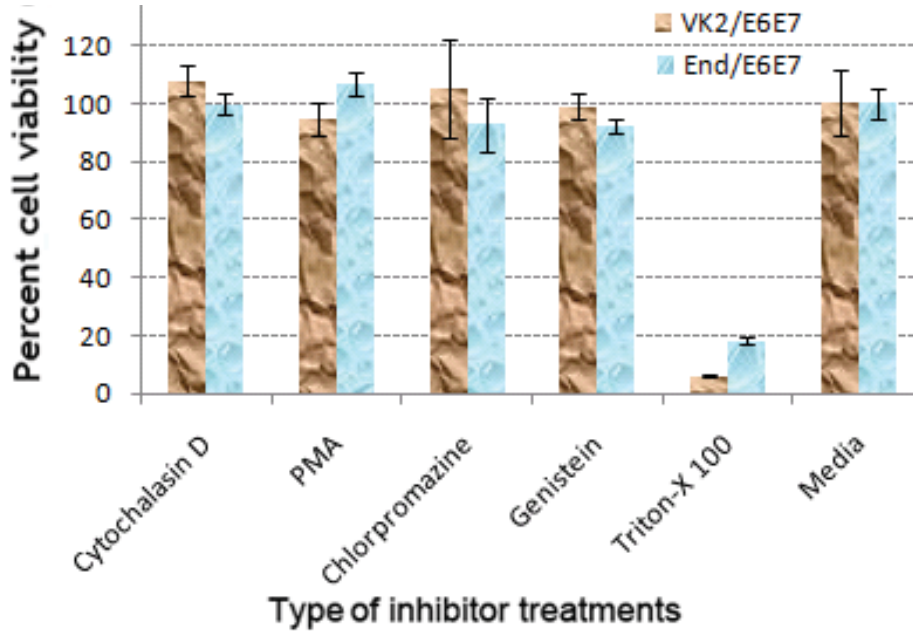


Fig. 4-9 Percent viability of VK2/E6E7 and End/E6E7 cell lines after treated with inhibitors.

The inhibitors did not reduce the cell viability. Cytochalasin D is an actin filament modifier that can inhibit actin polymerization¹⁰¹. Cytochalasin D led to 15% reduced internalization of TCS NPs in End/E6E7 cell line, indicating that cytoskeleton reorganization might be a route of the TCS NPs uptake by the End/E6E7 cell line, and actin microfilaments contributed significantly in End/E6E7 cell line. Indeed, actin microfilaments are identified in epithelial cells of rat uterine¹⁰². Actin is the driving force for uptake, which decreased in the absence of the actin filaments. Macropinocytosis is dependent on the actin assembly at the cell membrane¹⁰³. During macropinocytosis, the rims of the membrane fold extending from

the surface and fuse back with the plasma membrane, which is called membrane ruffling¹⁰⁴. Cytochalasin D induces depolymerization of actin filaments formed and as a result inhibits the membrane ruffling. However, this entrance mechanism is excluded in this study since phorbolmyristate acetate (PMA), a macropinocytosis stimulator, did not increase particle internalization in any cell line, indicating that the macropinocytosis is not involved in NP uptake. An actin assembly dependent entrance mechanism excluding macropinocytosis is involved in the uptake of the TCS NPs in the End/E6E7 cell line. Chlorpromazine inhibited clathrin-mediated permeation by disrupting the assembly-disassembly of clathrin¹⁰⁵. The clathrin pathway is also known as receptor-mediated endocytosis. Particles entering the cell via the clathrin pathway are believed to attach to the plasma membrane by specific binding to the receptor, then a coated pit which is a specialized region of the membrane that is coated with clathrin is formed¹⁰⁶. Treatment with chlorpromazine did not reduce the uptake of NPs significantly because there is no specific ligand present on the surface of these NPs that can interact with the receptors. Under genistein treatment, respectively, 51% and 35% reduction of the CS and TCS NPs in the VK2/E6E7 cell line, and 31% and 30% reduction of the CS and TCS NPs in the End/E6E7 cell line are observed. These reductions are statistically significant compared to the control. Genistein results in the greatest reductions in both cell lines. Caveolae is a specialized type of lipid rafts that is a flask-shaped invagination in the plasma membrane¹⁰⁷. The caveolae associated protein, such as caveolin-1 and caveolin-2, are expressed in a wide type of human cells, including epithelial cells¹⁰⁸. Genistein is an inhibitor of caveolin-dependent endocytosis that is used to block lipid raft-mediated endocytosis. In caveolae-mediated internalization, NPs interact through non-specific charge interactions with the cell. Since both the CS and TCS NPs are positively charged, the cationic charge on the

particle surface promotes their electrostatic interaction with the negatively charged cell surface, leading to an enhanced cellular uptake via caveolin pathway that is receptor-independent¹⁰⁹. It has been previously reported that the particle size also contributes to the internalization pathways. Particles with a diameter under 200 nm enter cells preferentially via clathrin-mediated endocytosis; particles over 200 nm are more likely to go through the caveolin-mediated endocytosis¹¹⁰. The mean diameters of both the CS and TCS NPs are above 200 nm. This could be another reason why the caveolae-mediated pathway favored these NPs. It is also consistent with a previous report that PLGA NPs with a mean diameter over 200 nm are primarily internalized via the same pathway[9]. Indeed, the internalized caveolae fuse with caveosomes, which could deliver their contents into other subcellular compartments. In comparison with the clathrin-dependent endocytosis, the caveolae internalization pathway could avoid the acidic and harmful milieu¹¹¹. In summary, caveolin-dependent endocytosis is the most productive route for uptake of these NPs on both cell lines, while cytoskeleton reorganization also contributes as a minor fraction, though the mechanism to which it occurs only on the End/E6E7 cell line is still not clear. A similar result has been reported using the CS-DNA complex on the HT1080 cells¹¹². However, since none of these inhibitors completely eliminate the particle uptake, it is evident that other internalization pathways are involved. The same NPs could be internalized via different pathways. For example, it remains to be known if megalin (an endocytic receptor in reproductive tissue for sex hormone binding globulin) also act as a pathway for these NPs' uptake¹¹³.

4.3.6 Bioadhesive studies

The mucus layer covering the epithelia could protect the epithelia against

mechanical and chemical damage. It consists mainly of glycoprotein chains with cysteine-rich subdomains¹¹⁴. The enhanced mucoadhesive properties of thiomers, such as TCS, are believed to be based on an interaction of thiolated groups of polymers with the cysteine-rich subdomains of mucus glycoprotein. The evidence of these disulphide bridges formations has been provided in previous literatures^{30, 115}.

Porcine vaginal tissue shows a high level of similarity to human vaginal tissue in not only ultrastructural organization and lipid composition, but also the secretions, in terms of pH and inflammatory responses⁷³. These similarities in structure and function have led to the use of porcine tissue as a promising experimental tissue model in studies of the vaginal drug delivery system. Preliminary study shows that the mucosal tissue remains vital after 3 h of death¹¹⁶; no significant difference has been shown in the histological structure or water permeability of the mucosal tissue snap frozen in liquid nitrogen as comparison with fresh tissue¹¹⁷.

Fig. 4-10 shows the mucoadhesion of the CS and TCS NPs.

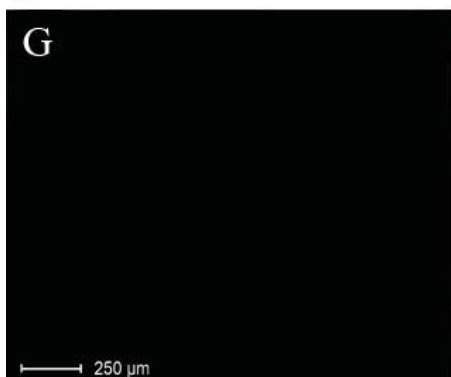
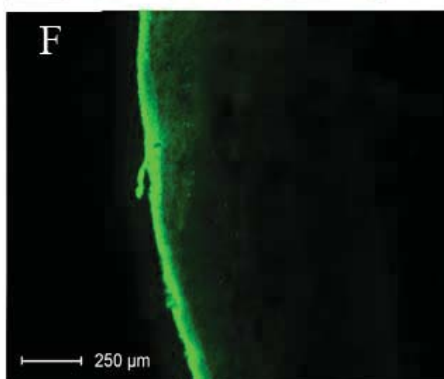
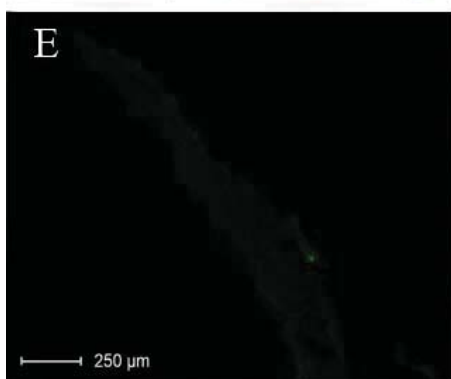
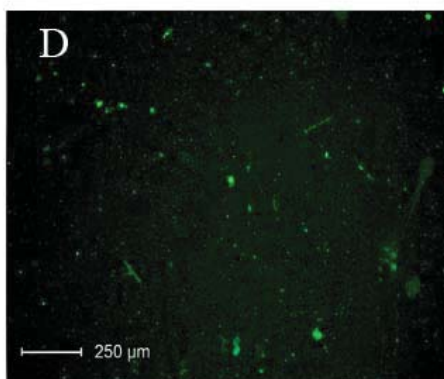
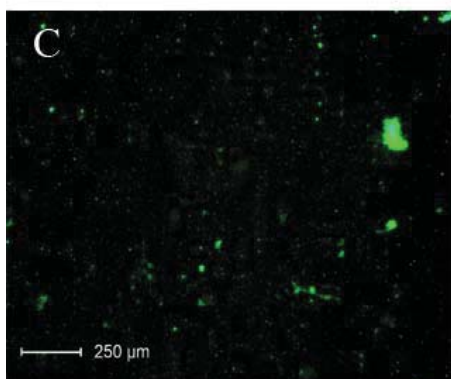
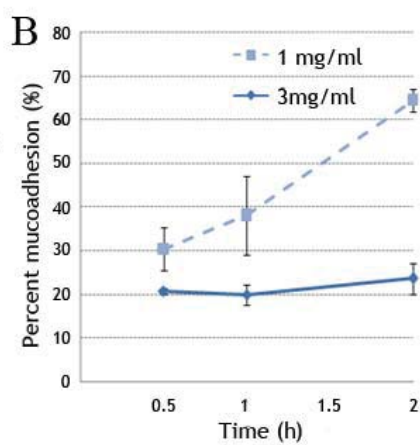
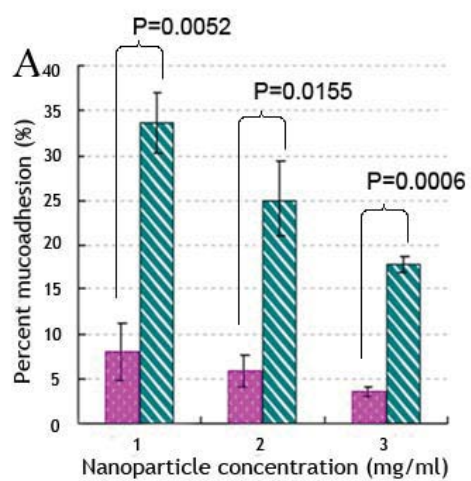




Fig. 4-10 Top panel: concentration dependent percent mucoadhesion by infusion method (A); and time dependent percent mucoadhesion by immersion method (B). : CS NPs; : CS-THA NPs. Bottom panel: fluorescence microcopy of FITC-CS NPs suspension (3 mg/ml) (C), FITC-TCS NPs suspension (3 mg/ml) (D), thin sections of porcine vaginal tissue treated with suspension A (E), suspension B (F) and media (G). H: H&E staining of porcine vaginal tissue. NPs are prepared with $X_1 = 1$, $X_2 = 0.96$ and $X_3 = -1$, respectively. Data are shown as mean \pm SEM (n=3).

According to Fig. 4-10 A, the mucoadhesive property of the TCS NPs is 4-5 fold higher in comparison with that of the unmodified CS NPs, which is consistent with the previous report¹¹⁸. The percent mucoadhesion of lower concentration TCS NPs increased considerably when the incubation time is prolonged as shown in Fig. 4-10 B. The formation of disulfide bonds between the TCS NPs and the mucus gel layer is based on a cross-linking process via the thiol/disulfide exchange reactions or a simple oxidation process of free thiol groups²⁹. By delaying the reaction time, more disulfide bonds can be formed from oxidation of the thiol groups. Hence, the mucoadhesion adhered covalently on the surface of the mucus layer. However, the increase of the percent mucoadhesion of higher concentration NPs (3 mg/ml) is not statistically significant compared to that of the lower concentration NPs (1 mg/ml); perhaps because of the limited number of reactive groups on the tissue surface. The maximum percent of bioadhesion is 65% (\pm 3%) with the 200 nm sized NP for a 2 h duration. The data indicates that mucoadhesion is a time and size dependent process.

The bottom panel of Fig. 4-10 shows the tissue sections visualized using a fluorescence microscopy. The tissue treated with the CS NPs shows a very weak fluorescence, while a strong intensity is observed from the tissue treated with fluorescently labeled TCS

NPs. The FITC label efficiency of the TCS is 1.5 times that of CS (data not shown). However, it is obvious that the amount of the TCS NPs adhered on the surface of the vaginal tissue is much larger than that of the CS NPs on the tissue.

4.4 Conclusion

In this work, it is reported for the first time that an anti-HIV microbicide (TFV) loaded thiolated CS can be a highly mucoadhesive (65%) and non-cytotoxic vaginal drug delivery system. The *in vitro* drug release, cytotoxicity assays, and mucoadhesion studies suggest that TCS NPs have the potential to be a controlled release, safe, and bioadhesive microbicide delivery system. These properties make thiolated CS NPs a good candidate for a topical vaginal microbicide delivery system for further study related to the quest of the prevention of HIV transmission.

CHAPTER 5

THIOLATED CHITOSAN COATED SODIUM ALGINATE MULTILAYER MICROPARTICLES FOR ENHANCED DRUG LOADING AND MUCOADHESION

5.1 Rationale

An ideal vaginal drug delivery system should be easy to administer, not cause discomfort to improve patient compliance and have a reduced number of doses required to the treatment¹¹⁹. To meet these requirements, various vaginal drug carriers have been developed^{79, 120}. However, in most of these formulations, the encapsulation of a water soluble small molecular drug is a serious problem associated with low drug %EE payload. Recently, a special attention has been focused on the development of spray dried microparticles (MPs)^{18a}.

Spray drying is a rapid and simple process based on the evaporation of the solvent. The atomized polymeric droplets containing the drug are transformed into solid particles by a stream of heated air¹²¹. The spray drying method not only typically produces spherical MPs with a narrow size distribution, but also enables the encapsulation of both hydrophilic and hydrophobic drugs with relatively high efficiency and yield¹²².

The main advantages of MPs over traditional vaginal dosage forms such as gels, creams, rings, and films are: the generation of a sustained long term drug release following the application of a single dose, a proper spreading over the vaginal epithelium, the protection of the drugs and capacity to reduce drug toxicity. To further prolong the residence time onsite of the treatment, a thiolated chitosan (TCS) is used to coat the MPs. TCS is chitosan (CS) with thiol groups immobilized on the polymer backbone. They have been shown to possess high mucoadhesive properties due to the thiol groups present on the CS

backbone can form disulfide bonds with the thiol groups present on the mucus substructures³⁰.

In this study, a hydrophilic anti-HIV microbicide, TFV (water solubility 1.87 mg.ml, logP -1.5), is encapsulated within the spray dried alginate MPs. The MPs are coated with TCS base on the charge-charge interaction between alginate and TCS. It is postulated that these MPs may provide prolonged retention time as well as controlled release, and could be a potential vaginal drug delivery system with increased encapsulation of water soluble small molecule drugs.

5.2 Materials and methods

5.2.1 Materials

Sodium alginate, CS with the weight molecular weight of 50-190 KDa, mucin, periodic acid, Schiff reagent kit and benzalkonium chloride (BZK, 2 %w/v) are purchased from Sigma Aldrich (St. Louis, MO, USA). TFV is purchased from Zhongshuo Pharmaceutical Co. Ltd. (Beijing, China). Sodium triphosphate pentabasic (TPP) is supplied by Fisher Scientific (Pittsburgh, PA, USA). The CytoTox-ONE™ and CellTiter 96™ Aqueous kits are purchased from Promega (Madison, WI, USA).

5.2.2 Methods

5.2.2.1 Formulation of spray dried MPs

To prepare TFV loaded alginate MPs, different amount of sodium alginate and TFV (Tab.1) is dissolved in 40 ml of deionized water, the ratio of sodium alginate to TFV is 5:1 (w/w). The solution is then spray dried using a Buchi Mini Spray Dryer, Model 290 (Buchi Laboratories - Technik AG, Flawil, Switzerland). Then, the formulated MPs are stored at 4 °C for further analysis.

In order to optimize the preparation conditions, a custom design with 3 factors and 16 run is used to study the effect of the formulation parameters on the yield. The independent variables, namely, molecular weight of sodium alginate, concentration of the sodium alginate solution, and inlet temperature, are represented by X_1 , X_2 and X_3 , respectively. The percent (%) yield, which is the dependent variable is represented by Y . These variables and their coded factors are listed in Tab. 5-1. All independent variables in this work are selected based on preliminary experiments performed (data not shown).

Tab. 5-1: Independent and dependent variables and their levels in custom design

Variables			Value
Independent	Molecular weight of sodium alginate (X_1)	Low	High
	Concentration of sodium alginate (X_2)	5 mg/ml	15 mg/ml
	Inlet temperature (X_3)	100 °C	150 °C
Dependent	Yield (Y)		

5.2.2.2 Percent yield

The yield is calculated by the ratio of total amount of the resulting sodium alginate MP powder to the total mass of amount of sodium alginate originally contained in the atomized liquid feed volume (Equ. 5-1).

$$\text{Yield(\%)} = \frac{\text{Total mass of MP powder collected}}{\text{Total mass of initial components in the formulation}} \times 100\% \quad (5-1)$$

5.2.2.3 Preparation of the multilayered MPs

For the preparation of MPs, a layer-by-layer method described by Li, et al. is employed¹²³. Briefly, 40 mg of CaCl_2 and 2 mg of TCS are dissolved in 1 ml of acidic acid

solution (pH 5). A total of 1 mg of spray dried alginate MPs are subsequently suspended into the above solution. After the resulting suspension is stirred for 2 h. The product is collected by centrifugation (Beckman Coulter Inc., Pasadena, CA, USA) at 10,000 rpm for 15 min and washed thoroughly with water once. This product is TCS coated single layer MP (SLMP). The multilayer MPs are obtained by alternately coating alginate and TCS on the surface of the particles. Firstly, alginate and TCS is dissolved in acetic acid solution (pH 5) at a concentration of 2 mg/ml, respectively. At this pH, both TCS (pKa 6.5) and alginate (pKa 4.2) mainly exist in ionized form¹²⁴. The SLMPs are suspended in 1 ml of alginate solution and stirred at room temperature for 10 min. The particles are centrifuged at 10,000 rpm for 10 min, washed, and suspended in 1 ml of TCS solution for 10 min. The resulting MPs are collected by centrifugation at 10,000 rpm for 10 min and washed with water once. These MPs are double layer MPs (DLMPs). The triple layer MPs (TLMPs) could thus be obtained by repeating the above operations and so on (Fig. 5-1).



Fig. 5-1 Schematic preparation scheme of the TCS coated multilayer MPs.

5.2.2.4 Percent drug loading determination using ³¹P SS NMR

³¹P-P90 MAS SS NMR spectra are acquired on a Tecmag Apollo console (Houston, TX) with 8.45 T magnet and homebuilt, 2-channel, wide-bore NMR probes. The

^1H and ^{31}P Larmor frequencies are 357.2 MHz and 144.596 MHz respectively. ^{31}P spectra are acquired on 3 mm probe with MAS spinning frequency and 45° pulse length is 8 KHz and 2 μs , respectively and signals are represented as chemical shift value; δ : ppm. About 40 mg of the MPs sample is taken for each analysis. All experiments are performed at ambient temperature without any corrections for sample heating.

5.2.2.5 Zeta sizer, FT-IR, and SEM is used to proof the formation of multilayers.

The zeta potential of the MPs is determined using Zeta sizer (Zetasizer Nano ZS, Malvern Instruments Ltd, Worcestershire, UK). Measurements are made in triplicate ($n = 3$) at 25 $^\circ\text{C}$.

The surface chemistry is determined by FT-IR. Before analyzing each sample, the background is collected at ambient conditions, then the MPs are scanned over the range of 650 and 4000 cm^{-1} . The FT-IR spectra are recorded by OMNIC V 7.0 spectra software.

The morphology of the MPs is analyzed by scanning electron microscopy (SEM). A small amount of the MP powder is mounted on a 1/2" aluminum stubs with double-sticky carbon tape, and sputter coated (Emitech EMS575SX) with approximately 20 nm thickness of gold–palladium alloy. The sample is then visualized under a FEI/Philips XL30 Field-Emission Environmental SEM (Philips/FEI, Eindhoven, Netherlands) at 5 kV. Digital images are acquired with ORIUSTM SC 1000 11 Megapixel CCD camera (Gatan, Pleasanton, CA, USA). The diameter of the MPs in the SEM images are estimated using Image Pro Plus software (Image Pro Plus 6.0, Media Cybernetics, Silver Spring, MD, USA). At least 100 particles counted to generate graph.

5.2.2.6 *In vitro* TFV release profile

The *in vitro* release of TFV from different MPs is evaluated using dialysis method¹²⁵.

One milligram/ml of MPs suspension is prepared in VFS or SFS media, prepared according to previous reports⁴⁵⁻⁴⁶. This suspension is then placed in Spectra/Por cellulose ester membrane dialysis bag (Spectrum Laboratories Inc. Rancho Dominguez, CA, USA) with 10-12 kDa molecular weight cutoff and is immersed into 20 mL of the same media at 37 °C in a thermostatically controlled shaking water bath (BS-06, Lab Companion, Seoul, Korea). At predetermined time intervals, the whole media is removed and replaced by fresh media. The concentration of the drug in the media is determined by a GENESYS 10 Bio UV-Visible Spectrophotometer (Thermo Scientific, Waltham, MA, USA) at 259 nm. Each experiment is run in triplicate together with a blank. In order to find out the mechanism of drug release from the formulations, the data distributions are fitted to various kinetics models (Tab. 5-2), using Microsoft Excel add-in DDSolver software¹²⁶.

Tab. 5-2 Different release models for model fit analysis of the *in vitro* data

Model	Equation	Parameter(s)
First-order	$F=100 \cdot (1-e^{-k_1 \cdot t})$	k_1
Higuchi	$F=k_H \cdot t^{0.5}$	k_H
Baker-Lonsdale	$\frac{3}{2} \left[1 - \left(1 - \frac{F}{100} \right)^{\frac{2}{3}} \right] - \frac{F}{100} = k_{BL} \cdot t$	k_{BL}
Korsmeyer–Peppas	$F=k_{KP} \cdot t^n$	k_{KP}, n

F represents the fraction of the drug released in time t, k_1 , k_H , k_{BL} , k_{KP} represent the release rate constant of different model, n is the release exponent.

5.2.2.7 Cytotoxicity studies

To perform the cytotoxicity studies, VK2/E6E7 (human vaginal keratinocyte) and End1/E6E7 (human endocervical epithelial) cell lines are grown in Keratinocytes-SFM medium Suped with 1% penicillin/streptomycin and 10% (v/v) fetal bovine serum (FBS).

Cells are seeded in 96 well plates at 37°C and humidified 5% CO₂ atmosphere till 80% confluence is achieved. Then the original cell culture media is removed and substituted with media containing alginate MPs, SLMPs, DLMPs and TLMPs with different concentration. Media with no MPs and 1% Triton-X 100 is used as negative and positive control samples, respectively. The well plates are then incubated at 37°C for 24 h and 48 h.

In order to determine the lactate dehydrogenase (LDH) assay, the plates are equilibrated at room temperature for 10 min. One hundred microliter of CytoTox-ONE™ Reagent is added in each well, followed by 30 s shaking and 10 min incubation at 37°C. Finally, 50 µl of stop solution is added. The fluorescence intensity is determined by a microplate reader at λ_{ex} 560 nm and λ_{em} 590.

For cell viability determination, after the incubation time, the media in the wells is removed and substituted with fresh media. Twenty microliters of CellTiter 96® Aqueous One Solution Reagent (Promega, Madison, WI, USA) is added to each well and incubated at 37°C for 4h. The absorbance is recorded at a wavelength of 490 nm.

5.2.2.8 Mucoadhesion study

To assess the amount of mucin adsorbed by the MPs, a periodic acid/Schiff (PAS) colorimetric method is used¹²⁷. Briefly, mucin is dissolved in VFS and SFS and the MP powder is suspended in the same solution at the ratio of 0.1, 1, and 2 of mucin:MPs. The suspension is maintained in the above shaking water bath at 37 °C for 30 min with an agitation speed of 100 rpm and then centrifuged at 4000 rpm for 2 min. The supernatant is removed, 0.2 ml of periodic acid reagent is added and incubated at 37°C for 2 h, followed by addition of 0.2 ml Schiff reagent and incubation at room temperature for 30 min. The absorbance of the solution is recorded at 555 nm by UV spectrophotometer. The mucin

content is calculated from the standard calibration curve. The sprayed alginate MPs and mucin solution without MPs is used as controls. Each experiment is performed in triplicate.

The mucin adsorption is estimated using the Equ. 5-2:

$$\text{Mucin adsorption(\%)} = \frac{\text{Total mass of mucin} - \text{free mucin}}{\text{Total mass of mucin}} \times 100\% \quad (5-2)$$

5.2.2.9 *In vivo* safety studies

Female C57/BL6 mice (8-12 weeks old) with an average body weight of 20 g are ordered from Jackson Laboratories (Harbor, ME). All mice are housed (maximum 5 per cage) under a 12 h light: dark regime in the University of Missouri-Kansas city (UMKC) Laboratory Animal Resource Center (LARC) facility with temperature, humidity, and lighting controlled systems and allowed to acclimate for 7 days. Mice are treated with 2 mg of subcutaneous medroxyprogesterone acetate (Greenstone, Peapack, NJ, USA) diluted in Lactated Ringer's saline solution 4-5 days before the treatment to induces and maintain a diestrus-like state.

The DLMP is suspended in PBS at a concentration of 475 mg/kg. Benzalkonium chloride (BZK, 2 %w/v) is used as positive control due to its well-known toxic effects on genital tracts, PBS is used as negative control. Once-daily administration is carried out using a flexible feeding needle (Cadence, Inc. Staunton, VA, USA). After completion of the 1-day and 7-day intravaginal application, mice are euthanized by carbon dioxide (CO₂) asphyxiation. Their cervico-vaginal tissues are harvested. The collected tissues are formalin fixed and embedded in paraffin, and cut into 5-mm sections.

5.2.2.9.1 H&E staining

Serial sections are used for staining with hemotoxylin and eosin (H&E). Images are captured using a Nikon Labophot-2 microscope (Nikon Instruments, Inc., Melville, NY)

equipped with a PAXCam digital microscope camera and analyzed using PAX-it image management and analysis software (Midwest Information Systems, Inc., Villa Park, Illinois).

5.2.2.9.2 Immunohistochemical (IHC) staining

In order to identify the inflammatory cell (CD45) infiltrate, immunohistochemical staining is performed in genital tissue sections. Briefly, the sections are de-paraffinized and rehydrated using the standard protocol. Antigen retrieval is performed using steam heat method in citrate buffer/0.05%Tween-20 for 20 min. The tissue sections are then rinsed with Tris buffered saline/0.05%Tween-20 three times, followed by treating with 3% v/v hydrogen peroxide in PBS for 10 min and blocked with 10% normal goat serum for 2 h (Vector Laboratories, Burlingame, CA). Anti-CD45 from Santa Cruz Biotechnology, Inc. (Dallas, Texas) are diluted in 1.5% normal goat serum to 5 µg/mL (1:50) and applied to the tissue sections overnight at 4°C in a humidified chamber. Following the incubation with primary antibody, tissue sections are rinsed three times. The appropriate biotinylated secondary antibody (Santa Cruz Biotechnology, Inc., Santa Cruz, CA) is then diluted to 5 µg/mL (1:50) and applied to tissue sections at room temperature for 1 h. After the incubation with the secondary antibody, visualization of the cells is performed using the DAB: Peroxidase Substrate Kit (Sigma, Saint Louis, MO) under a Nikon Labophot-2 microscope. The tissue is then counter-stained using hematoxylin (Sigma, Saint Louis, MO) and processed through an alcohol gradient and xylene before application of a coverslip mounted using cyto seal 60 mounting media (Richard Allan Scientific, Kalamazoo, MI). Images are viewed and captured as described above.

5.2.2.10 Statistical analysis

The result of the custom experimental design is performed and analyzed using JMP software (version 8.0, SAS Institute Inc., Cary, NC, USA). Unless otherwise stated, data are expressed as mean \pm standard deviations ($n = 3$). Compared to controls, the statistical significant difference of a given mean is determined using a student's *t*-test. A *P* value < 0.05 is considered statistically significant.

5.3 Results and discussion

5.3.1 Experimental design and optimization of spray dried MPs

The responses obtained by the custom design are described in Tab. 5-3.

Tab. 5-3 responses obtained by the custom design.

No.	Mw	Concentration (mg/ml)	Inlet T (°C)	Yield (%)
1	Low	15	150	48.3
2	Low	10	100	43.9
3	High	5	150	56.1
4	High	5	100	44.9
5	High	15	150	17.4
6	High	5	150	54.9
7	Low	5	125	52.5
8	High	15	100	5.37
9	Low	5	150	61.2
10	High	5	100	50.5
11	Low	5	100	48.6

12	High	15	150	20.2
13	High	10	125	43.2
14	Low	15	125	40
15	Low	15	100	14.6
16	Low	10	150	49.5

The overall yield varies from 15% to 60%. The R^2 value of the dependent variable is 0.95, greater than 0.9. From the results of the ANOVA study (Tab. 5-4), the P value is 0.0007, less than 0.05. These results indicating a statistically significant model fit at 95% confidence.

Tab. 5-4 ANOVA analysis of the spray dried MPs

Response	Source	DF	Sum of squares	Mean square	F ratio	P value
C1	Model	8	4004.39	500.55	16.57	0.0007*
C2	Error	7	211.52	30.22		
C3	Total error	15	4215.91			

The polynomial Equations for the response value is:

$$Y=46.89-5.31X_1-14.93X_2+7.14X_3-5.04X_1X_2-1.51X_1X_3+2.83X_2X_3-5.14X_2^2-4.70X_3^2 \quad (5-3)$$

In Equ. 5-3, the coefficients of the independent variables show their effects on the yield. The coefficients of interaction terms show how the yield changes when the two independent variables changed simultaneously. The main effect of all independent variables and their interactions on the dependent variable (yield) is shown in Fig. 5-2. The values on the x-axis of the Pareto charts represent the standardized effects. The factors whose length

passed the blue vertical line ($t_{\text{critical}} = 2.36$ at $P < 0.05$) are identified as statistically significant⁴².

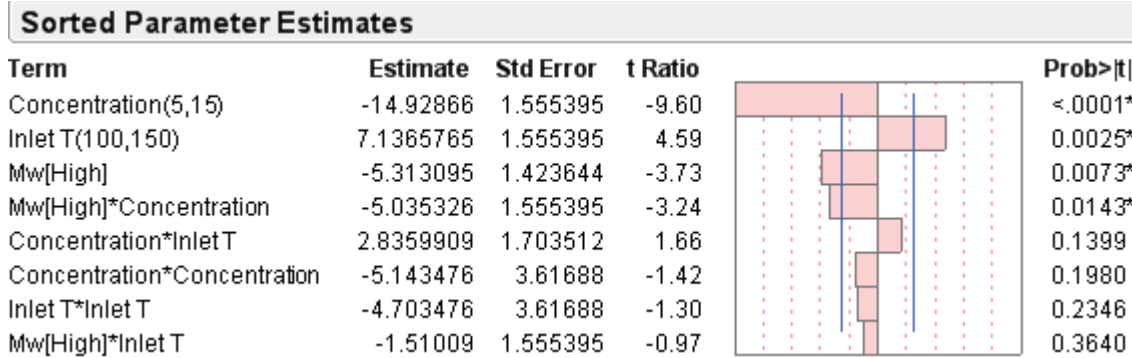


Fig. 5-2 Standardized effect of variables and their interaction on yield. The x-axis shows the t ratio of the variables, bars extending pass the vertical line indicate values reaching statistical significant ($P < 0.05$).

Fig. 5-3 is a desirability and prediction plot showing the effect of the independent variables on the yield. The solid black line and the dashed boundary lines represent the predicted values of the yield with their 95% confidence data distribution limit, respectively. In order to maximize the yield, the optimum condition is selected through the mathematical optimization process: low molecular weight, alginate concentration 6.13 mg/ml, inlet temperature 142 °C.

It is found that decreasing the alginate concentration can significantly improve the yield. High inlet temperature and low molecular weight are also capable of improving the yield.

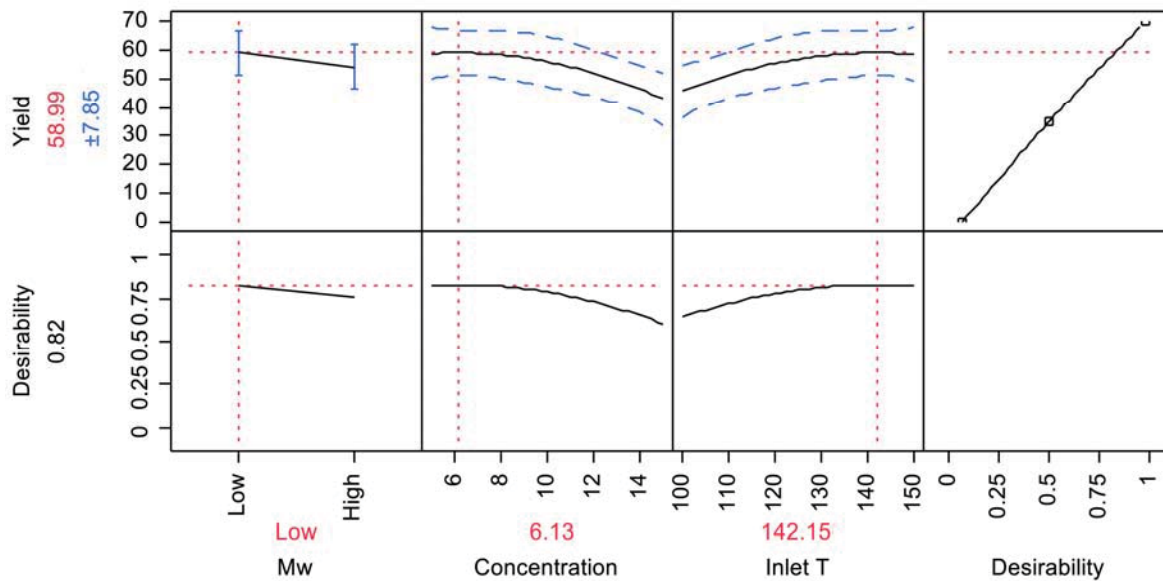


Fig. 5-3 prediction profiler and desirability plot showing the effect of independent variables on yield.

To obtain well-dispersed MPs, the concentration of the initial solution has to respect some conditions: (1) to generate particles with a relatively high density and good mechanical characteristics, the concentration of the polymer should be sufficiently high. (2) to allow its homogenous atomization, the viscosity of the solution should be relatively low¹²¹.

Alginate solution at concentration lower than 5% (w/v) results in the formation of droplets but dried powders based on past experience. With low concentration, low content of solid and high proportion of water, more water need to be removed at constant temperature and flow rate, which leads to incomplete evaporation. To run the spray-drying process efficiently and smoothly, 5% (w/v) is selected as the lowest limit of the polymer concentration. On the other hand, with increasing concentration resulting in increased viscosity. The viscosity is directly proportional to the degree of atomization, which largely determines the efficiency of spray drying.

The mechanism of the atomization in spray drying can be summarized as the immediate disintegration of liquid. At the nozzle orifice, the contact of the liquid with the high velocity gaseous medium creates high frictional force over liquid surface, the liquid is broken up by the kinetic energy, forms into smaller droplets. The entire process is the result of turbulence in the issuing liquid and the action of air force, however, it is opposed by viscosity. As the feed solution's viscosity increases, more kinetic energy is used to overcome larger viscous force. This can be explained using the Reynolds number shown in Equ. 5-4:

$$Re = \frac{\rho w d}{\eta} \quad (5 - 4)$$

Where Re denotes the Reynolds number, ρ is the density of the liquid, w is the fluid velocity of the liquid, d is the inner nozzle diameter, η is the viscosity¹²⁸.

An increase in viscosity lowers the Reynolds number and makes turbulence generation more difficult. Therefore, less energy of atomization is available for breaking up the droplets. The insufficient turbulence and energy transfer causing a wide droplet-size distribution throughout the resulting spray, and even a high percentage of liquid remains in the center of the spray as a solid jet. These large particles or jet cannot be completely dried before they deposit on the drying chamber wall¹²⁹. Therefore, when viscosity is high, these semi-wet particles build up form a wet deposit, or even break off as wet lumps and stream down the wall. This is a well-known phenomenon that results in a reduced powder yield¹³⁰.

The effect of molecular weight to the viscosity is shown in the Mark-Houwink Equation as follow¹³¹:

$$[\eta] = KM^a \quad (5 - 5)$$

Where K and a are constant (MH constant). Lower molecular weight lead to lower viscosity, hence results in higher yield. By increasing inlet temperature, the overall thermal efficiency is increased, leading to better drying and higher yield. With larger molecular weight resulting in higher viscosities and hence lower yields.

Moreover, by increasing inlet temperature, the overall thermal efficiency is increased, leading to better drying and higher yield. The effect of inlet temperature on spray drying is shown as follow¹³²:

$$\eta_{\text{overall}} = \frac{T_1 - T_2}{T_1 - T_0} \times 100 \quad (5 - 6)$$

Where η_{overall} denotes the overall thermal efficiency, T_1 is inlet temperature, T_2 is outlet temperature, and T_0 is the atmospheric temperature.

The relationship between the actual values and the theoretical values of the yield is investigated by a check point analysis. The measured and predicted values of the yield at three selected point (two random points and the optimal point) are shown in Tab. 5-5. The differences of all the points appear to be statistically insignificant, indicating that this model is valid for predicting the yield.

Tab. 5-5 Checkpoint experiments comparing measured and predicted responses ($n = 3$)

Run NO.	X1	X2 (mg/ml)	X3 (°C)	Measured Y (%)	Predicted Y (%)	Error %	t valu e	P value
C1	Low	7.5	113	53.23 ± 4.75	51.26	4.23	0.41	0.72
C2	High	12.5	138	37.67 ± 7.54	32.68	15.41	0.66	0.58
C3	Low	6.13	142	62.62 ± 6.67	58.97	6.19	0.55	0.64

5.3.2 Characterization of the MPs

Tab. 5-6 describes about the amount of TFV encapsulated in MPs with different layers. The amount is presented as a percentage, in comparison with pure TFV (considered as 100 %). Three trials for each type of NPs are carried out in order to be able to calculate the standard deviation by utilizing ^{31}P solid state NMR spectroscopic technique. The drug loading slightly decreases when a new layer, which increases the total mass of polymer, is coated. The MPs are washed after each coating step, this may also lead to the loss of drug dye to the high water solubility of TFV.

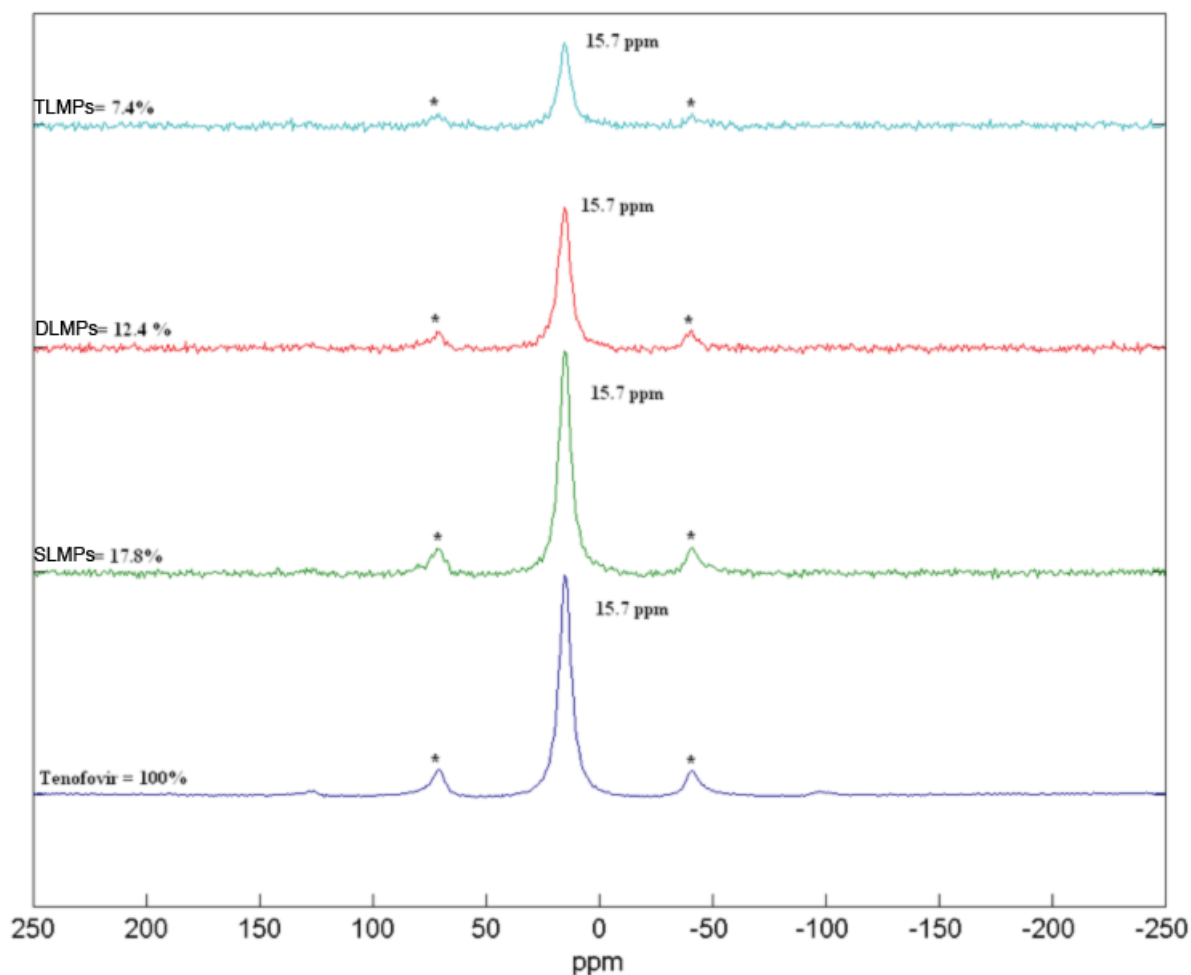


Fig. 5-4 ^{31}P solid state NMR spectroscopy of the MPs

Tab. 5-6 Drug loading in the multilayer MPs, pure TFV is considered as 100 %.

Formulation	Drug loading (%)
SLMP	17.80±0.30
DLMP	12.27±0.23
TLMP	7.17±0.21

The dominated component on the MPs surface during the coating process can be estimated from the zeta potential measurement. A reversal in the surface charge of the MPs is expected as oppositely charged polymers are adsorbed onto the surface of the MPs¹³³. As shown in Fig. 5-5 A, the zeta potential of alginate and TCS are found to be -42 ± 1.5 mV and $+35.5 \pm 1.5$ mV ($n = 3$). The zeta potential of the spray dried alginate MPs is -41.1 mV . After the first coating, the cationic TCS is deposited on the negative charged surface to form TCS coated single layer MPs with zeta potential of $+25$ mV. To generate the double layer MPs, the anionic alginate is assembled on the surface, followed by coating of the second layer of TCS, for which the zeta potential reversed from -40 mV to $+33.0$ mV. Finally, the last layer of alginate and TCS is conjugated respectively to obtain the trip layer MPs. And the final zeta potential changed from -42 mV to $+35$ mV, suggesting TCS is exposed on the surface.

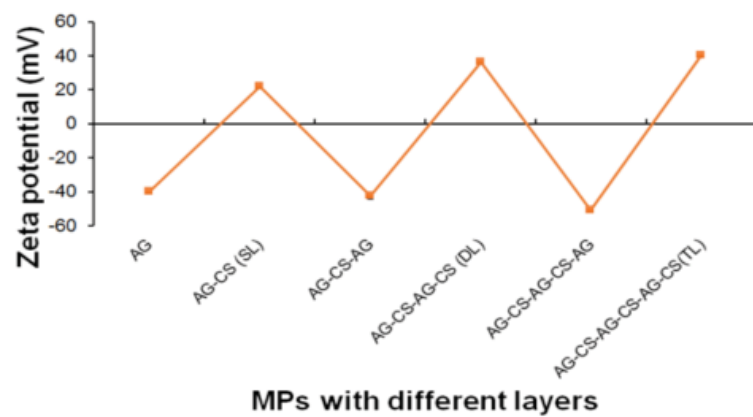
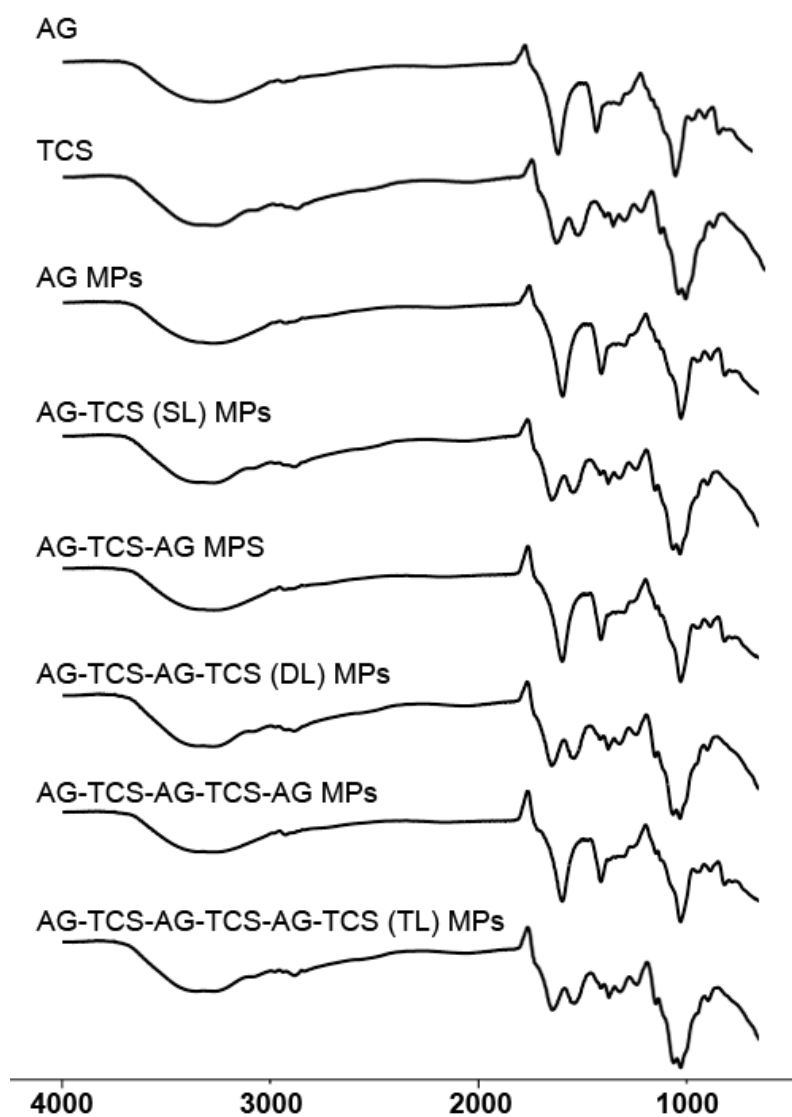
A**B**

Fig. 5-5 Change in zeta potential values (A) and FTIR (B) after coating with oppositely charged TCS and sodium alginate (n=3).

The coating of different layers is further confirmed by FT-IR (Fig. 5-5 B). Both native alginate and native TCS exhibit a broad absorption peak at around 3100 to 3650cm^{-1} and weak absorption peaks at 2890 cm^{-1} , attributed to the hydrogen bond stretching vibration and the CH stretch, respectively. TCS shows two peaks at 1520 and 1650 cm^{-1} are due to the amide (CO-NH-) and the amine (-NH₂) absorption band, respectively. The native alginate reveals two sharp peaks at 1610 and 1415 cm^{-1} assigned to the carboxylic acids (COO⁻). After coating by TCS or alginate, the dominated component on the MPs surface is the same polymer.

Layer by layer deposition results in a slight increase in the particle size. The average diameter of spray dried alginate MPs, SLMPs, DLMPs and TLMPs is found to be $2.01\mu\text{m}$, $2.06\text{ }\mu\text{m}$, $2.66\text{ }\mu\text{m}$ and $2.83\text{ }\mu\text{m}$, respectively, As the SEM images and size distribution shown in Fig. 5-6. A minimum of 100 PMs for each sample are analyzed. The MPs appear to be well dispersed, the increasing in mean diameter with each coating step indicating the layer growth.

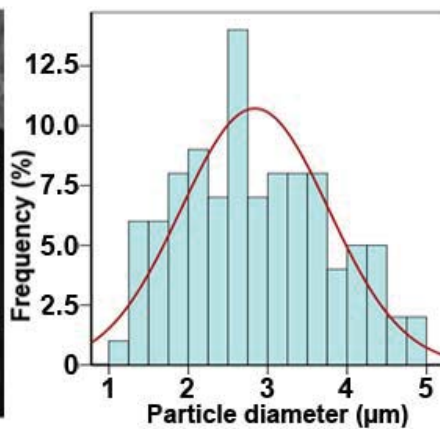
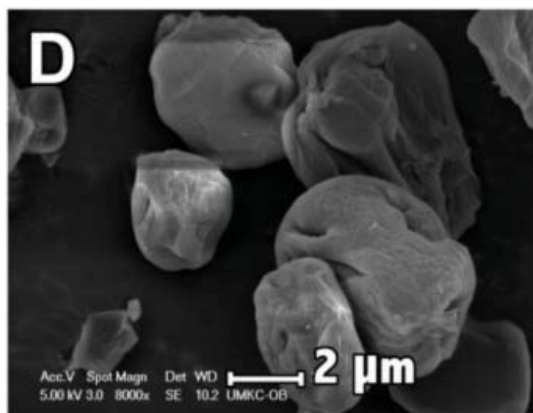
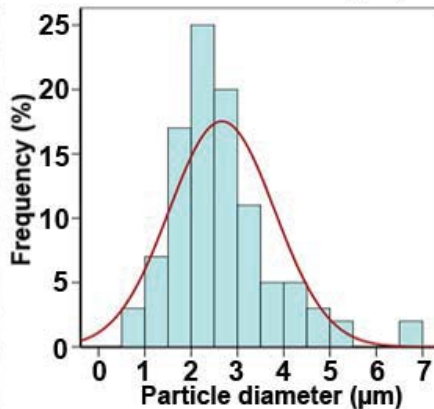
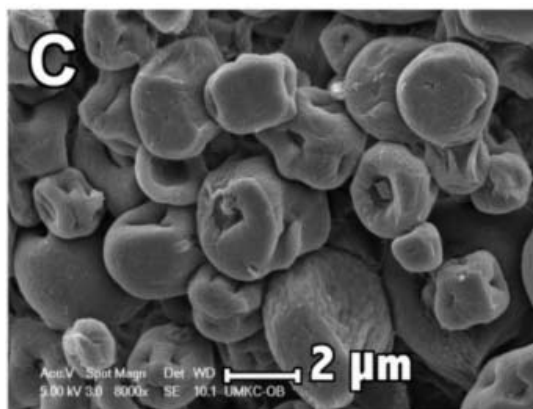
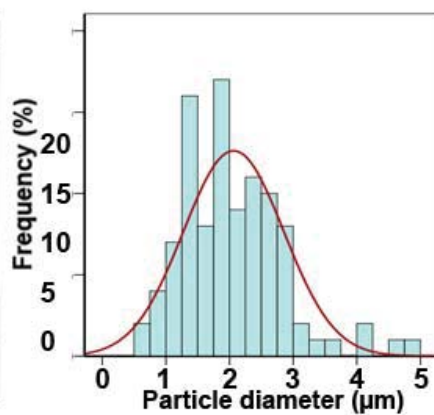
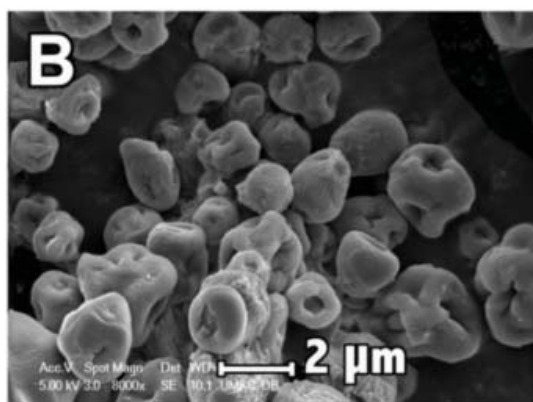
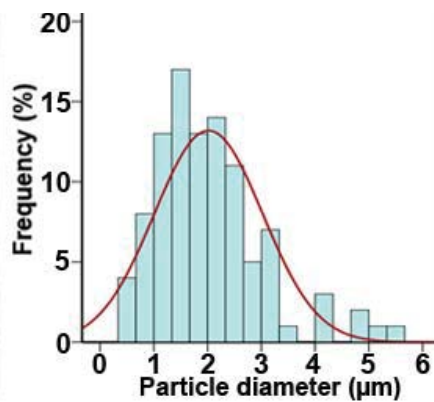
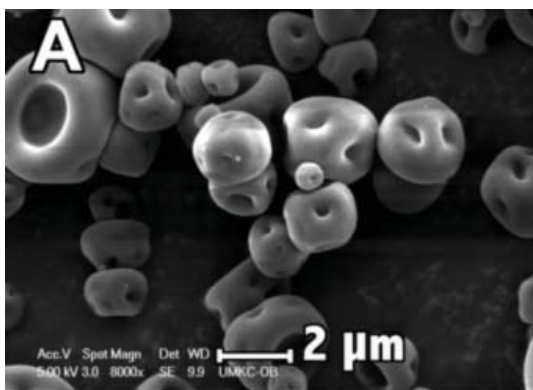


Fig. 5-6 SEM image (left) and size distribution (right) of A: alginate MPs, B: TCS coated single layer MPs, C: TCS coated double layer MPs, D: TCS coated triple layer MPs.

5.3.3 *In vitro* release profile of the MPs

The *in vitro* release of TFV from the MPs is analyzed up to 5 days. From the release profile of the MPs in both VFS and SFS media shown in Fig. 5-7, the release pattern is characterized by a short-lasting burst release followed by a longer-lasting sustained release. The release rate of TFV is decreased as the number of layers is increased. The spray dried alginate MPs are used as control, in which, a burst release is observed. Almost 100% of its pay load is released within the first 24 h, as alginate is entirely solubilized without calcium chloride and TCS. Calcium chloride is added as a cross-linking reagent. The calcium ions and the glucuronic sequences of alginate can interact via charge-charge interaction, each calcium ion can attach to two of the alginate strands to form a matrix texture (Fig. 5-1)¹³⁴. Then TCS is deposited on to the surface of the MPs to generate a core-shell structure. After TCS coating, the cumulative drug release reduces to 65% and 78% in VFS and SFS, respectively. However, TFV can easily diffuse out of the MPs across the single layer of TCS shell. In order to further reduce the release rate, the second and third layer of TCS is coated as previously described. As a result, the percentage release rate of drug from DLMPs and TLMPs decreased to 49% and 41% in VFS, 58% and 43% in SFS media, respectively, as analyzed after 24 h.

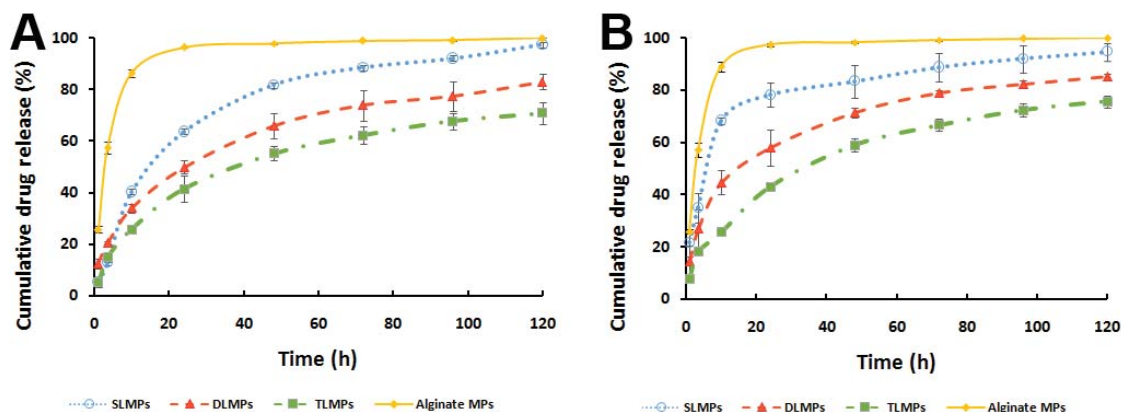


Fig. 5-7 *In vitro* release profile of drug from alginate MPs, SLMPs, DLMPs and TLMPs in VFS (A) and SFS (B) (n=3).

To elucidate the release mechanism of the core-shell MPs, their drug release profiles are fitted to a series of known release kinetic models in Tab. 5-2. The first-order release model represents the system where the drug release rate is concentration dependent. Higuchi model is developed to describe the release of water soluble (or low soluble) drugs incorporated in solid (or semi-solid) matrixes. Baker-Lonsdale model is developed by Baker and Lonsdale from the Higuchi model to characterize the controlled drug release from a spherical matrix. This model is generally applied to analyze the release of nano and micro-particles. Korsmeyer–Peppas model is a semi-empirical model the n value is used to study different mechanisms of the pay load release, of $n \leq 0.5$ for diffusion and $0.5 < n \leq 1$ for mass transfer following a non-Fickian model⁶⁷.

The results of the release data modeling are summarized in Tab. 5-7, In VFS, the drug release from SLMPs follow mostly the first-order kinetic, since the value of correlation coefficient (r^2) is the highest when the data is fit to first-order model, while The drug release from DLMPs and TLMPs is governed by the Baker-Lonsdale model. In SFS, the release of TLMPs fit the same model as it in VFS, while the release profile of SL and DLMPs can be

better described by Korsmeyer–Peppas model, the Korsmeyer–Peppas release exponent (n) is less than 0.5, indicating that diffusion is the controlling factor for drug release.

Tab. 5-7 Mathematical modeling for drug release from different MPs in VFS and SFS.

Media	MP	First-order		Higuchi		Baker-Lonsdal		Korsmeyer–Peppas		
		s		e						
		k_1	r^2	k_H	r^2	k_0	r^2	k_0	n	r^2
VFS	SL	0.04	0.9848	10.04	0.9257	0.003	0.9702	14.895	0.408	0.9471
(pH 4.2)	DL	0.022	0.8462	8.43	0.9344	0.002	0.9909	14.844	0.367	0.9890
	TL	0.014	0.8587	7.13	0.9654	0.001	0.9898	10.182	0.417	0.9824
SFS	SL	0.106	0.8465	10.58	0.4389	0.004	0.8189	32.331	0.237	0.9074
(pH7.2)	DL	0.032	0.7557	9.063	0.8209	0.003	0.9554	20.424	0.309	0.9776
	TL	0.017	0.8796	7.603	0.9681	0.001	0.9932	11.011	0.413	0.9866

5.3.4 Cytotoxicity study

As shown in Fig. 5-8, no significant increasing of LDH release is observed in the TFV loaded MPs treated cells compare to that of the negative control (media) .

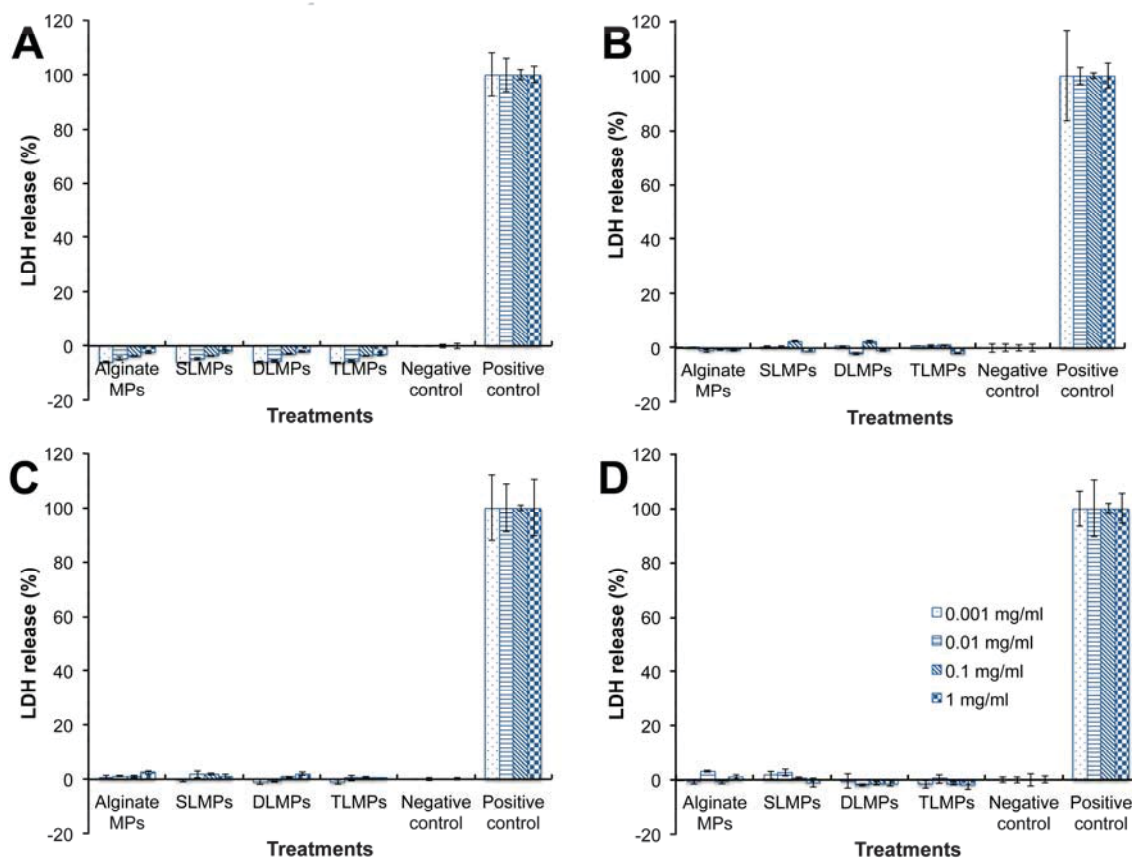


Fig. 5-8 LDH release of cells treated by alginate MPs, SLMPs, DLMPs and TLMPs for 24 and 48 h. A: VK2/E6E7 cell line 24h; B: VK2/E6E7 cell line 48 h; C: End1/E6E7 cell line 24 h; D: End1/E6E7 cell line 48 h, (n=3).

3-(4,5-dimethylthiazol-2-yl)-5-(3-carboxymethoxyphenyl)-2-(4-sulfophenyl)-2H-tetrazolium (MTS) is a tetrazolium compound. MTS can be converted to a brown formazan compound by active mitochondrial reductase enzymes, which exist in living cells only. Therefore, this reduction can be directly related to the number of living cells, the formazan product is used as an indicator of the cell viability. No significant difference is found between the cells incubated with drug loaded MPs and media (Fig. 5-9). These results suggest that the

TFV loaded MPs are not toxic to both vaginal (VK2/E6E7) and endocervical (End1/E6E7) epithelial cell lines.

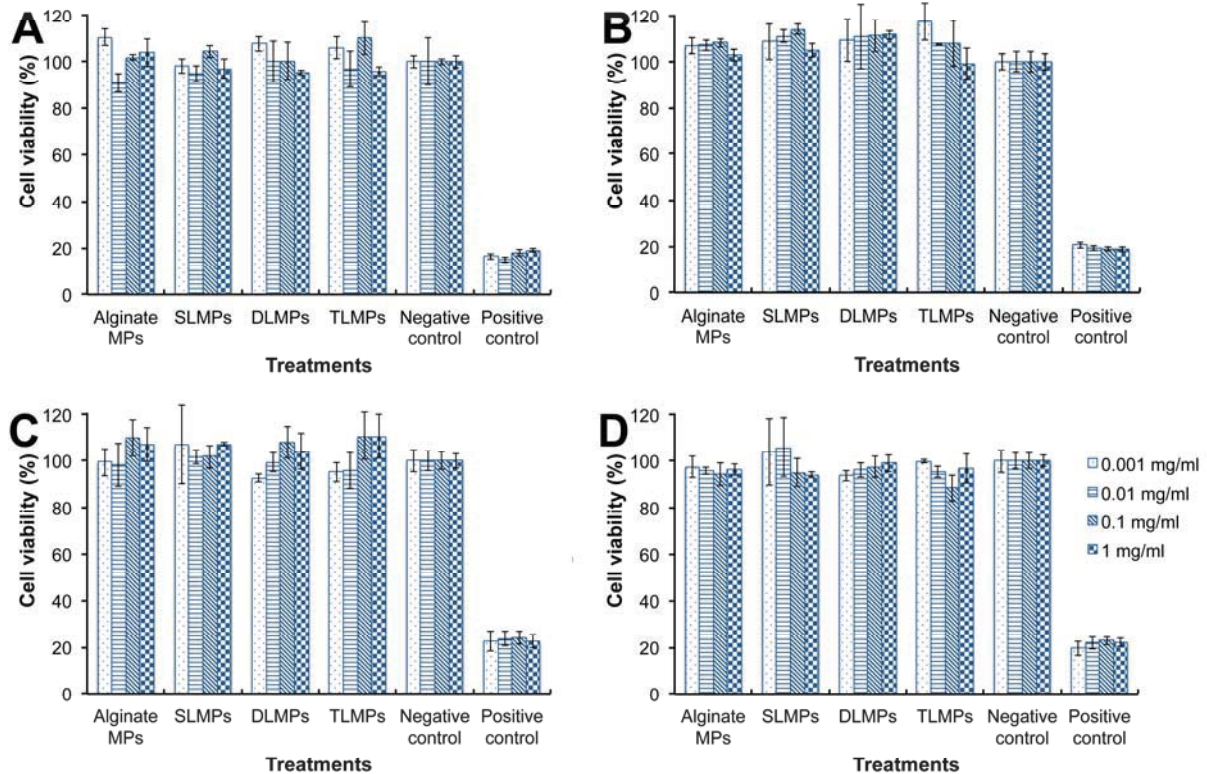


Fig. 5-9 Viability of cells treated by alginate MPs, SLMPs, DLMPs and TLMPs for 24 and 48 h. A: VK2/E6E7 cell line 24h; B: VK2/E6E7 cell line 48 h; C: End1/E6E7 cell line 24 h; D: End1/E6E7 cell line 48 h, (n=3).

5.3.5 Mucoadhesion of the MPs

Mucus, which is secreted by epithelium of the cervix, plays an important role in female reproductive function by facilitating the wriggling of the sperm toward the uterus¹³⁵. Mucus also provides a protective covering for the vaginal epithelium. It can be present as a luminal soluble, suspended form, or gel layer adherent to the mucosal surface¹³⁶. Mucin

glycoprotein is the major components of mucus gels. In this study, the Mucoadhesion of the MPs is assessed through the adsorption of mucin by MPs. It is reported that the mucus compositional differences exist among individuals¹³⁷. Even for the same person, the amount of mucin in the female reproductive tract changes during the menstrual cycle. Prior studies suggest that in healthy women, the daily production of cervix mucus is around 20–60 mg. During the midcycle, it increases up to 700 mg/day and becomes less viscous in order to allow sperm penetration¹³⁸. Therefore different concentration of mucin, low (0.1 mg /ml), medium (1 mg/ml) and high (2 mg/ml) is selected, respectively. The results are shown in Fig. 5-10, the mucin adsorption of the TCS coated MPs is increased by 10-20 fold Compare to that of the non-mucoadhesive MPs (alginate). In both VFS and SFS, the mucin adsorption is quite low, around 20%, when mucin concentration is relatively low (0.1 mg/ml), the possible reason is, both vaginal fluid and semen fluid contain soluble proteins, which is substituted by BSA in VFS and SFS. The negatively charged protein can interact with positively charged MPs by charge-charge interaction. With low mucin concentration, MPs have less chance to collide with mucin molecules, the protein occupies the surface of MPs and results in low mucin adsorption. When mucin and MPs has the same concentration (1 mg/ml), the mucin adsorption increases to approximately 50%. After the mucin concentration is increased to 2 mg/ml, the percentage of mucin adsorption decreases to about 40% compare to that of the 1 mg/ml solution, however, given the difference in concentration, it is reasonably computed that the amount of mucin adhered to the MPs in 1 ml of buffer is increased approximately from 0.5 mg to 0.8 mg.

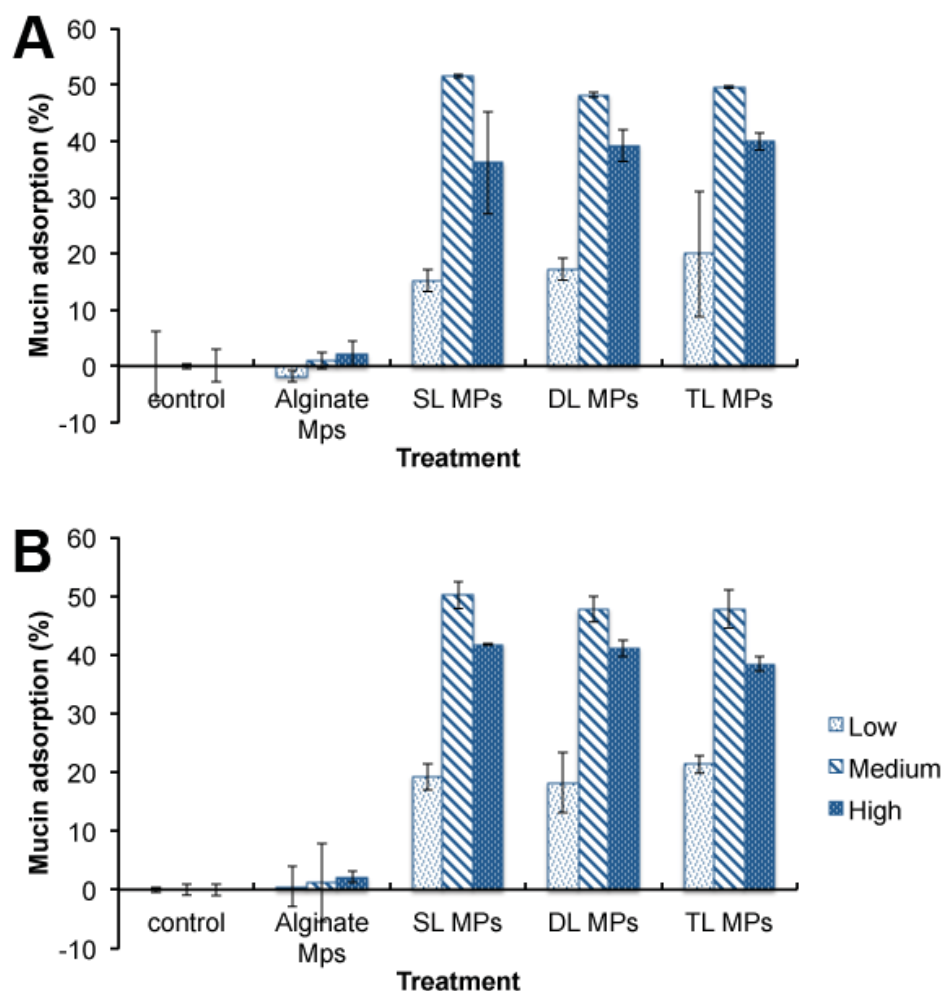


Fig. 5-10 Mucin adsorption in VFS (A) and SFS (B), (n=3).

5.3.6 *In vivo* safety studies

DLMPs, which show relatively high drug loading and slow release rate, are applied intravaginally to female C57/BL6 mice, the light micrographs of their genital tissues are analyzed. A representative H&E stained vaginal tissue section is presented in Fig. 5-11. Daily intravaginal exposure to the DLMPs does not lead to significant microscopic abnormalities. As a comparison, severe histopathologic changes, including ulceration and denudation (red arrows) are evident among mice treated with 4% N-9 for 24h. The

substantive difference of the vaginal epithelium integrity is found to be insignificant due to the recovery of the vaginal epithelium after 24 h postapplication¹³⁹.

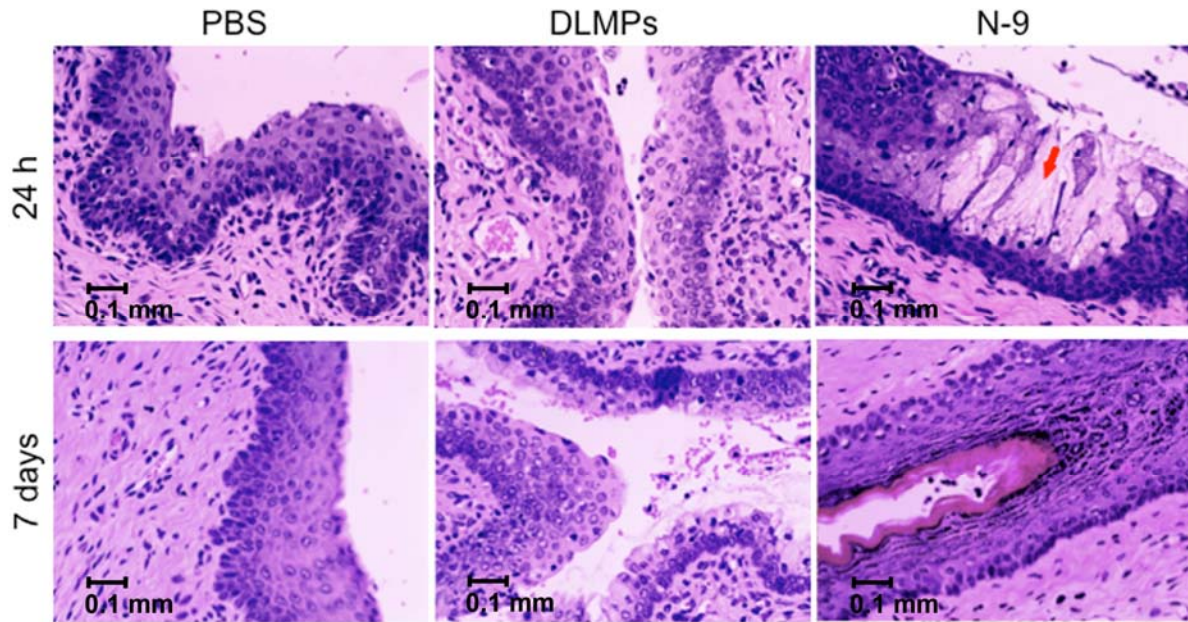


Fig. 5-11 H&E stain *in vivo* safety evaluation in C57BL/6 mice after 24 h (top row) and 7 days (bottom row) exposure with PBS, DLMPs, and N-9. Scale bar = 0.1 mm.

Therefore, to determine whether the MPs treatment can induce the infiltration of immune cells, the distribution of CD45-positive cells is examined using IHC analyses, which is indicative of inflammation, into the cervico-vaginal mucosa. After 4% N-9 application for 24 h and 7 days, Compare to the PBS treated tissue (negative control), the level of CD45-positive cells distributed within the N-9 treated vaginal epithelium is slightly elevated, Whereas the distribution of immune cells within the DLMPs treated vaginal tissue is similar to that of the negative control. The CD45-positive cells are identified by arrowhead marks in Fig. 5-12. The results indicate that there is no considerable inflammation of the vaginal epithelium after DLMPs exposure for 24 h and 7 days.

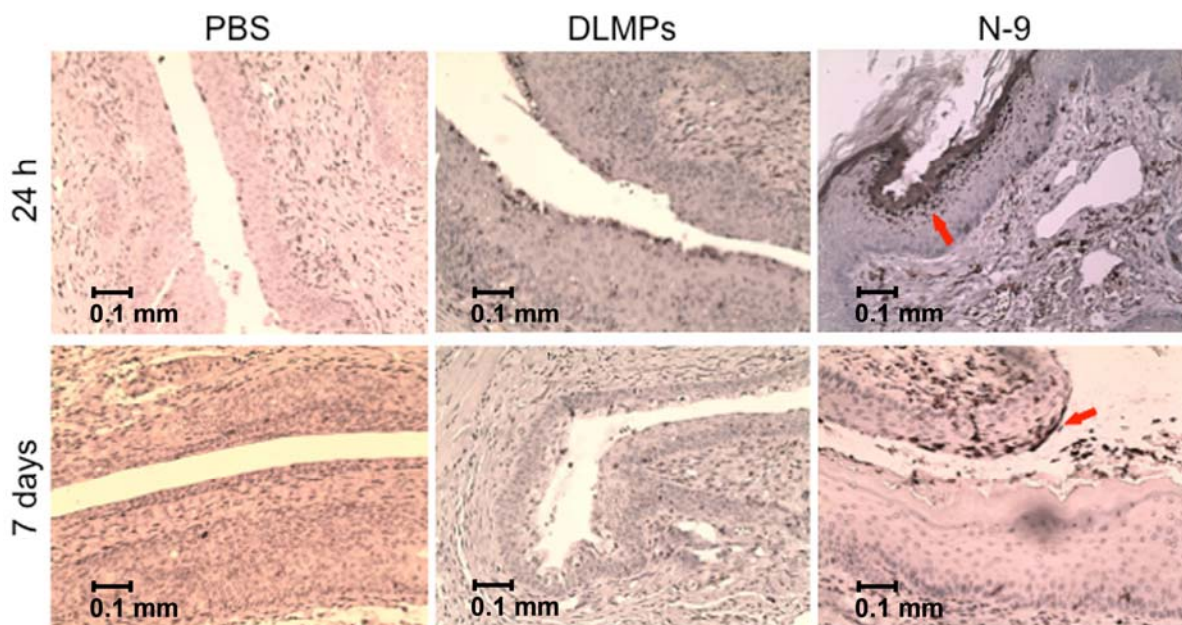


Fig. 5-12. Immunohistochemical stain *in vivo* safety evaluation in C57BL/6 mice after 24 h (top row) and 7 days (bottom row) exposure with PBS, DLMPs, and N-9. Scale bar = 0.1 mm.

5.4 Conclusions

In this study, a custom experimental design is used to optimize the formulation and process parameters of a spray dried alginate MP. Base on the optimized MP, thiolated CS coated multilayer MPs are prepared utilizing a layer-by-layer technique. These microspheres have non-cytotoxic to vaginal and endocervical epithelial cells, as well as high mucoadhesion property in both vaginal fluid and semen fluid. These data suggests that these MPs are effective for intravaginal delivery of anti-HIV microbicides.

CHAPTER 6

TENOFOVIR CONTAINING THIOLATED CHITOSAN CORE/SHELL NANOFIBERS: *IN VITRO* AND *IN VIVO* EVALUATIONS

6.1 Rational

The study of nanomedicine has been dominated by spherical particle design, mainly because it minimizes the interfacial energy during the particles formation¹⁴⁰. However, very few non-spherical delivery systems are studied even though they could potentially exhibit superior properties. One of the most promising non-spherical delivery systems are nanofibers (NFs), which can be designed by electrospinning (ESP)¹⁴¹. ESP utilizes electrostatic forces as its driving force to produce polymeric fibers¹⁴². It provides an effective and alternative way to directly encapsulate both hydrophobic and hydrophilic drugs into the fibers directly¹⁴³. Biocompatible polymers can be electrospun into nano-sized mesh that is composed of fibers with a high surface area¹⁴⁴. The high surface-to-volume ratio of NFs makes them suitable for mucoadhesive drug delivery systems.

In this study, thiolated chitosan (TCS) is used as the mucoadhesive material in NF formulation. Its mucoadhesive property has been proven in various studies^{35a, 145}. TCS on the surface of the formulation can bind to the mucosa, which lines the surfaces of body cavities, such as the vagina and rectum, to maintain a certain level of moisture¹⁴⁶. Therefore, the adhesive property of a formulation is largely depended on its surface-to-volume ratio. Compare to spherical NPs, NFs have higher surface-to-volume ratio resulting in more interfacial area available to interactions thereby aiding the adhesion^{27, 147}. Once applied topically, the mucoadhesive NFs intend to stay in close contact with the mucosa, prolong the

residence time on the application site, provides long-lasting protection to women¹⁴⁸, since heterosexual contact is the major route of acquiring HIV for women²⁶.

In this study, it is hypothesized that ESP can improve the drug loading significantly, in comparison with other forms of drug delivery systems produced by conventional methods, such as hydrogel, liposomes, and nanospheres¹⁴⁹; the electrospun TCS NFs can provide long-lasting drug release due to their mucoadhesivity, and are safe *in vivo*.

6.2. Materials and methods

6.2.1 Materials

Chitosan (CS) (Mw 50-190 kDa), thioglycolic acid, poly(ethylene oxide) (PEO) (Mw 900 kDa), formic acid, mucin (Type III), periodic acid Schiff reagent kit and DAB: Peroxidase Substrate Kit are purchased from Sigma Aldrich (St. Louis, MO, USA). Poly (DL-lactide) (PLA) (PDL 05) is a gift from Purac Biomaterials (Lincoln, IL, USA). 1-ethyl-3-(3-dimethylaminopropyl) carbodiimide hydrochloride (EDC) and *N*-hydroxysuccinimide (NHS) and sodium triphosphate penta-basic (TPP) are supplied by supplied by Thermo Fisher Scientific (Pittsburgh, PA, USA). TCS is synthesized as described in the Supary material file. Tenofovir (TFV) is purchased from Zhongshuo Pharmaceutical Co. Ltd. (Beijing, China). The CytoTox-ONE™ and CellTiter 96™ Aqueous kits are purchased from Promega (Madison, WI, USA). Anti-CD45 and biotinylated secondary antibody is obtained from Santa Cruz Biotechnology, Inc. (Dallas, Texas, USA).

6.2.2 Methods

6.2.2.1 Preparation of the TCS core/shell NFs

A blend of TFV and PEO is used as the core material. A coaxial spinneret is used to allow for the injection of PEO solution into the TCS solution as shell material at the

syringe tip.

The core composite solution is prepared by dissolving PEO into 50% v/v formic acid solution and stirring over night to yield a 3% (w/v) homogeneous solution. TFV is dissolved in the same solution at the concentration of 1% (w/v). To prepare the core composite solution, TCS is mixed with PLA in a ratio of 1:1 (w/w). Then, TCS or TCS-PLA blend is dissolved in pure formic acid at the concentration of 3% (w/v) and TPP is added in the solution at the ratio of TCS:TPP is 8:1 (w/w).

An electrospinning system with a coaxial nozzle (NaBond Technologies Co., Ltd., HongKong, China) is used for NF production. The core and shell composite solutions are placed in two separate glass syringes (Becton, Dickinson and Company, NJ, USA). Two syringe pumps (Cole-Parmer Instrument Company, IL, USA) are used to supply a continuous and constant amount of solution. The feeding rate of both the solutions is 50 μ l/h. A voltage of 15 kV is applied to the nozzle by a high voltage power supply (Gamma High Voltage Research, Inc., FL, USA). The NFs are collected onto an aluminum collector connected to the ground. The distance between the collector and the syringe tip is 10 cm. After electrospinning, the prepared NF mat is peeled from the surface of the collector and stored in a vacuum desiccator.

6.2.2.2 Percent drug loading and yield

To determine the drug loading, approximately 1 mg of TFV loaded NFs is submerged in 50 ml water for 48 h to allow complete dissolution of the PEO core and vortexed for 5 min. After centrifugation (Micro 18R Ultracentrifuge, VWR International LLC., PA, USA) at 10,000 rpm for 20 min, the supernatant is analyzed by using a high

performance liquid chromatography (HPLC) assay at 259 nm¹⁵⁰. The percent drug loading is calculated by using Equ. 6-1:

$$\text{Drug loading(\%)} = \frac{\text{Total amount of TFV}}{\text{Total amount of NFs}} \times 100 \quad (6-1)$$

The yield of the NFs fabrication process is calculated by the ratio of total mass of the electrospun NFs to the total mass of the initial ingredients combined (Equ. 6-2).

$$\text{Yield(\%)} = \frac{\text{Total mass of NF}}{\text{Total mass of initial components combined}} \times 100\% \quad (6-2)$$

6.2.2.3 Morphological analysis study

The morphology and surface characteristics of the NFs are analyzed by scanning electron microscopy (SEM) and transmission electron microscopy (TEM). For SEM analysis, small amount of NFs is mounted to aluminum stubs with conductive tape, and sputter coated with approximately 20 nm thickness of gold–palladium alloy. The NFs are then examined using a FEI/Philips XL30 Field- Emission Environmental SEM (Philips, Eindhoven, Netherlands) at 5 kV. Digital images are acquired with ORIUSTM SC 1000 11 Megapixel CCD camera (Gatan, Pleasanton, CA, USA). The SEM images are analyzed using Image Pro[®] Plus software (Image Pro Plus 6.0, Media Cybernetics, Silver Spring, MD, USA). The following measurements are made: average fiber diameter, average bead diameter, and the approximate ratio of bead area to total bead and fiber area.

For TEM analysis, NFs are deposited onto a copper grid with a carbon support film. The copper grid is submerged in water and then dried. The NFs are observed under a Scanning Transmission Electron Microscope CM12 (FEI, Hillsboro, OR, USA) at 80 kV accelerating voltage. Digital images are acquired as described above.

6.2.2.4 Fourier transform infrared (FT-IR) spectroscopy analysis

In order to elucidate the surface chemistry, the NFs are directly scanned over the range of 650 and 4000 cm^{-1} . The background is collected at ambient conditions before analyzing each sample. The FT-IR spectra are recorded by OMNIC V 7.0 spectra software.

6.2.2.5 *In vitro* drug release profile from the NFs

One milligram of NFs is immersed in a tube containing 40 ml of vaginal fluid simulant buffer (VFS), prepared according to previous reports⁴⁵. The tubes are kept in a thermostatically controlled water bath (BS-06, Lab Companion, USA) at 60 rpm, the temperature is maintained at 37°C. At predetermined time intervals, 1 ml of the VFS buffer solution is taken out and replaced by fresh buffer to maintain the sink conditions. The concentration of drug in the buffer solution is determined by the above HPLC assay. Each experiment is run in triplicate ($n = 3$) together with a blank control.

6.2.2.6 *In vitro* cytotoxicity studies

Human vaginal keratinocyte cell line (VK2/E6E7) and human endocervical epithelial cell line (End1/E6E7) are grown in the Keratinocytes-SFM medium, the media is Suped with 10% (v/v) fetal bovine serum (FBS) and 1% penicillin/streptomycin. Cells are cultured at 37°C in a humidified 5% CO_2 atmosphere and sub-cultured prior to confluence using trypsin. *Lactobacilli crispatus* is grown in an ATCC medium 416 *Lactobacilli* MRS broth (BD, Franklin Lakes, NJ, USA) and cultured at 37°C in a humidified 5% CO_2 atmosphere.

6.2.2.7 Cell culture

6.2.2.7.1 Cellular membrane integrity assay

The NFs membrane with an area of 0.25 cm^2 (approximately 0.1 mg), is peeled from the collector and laid at the bottom of each well in the 96-well plates. VK2/E6E7 and

End1/E6E7 cell lines are seeded in the plates with the NF membrane to ensure 1×10^4 cells per well. The plates are then incubated at 37°C for 24 or 48 h. The cells incubated with media alone or 1% Triton X-100 (both without NFs) are used as the negative and positive controls, respectively.

To measure the lactate dehydrogenase (LDH) release, after the 24 or 48 h incubation time, the plates are taken out of the incubator and equilibrated to 22 °C. In each well, 100 µl of CytoTox-ONE™ Reagent is added. The plates are shaken for 30 s and then incubated at 22 °C for 10 min. After this, 50 µl of stop solution is added and the fluorescence intensity is determined by a microplate reader at λ_{ex} 560 nm and λ_{em} 590^{120c}.

6.2.2.7.2 Cell viability assay

To determine the cell viability, after the incubation time, the media in the wells is removed and substituted with fresh media. Twenty microliters of Cell Titer 96® Aqueous One Solution Reagent (Promega, Madison, WI, USA) is added to each well and incubated at 37°C for 4h. The absorbance is recorded at a wavelength of 490 nm.

6.2.2.7.3 *Lactobacillus* viability assay

The *Lactobacillus* viability assay is performed using an established method⁴⁷. The *L. crispatus* bacteria density is adjusted to an OD₆₇₀ of 0.06, corresponding to a 0.5 McFarland Standard or 10⁸ CFU/ml^{48a}. It is then plated in the plates with NFs at a volume of 100 µl per well, and then incubated at 37 °C. The *Lactobacillus* incubated without NFs is used as the negative control and those incubated with a commercially available 10 µg/ml of Penicillin-Streptomycin solution (Invitrogen, Carlsbad, CA, USA) is used as a positive control. After 24 or 48 h, 20 µl of MTS reagent is added to each well, and the bacterial viability is determined by measuring the absorbance at a wavelength of 490 nm by a

microplate reader.

6.2.2.8 Mucoadhesion study

A periodic acid/Schiff (PAS) colorimetric method is used to determine the free mucin concentration in order to assess the amount of mucin adsorbed on the NFs¹²⁷. Periodic acid reagent is freshly prepared by adding 10 µl of 50% periodic acid solution to 7 ml of 7% (v/v) acetic acid solution. One milligram of PEO, PEO/TCS, and PEO/TCS-PLA NFs is added in the mucin solution of VFS at the concentration of 1 mg/ml. The solution is incubated in a shaking water bath for 30 min at 37°C to enable NFs-mucin interaction. Then, the dispersions are centrifuged at 4000 rpm for 2 min to separate NF-mucin conjugate, and the supernatant is used for the measurement of the free mucin content. For each sample, 0.2 ml of periodic acid reagent is added, the samples are incubated at 37°C for 2 h in a water bath. Then, 0.2 ml of Schiff reagent is added at room temperature. Thirty minutes later, the absorbance of the solution is recorded at 555 nm by using the Genesys 10 Bio UV–Vis Spectrophotometer (Thermo Electron Sci. Inst., LLC, Madison, WI, USA). Standard calibration curve is prepared from 1 ml of mucin standard solutions in the concentration range of 0.25 - 2 mg/ml. The mucin content is calculated from the standard calibration curve. The mucin solution without NFs is used as a control and assessed using the above procedure. Each experiment is performed in triplicate (n = 3). The percentage of mucin adsorption is estimated using Equ. 6-3:

$$\text{Mucin adsorption(\%)} = \frac{\text{Total mass of mucinmated using}}{\text{Total mass of mucin}} \times 100 \quad (6-3)$$

The above method is developed for the quantification of the mucoadhesion, however, it is limited due to no biological tissue is used. To assure the NFs can adhere to the real vaginal mucus, an infusion method is employed. The porcine vaginal tissues are

obtained from the local abattoir (Fairview Farm Meat Co., Topeka, KS, USA). These tissues are washed using normal saline, snap frozen in liquid nitrogen, and then stored at -80°C. Before the experiment, the frozen tissues are thawed in normal saline at 37°C for 3 min. the FITC labeled TCS is synthesized as previously described⁵⁰. The tissue is cut into pieces of 2 cm length and 1 cm width and stuck to a plastic strip by cyanoacrylate glue, which is resistant to water and harmless to the tissue. Approximately 0.1 mg of FITC labeled PEO/TCS and PEO/TCS-PLA NFs are distributed over the surface of the tissue. The strip is put into a tube that is placed in a water bath of at an angle of 75° to allow buffer flow by gravity. The tissue is then placed in a container maintains at 37°C and relative humidity for 20 min to allow the NFs to hydrate and to interact with the mucin layer of the tissue. After 20 min, the mucosa is continuously washed for 10 min with VFS at the rate of 1 ml/min. The tissue is then cut into small cubes, embedded into Histoprep, frozen by liquid nitrogen, and sectioned vertically using a cryostat microtome. The skin sections (5 mm) are mounted on glass slides and visualized through a fluorescence microscopy (Nikon, Shizuoka Prefecture, Japan)⁸⁹.

6.2.2.9 *In vivo* safety studies

The animal experiments are duly approved by the University of Missouri - Kansas City Institutional Animal Care and Use Committee (IACUC). Female 8-12 weeks old C57Bl/6 mice, weighing about 18-22 g, are obtained from Jackson Laboratories (Bar Harbor, Maine, USA.) and allowed to acclimate for 7 days. All mice are housed (no more than 5 per cage) under a 12 h light: dark regime in the University of Missouri-Kansas city (UMKC) Laboratory Animal Resource Center (LARC) facility which is a fully AAALAC accredited with HEPA-filtered, temperature, humidity, and lighting controlled systems. In order to

maintain a constant diestrus-like vaginal cytology for reproducible experimental conditions, mice are s.c. injected with 2 mg of medroxyprogesterone acetate (Depo-Provera®, Greenstone, Peapack, NJ, USA)) in a total volume of 200 µl of in Lactated Ringer's saline solution 4-5 days before the treatment to induces and maintain a diestrus-like state..

The mice are divided randomly in three groups (n = 4). Group 1 is treated with 20 µl Benzalkonium chloride (BZK, 2 %w/v), as positive control; group 2 is treated with PBS is used as negative control; group 3 is treated with freshly prepared PEO/TCS-PLA NFs , the dose is 475 mg/kg. Intra-vaginal instillation is carried out Once daily using a flexible feeding needle (Cadence, Inc. Staunton, VA, USA). After 1-day and 7-day intravaginal application, mice are euthanized by carbon dioxide (CO₂) asphyxiation. Their vaginal tissues are collected, formalin fixed in paraffin, and cut into 5-mm sections.

6.2.2.9.1 Hematoxylin and eosin (H&E) staining

Serial sections are stained with hemotoxylin and eosin (H&E). Images are captured using a Nikon Labophot-2 microscope (Nikon Instruments, Inc., Melville, NY) equipped with a PAXCam digital microscope camera and analyzed using PAX-it image management and analysis software (Midwest Information Systems, Inc., Villa Park, Illinois).

6.2.2.9.2 Immunohistochemical staining

To identify the inflammatory cell (CD45) infiltrate, immunohistochemical staining is performed in genital tissue sections. Briefly, the de-paraffinized and rehydrated tissue sections are pretreated with citrate buffer/0.05%Tween-20 (antigen retrieval reagents) for 20 min using steam heat method, rinsed with Tris buffered saline/0.05%Tween-20 three times, incubated with 3% v/v hydrogen peroxide in PBS for 10 min, and blocked with 10% normal goat serum (Vector Laboratories, Burlingame, CA) for 2 h. The slides are then incubated

with the primary anti-CD45 antibody overnight in a humidified chamber at 4°C, rinsed three times with PBS, followed by application of biotinylated secondary antibody at room temperature for 1 h. The cells are visualized using the DAB: Peroxidase Substrate Kit under a Nikon Labophot-2 microscope. The tissue is then counter-stained by hematoxylin (Sigma, Saint Louis, MO) and treated with alcohol gradient and xylene before application of a coverslip mounted using cyto seal 60 mounting media (Richard Allan Scientific, Kalamazoo, MI). Images are viewed and captured as described above.

6.2.2.10 Statistical data analysis

The results are expressed as the mean of at least 3 experiments ($n=3$) \pm the standard error of the mean (SEM). Statistical data analysis is performed using the student t-test; two tails with 95% confident interval ($p < 0.05$) as the minimal level of significance.

6.3 Results and discussions

6.3.1 Formulation of NFs

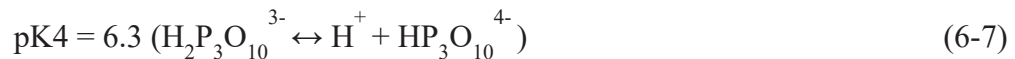
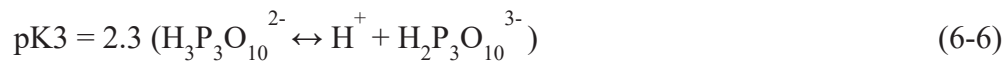
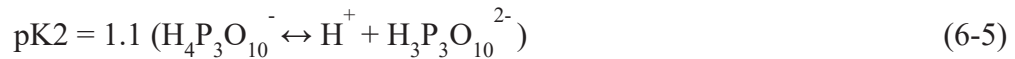
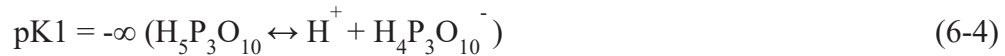
Electrospinning is a simple, flexible, and cost-effective process that can form a broad range of polymeric fibers. During the electrospinning process, when a sufficiently high electrical potential is applied to the droplet of polymer solution, the droplet becomes charged. At a critical voltage, the electrical energy overcomes the surface energy of the polymer droplet, and a jet erupts from the surface. The jet is then elongated under the electrostatic force while the solvent of the polymer is being evaporated until it is finally deposited on a grounded collector¹⁵¹.

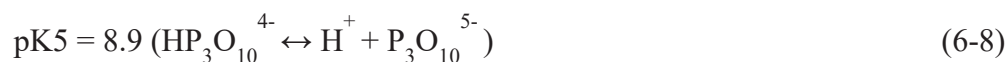
TCS is a derivative of CS, it presents on the surface as the shell can interact with the mucosa while the TFV is released from the core in controlled manner. CS is a cationic polysaccharide. The amino groups on the polymer backbone are ionizable and positively

charged under acidic condition. During the electrospinning process, the repulsive force between ionic amino groups within polymer backbone limit its electrospinnability and inhibits the formation of continuous fiber under the high electric field¹⁵². Therefore, the electrospinning of pure TCS typically forms beads and droplets instead of ultrafine fibers¹⁵³. To overcome this drawback and obtain continuous fiber, the following three alternative strategies are used.

Firstly, TCS is blended with Polylactic acid (PLA), which is a biodegradable aliphatic polyester. PLA has been approved by the FDA for human clinical applications, and has excellent film forming mechanical properties, attractive molding and shaping properties. It can be fabricated into porous NFs and many other types of structures¹⁵⁴. Some works have been devoted to manufacture PLA/CS composites¹⁵⁵. In our preliminary study, it is observed that the obtained NFs became more uniform when equal amounts of TCS and PLA are used.

Secondly, formic acid is the solvent of choice. This could be attributed to several reasons. 1) Formic acid is a good solvent of PLA/TCS composite, both TCS and PLA are soluble in formic acid. 2) The TPP is used to cross-link CS via charge-charge interaction between the phosphate groups of TPP and the amino groups of CS³⁸. The crossing linking is dependent on the availability of the cationic sites and the anionic sites. CS is polycationic in acidic environment, TPP has 5 pKa values as follow¹⁵⁶:





Since the pH of pure formic acid is lower than 1, only $\text{H}_4\text{P}_3\text{O}_{10}^-$ ions are present, the negative charge is too low to cross-link the positively charged CS. TPP and CS are free in the solution. After electrospinning, when the NFs are immersed in the VFS (pH 4.2), both CS and TPP dissociate to provide sufficient cationic sites and the negative sites, not until then will they crosslink and form the insoluble shell. This is supported by the fact that the solution of CS and TPP in pure formic acid is dropped into water or VFS, it precipitates as white flocky sediment (Fig. 6-1). 3) CS solution has high viscosity, which limits its spin ability¹⁵⁷. As a comparison with other solvent of CS, such as acetic acid (intrinsic viscosity $[\eta] = 28.21 \times 10^2 \text{ dL/g}$), the viscosity of the solution of CS in formic acid (intrinsic viscosity $[\eta] = 6.72 \times 10^2 \text{ dL/g}$) is relatively low at equal concentration¹⁵⁸. This facilitates the formation of the jet during the electrospinning process. 4) The vapor pressures of formic acid and acetic acid is 45 mm Hg and 11 mm Hg at 20 °C, respectively¹⁵⁹. The high volatility of formic acid is also advantageous for the rapid solidification of the electrified jet.

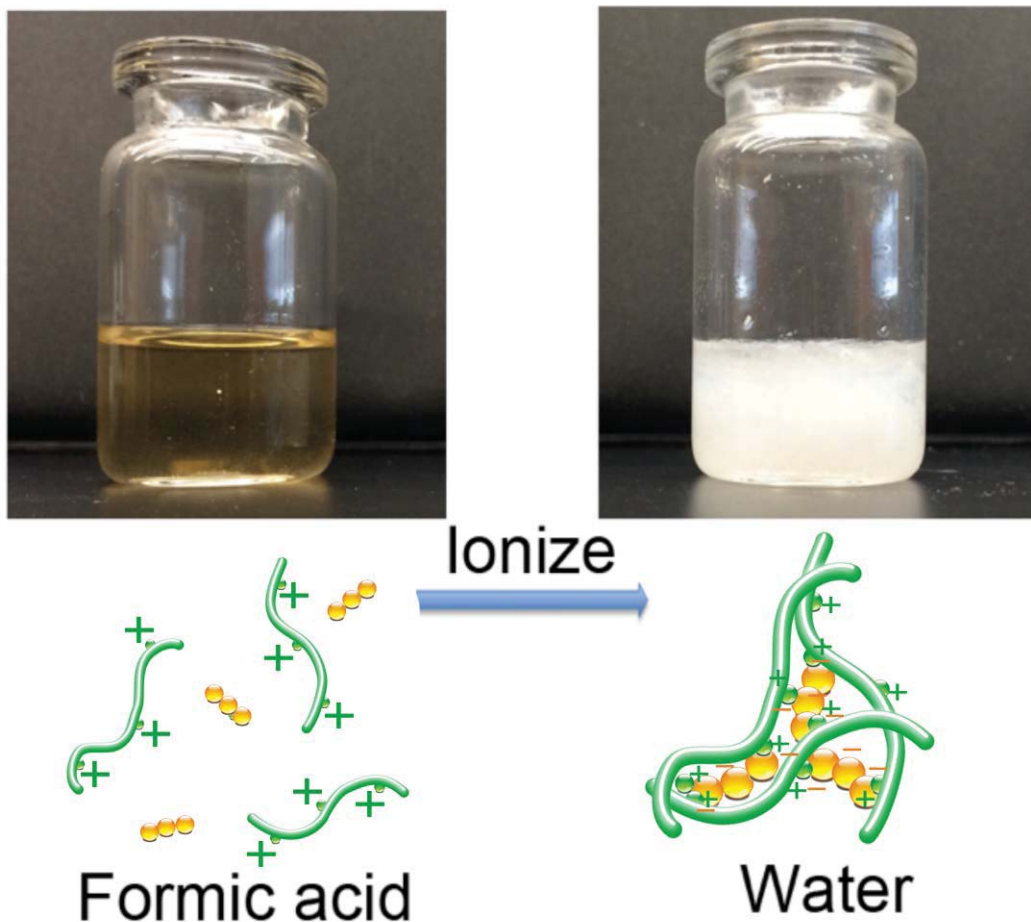


Fig. 6-1. Ionization of CS and TPP blend from formic acid to water.

Thirdly, PEO serves not only as a core material, but also as a spinning aid. The PEO core solution is believed to act as a carrier that forms a stable Taylor cone and draws out the shell CS solution by forming a continuous jet ejection¹⁶⁰. Moreover, PEO is nontoxic and has been approved by the FDA for use in different pharmaceutical formulations¹⁶¹. To successfully prepare the core/shell NFs, 50% formic acid is used as the solvent of PEO. Using the same solvent in the two streams can reduce the interfacial tension between the two solutions. The surface tension of 50% formic acid at 20 °C is 43 dyn/cm, very close to that

of the pure formic acid (37 dyn/cm at 20°C)¹⁶², it is in favor of coaxial electrospinning¹⁶³. If water (72 dyn/cm at 20°C) is used as the core solvent instead of acid solution, it appears that no fiber can be formed. This result is also confirmed by Pakravan et al.¹⁶⁰.

NF drug loading and percent yield

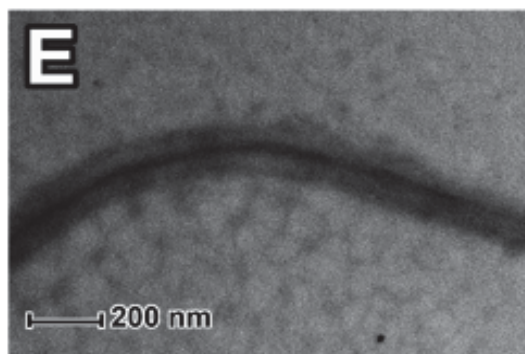
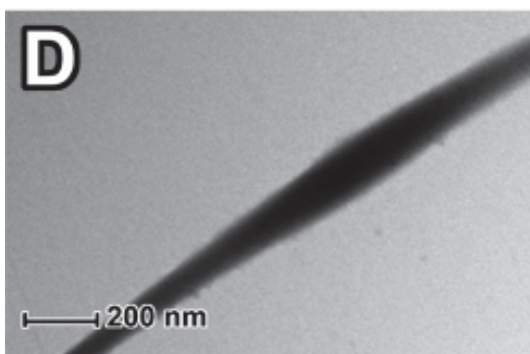
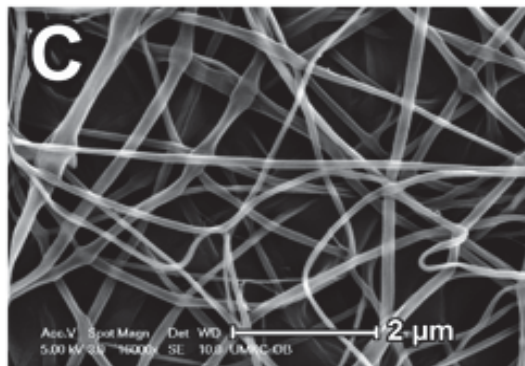
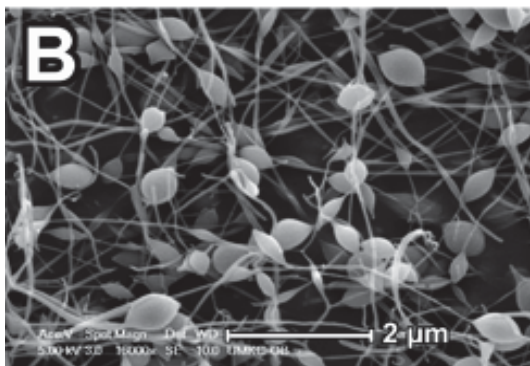
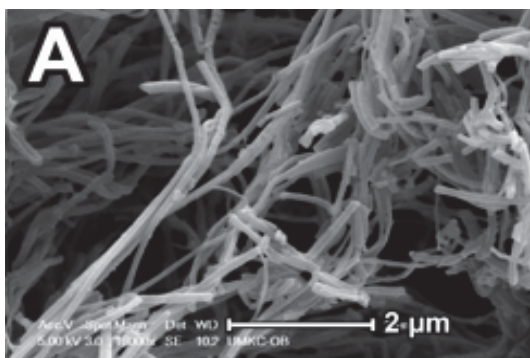
As shown in Tab. 6-1, the drug loading of the PEO, PEO/TCS and PEO/TCS-PLA NFs are 25.62%, 13.42% and 14.20% w/w, which is in close agreement with the theoretical values. Their respective yields are 102.48%, 53.65% and 63.18%. The jet stretches by whipping and bending. The nature of the whipping motion and bending instability of the charged jet in the electrospinning process may cause some shift in the direction, and distribute the fibers over a larger area. For PEO/TCS and PEO/TCS-PLA NFs, the area of NFs deposit exceeds that of the collector, not all the NFs can be collected on the aluminum foil, which lead to a lower yield (Tab. 6-1).

Tab. 6-1 Composition, drug loading, yield and mean diameter of the NFs. Data are given as mean \pm SEM for n=3.

NF	Component		Drug loading (%)	Yield (%)	Mean diameter of fibers (nm)
	Core	Shell			
PEO NF	PEO	N/A	25.62 \pm 0.93	102.48 \pm 0.95	118.56 \pm 4.77
PEO/TCS NF	PEO	TCS	13.42 \pm 3.51	53.65 \pm 0.26	9.95 \pm 0.64
PEO/TCS-PLA NF	PEO	TCS PLA blend	14.20 \pm 2.12	63.18 \pm 1.16	99.52 \pm 5.52

6.3.2 Morphology studies

The SEM images (Fig. 6-2) shows that the pure PEO fibers and the core-shell fibers has been successfully produced using the electrospining technique. All the electrospun NFs are in nanoscale size in diameters. To characterize the NFs, the average fiber diameter, average bead diameter, and the approximate ratio of the bead area to the total NFs area are summarized in Tab. 6-1. Both PEO and PEO/TCS-PLA NFs are highly smooth without the occurrence of beads. However, for the PEO/TCS NFs, beads with the mean diameter of 58.81 nm are observed. Besides the morphological difference, there is also a difference in diameter between the pure PEO NFs and the PEO/TCS ones. The mean diameters of the PEO, PEO/TCS and PEO/TCS-PLA NFs are 118.56 nm, 9.95 nm and 99.52 nm, respectively. Compared to the pure NFs, the diameters of the PEO/TCS core shell NFs are significantly lower due to the strength of the repulsive force as explained above. The incorporation of PLA into the TCS shell solution leads to continuous, defect-free, cylindrically-shaped fibers. The NFs which are significantly uniform without beads are observed again.



Extraction

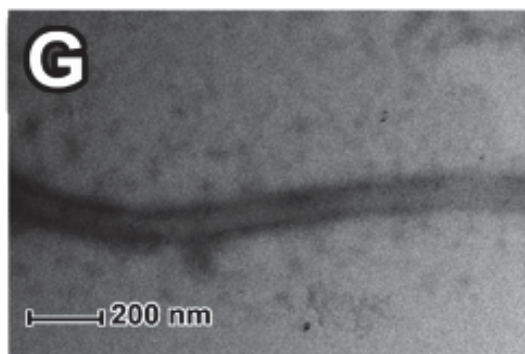
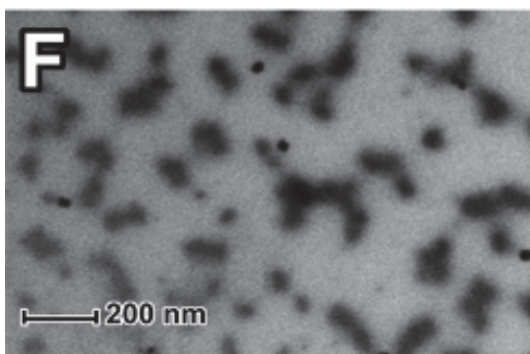


Fig. 6-2. Morphology of the nanofibers (NFs). Scanning electron microscopy (SEM) image of PEO NFs (A), PEO/TCS NFs (B), PEO/TCS-PLA NFs (C), Transmission electron microscopy (TEM) image of PEO/TCS NFs before PEO core extraction (D), PEO/TCS-PLA NFs before PEO core extraction (E), PEO/TCS NFs after PEO core extraction (F), PEO/TCS-PLA NFs after extraction (G). Scale bar = 2 μ m for SEM, scale bar = 200 nm for TEM.

To further identify the core/shell structures, the morphological detail of the produced core/shell NFs is shown in a TEM micrograph in Fig. 6-2 D-G. The contrast, which represents the distinctive phases in the NFs, is due to the absorption of electron beam in the organic molecules with different electron density used in TEM samples¹⁶⁴. In Fig. 6-2 D and E, the bright and dark regions represent the shell and core of the NFs, respectively. The electrospun NFs are soaked in water in order to selectively remove the PEO, since the water is a good solvent for PEO but poor solvent for TCS and TCS-PLA blend. The NFs are then examined under the TEM, the resulting structure is shown in Fig. 6-2 F and G. It appears that the PEO/TCS NFs are broken after aqueous extraction; fragments of the NFs instead of intact fibers are observed, revealing a discontinuous core-shell structure. Comparatively, the PEO/TCS-PLA NFs show very uniform core-shell structure with obvious boundary: the core is about 30 nm in diameter while the shell is approximately 20 nm in thickness. After the core (dark region) is completely removed, an integrated hollow fiber is observed. According to the SEM and TEM image, it is speculated that the PEO/TCS NFs have a necklace-like structure (Fig. 6-3 A), where TCS beads of different size are on the PEO string. Unlike PEO/TCS NFs that have a fine core/shell structure (Fig. 6-3 B), PEO is mainly located in the core while TCS-PLA blend constitutes the shell.

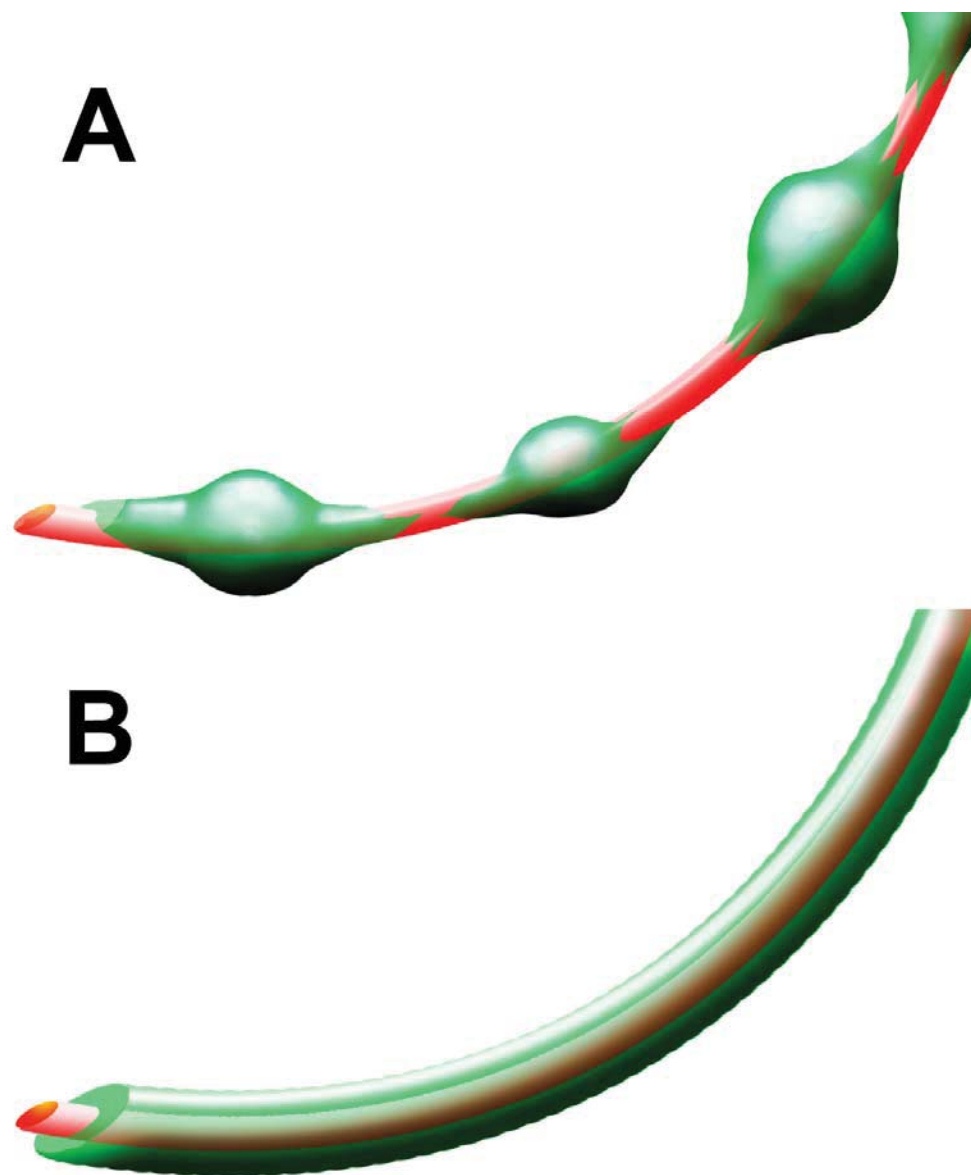


Fig. 6-3. Schematic description of PEO/TCS nanofibers (NFs) (A) and PEO/TCS-PLA NFs (B).

6.3.3 FTIR analysis

Fig. 6-4 displays the FTIR spectra of native PEO, TCS, PLA and the core/shell NFs. The native PEO shows a characteristic band at 2890 cm^{-1} corresponding to the CH_2 stretching vibration, which overlaps with that of CS. Absorption bands of hydroxyl ($-\text{OH}$)

groups are negligible as a high molecular weight (900 kDa) PEO is used. Other feature bands of PEO observed from 1240 to 1360 cm^{-1} are due to CH deformation of the methyl groups ($-\text{CH}_3$). The triplet peaks at 1065, 1095 and 1150 are referred to C–O–C stretching vibrations¹⁶⁵. The native TCS exhibited a broad absorption peak at around 3100 to 3650 cm^{-1} and weak absorption peaks at 2890 cm^{-1} , which are attributed to N–H and OH–O (hydrogen bond) stretching vibration and the CH stretch, respectively. The two peaks at 1520 and 1650 cm^{-1} are respectively due to the amide (CO–NH–) and the amine ($-\text{NH}_2$) absorption band. The FTIR spectra of native PLA reveals a sharp peak at 1750 cm^{-1} and characteristic bands from 1050 to 1200 cm^{-1} , 1187, 1131 and 1093 are assigned to the ester groups ($-\text{CO}-\text{O}-$) of PLA^{155a}. The peak of 1758 cm^{-1} which belonged to the carbonyl group in PLA is decreased.

In the spectrum of the PEO/TCS NFs, the absorbance intensity of amide and amine groups stretching at 1520 and 1650 cm^{-1} is decreased and the absorbance intensity of CH_2 stretching vibration at 2890 cm^{-1} is increased, indicating that the PEO exists not only in the inner core, but also on the surface of the NFs. For the PEO/TCS-PLA NFs, the increasing of the peak at 2890 cm^{-1} is not apparent, three characteristic bands at 1520, 1650 and 1750 cm^{-1} are observed, suggesting that the shell of these NFs are composed mainly of TCS and PLA, no PEO or perhaps a very minute quantity of PEO distributes on the surface of the NFs due to the fine core–shell morphology.

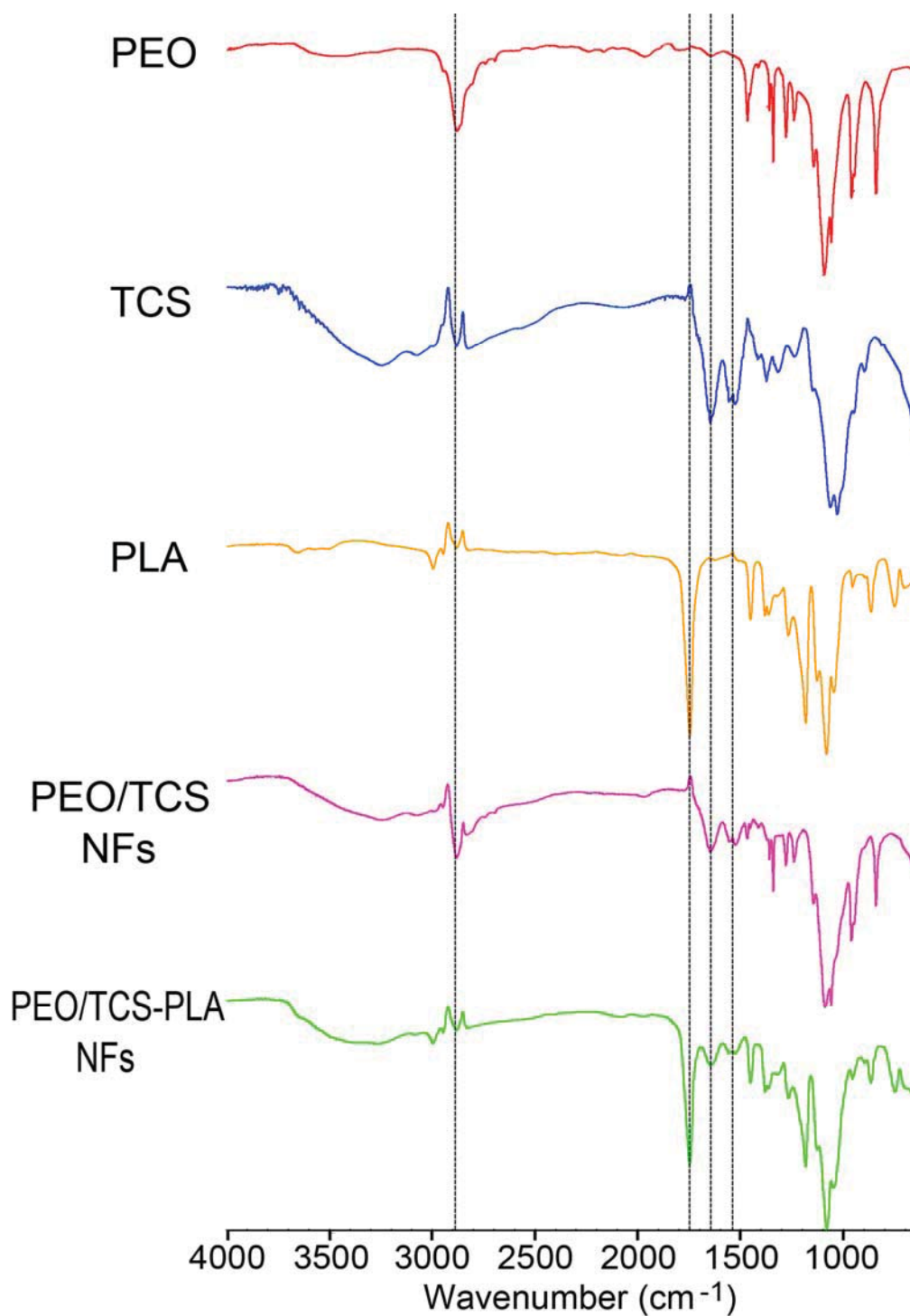


Fig. 6-4 The FT-IR reflectance spectra of neat PEO, TCS, PLA powder, PEO/TCS and PEO/TCS-PLA nanofibers (NFs).

6.3.4 *In vitro* drug release study

The drug release profiles for the NFs are shown in Fig. 6-5. In order to compare release kinetics of PEO NFs and the core/shell NFs, a simple model independent approach of FDA guidance is applied. The difference factor (f_1) and similarity factor (f_2) are calculated as follow:

$$f_1 = \left\{ \left[\sum_{t=1}^n |R_t - T_t| \right] / \left[\sum_{t=1}^n R_t \right] \right\} \times 100 \quad (6-11)$$

$$f_2 = 50 \times \log \left\{ \left[1 + \left(\frac{1}{n} \right) \sum_{t=1}^n (R_t - T_t)^2 \right]^{-0.5} \times 100 \right\} \quad (6-12)$$

Where n is the number of time points, R_t and T_t are the cumulative degradation and drug release (%w/w) at time t for reference (PEO NFs) and the test formulation (PEO/TCS NFs or PEO/TCS-PLA NFs), respectively⁶⁷.

Here f_1 is a measurement of the percent difference between the reference and test sample at each time point, while f_2 calculates the similarity in the percent dissolution between the two samples. Two curves can be considered similar if the values of f_1 and f_2 are close to 0 and 100, respectively. In this study, f_1 values of PEO/TCS and PEO/TCS-PLA NFs are 41.23 and 56.73; f_2 values are 8.24 and 1.31, respectively, indicating significant difference between the PEO NFs and the core/shell NFs.

For the PEO NFs, approximately 95% of drug is released within 5 h, which is attributed to the hydrophilic nature of PEO; the mechanism of drug release is based on dissolution of the drug. In the case of PEO/TCS and PEO-TCS-PLA NFs, The release profiles are simulated to a series of known release kinetic models: first-order model, Higuchi model, Korsmeyer-Peppas model, and Weibull model¹⁶⁶, The model with the highest determination coefficient (R^2) is chosen as the best fit, data is analyzed using the Excel add-in DDSolver program¹²⁶. It appears that they both follow Weibull model, $R^2 = 0.983$

and 0.991 for PEO/TCS NFs and PEO/TCS-PLA NFs, respectively. Weibull model is commonly used to describe the release profiles of matrix type delivery system. Given the fact that the effective molar EC_{50} of TFV is 5.0 to 7.6 μM , if the concentration of the NFs in VFS is 1 mg/ml, it is equivalent to a TFV concentration of 350 μM bases on the average drug loading ($\sim 10\%$), which means the drug could exhibit its effect when approximately 1.4% of drug is released from the NFs. According to the predicted release profiles in Fig. 6-5, both PEO/TCS and PEO/TCS-PLA NFs could release 1.4% of TFV within 2 min after application. Therefore, it is reasonable to speculate that both NFs are able to provide sufficient TFV concentration to exhibit an anti-HIV activity. After 24h, more than 80% of the drug is released from the PEO/TCS NFs, whereas approximately 60% of the drug is released from the PEO/TCS-PLA NFs. The release rate of the former is faster due to its discontinuous core-shell structure. Over all, the PEO/TCS-PLA NFs provide a better control on the drug release.

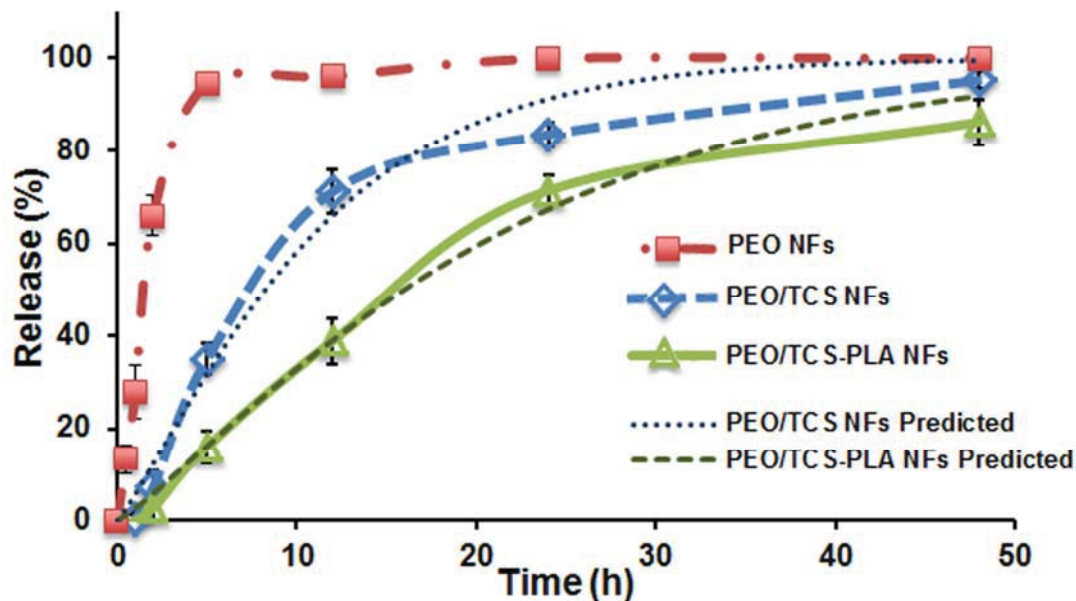


Fig. 6-5. *In vitro* drug release profiles from PEO nanofibers (NFs), PEO/TCS NFs, and PEO/TCS-PLA NFs in vaginal fluid simulant buffer ($n = 3$). Data are shown as mean \pm SEM

(n = 3).

6.3.5 Cytotoxicity assays

A vaginal drug delivery system must have safety profiles that justify its application, especially for the vaginal ecology¹⁶⁷. Thus, it is important to test the impact of the drug-loaded NFs on the viability and structural integrity of the vaginal epithelial cells as well as the natural flora in the vagina. The cellular membrane integrity is determined by the release of lactate dehydrogenase (LDH) from cells with damaged membranes. MTS is a tetrazolium compound that is convertible into a brown colored formazan product by viable cells with active metabolism, the amount of formazan produced is proportional with the number of viable cells⁹⁹. Fig. 6-6 A-D shows the results of the LDH release and the cellular viability (MTS assay) using the selected vaginal epithelial (VK2/E6E7) cell line and human endocervical epithelial (End2/E6E7) cell lines. After 24 h or 48 h, the TFV loaded NFs cause a statistically non-significant ($p>0.05$) release of LDH as a comparison with that caused by the media. The cellular viability test results are consistent with those of LDH assay, as no statistical difference ($p>0.05$) is observed by the Student t-test between the media and the TFV loaded NFs. The *Lactobacillus* viability assay (Fig. 6-6 E-F) also shows that no statistically significant loss of bacterial viability is observed during the incubation period.

The results indicate a non-cytotoxic nature of the NFs on both vaginal and endocervical epithelial cell lines and the vaginal flora at the concentration of 1 mg/ml up to 48 h.^{21a}

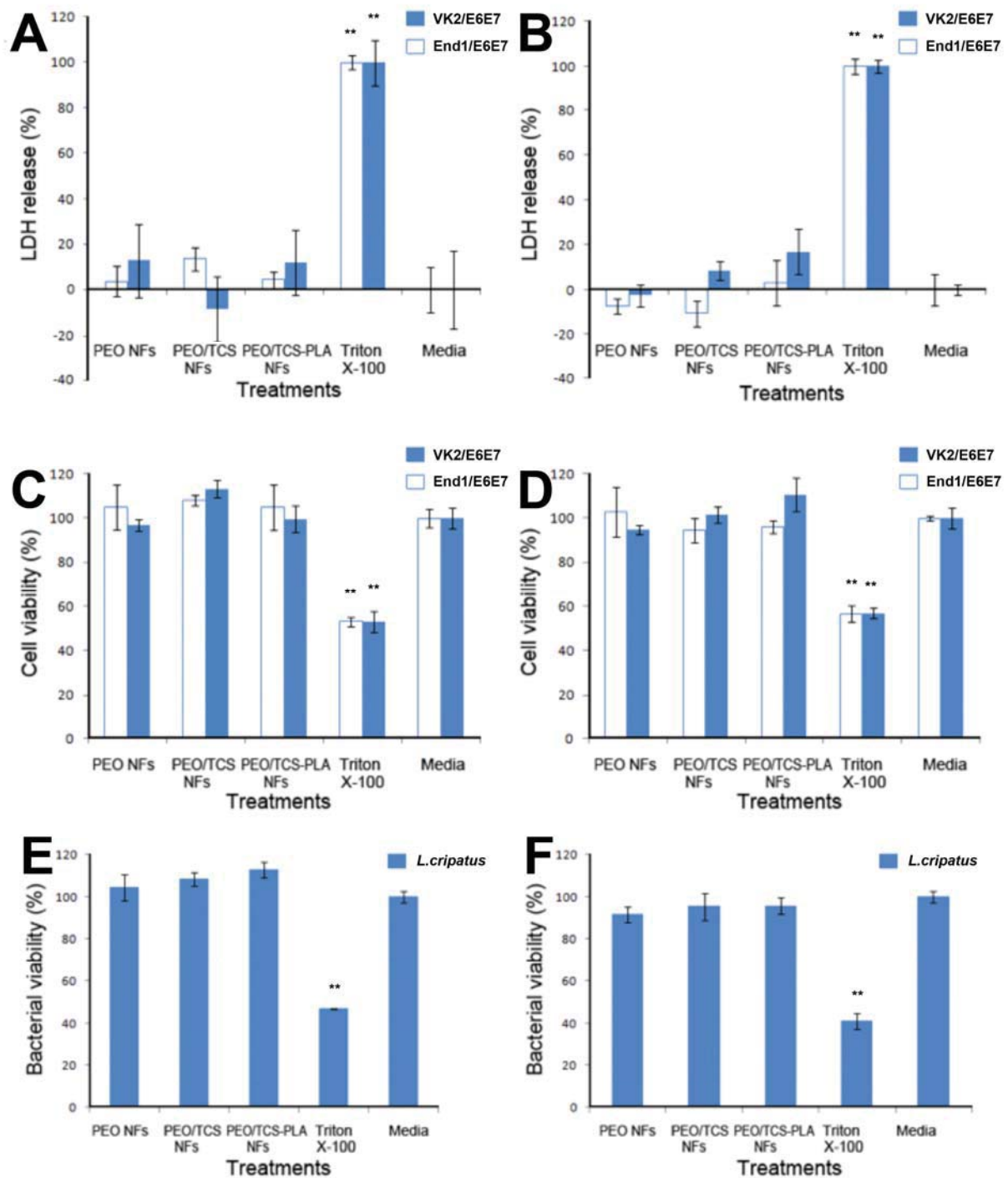


Fig. 6-6 Cytotoxicity study of PEO nanofibers (NFs), PEO/TCS NFs, and PEO/TCS-PLA NFs. CS and TCS NPs. LDH release of VK2/E6E7 cell line (A) and End1/E6E7 cell line (B), percent viability of VK2/E6E7 cell line (C) and End1/E6E7 cell line (D), percent viability of

L.cripatus after incubated with the NFs for 24 h (E) and 48 h (F). Data are shown as mean \pm SEM (n = 3). *: p<0.05 vs media, **: p<0.01 vs media.

6.3.6 Mucoadhesive studies

The enhanced mucoadhesive property of the core/shell NFs is based on the covalently attaching of thio-glycolic acid thiolation to CS backbone. TCS displays thiol side chains that mimic the natural structure of the secreted mucus glycoproteins. These side chains can form disulfide bound with the cysteine-rich subdomains of mucin via thiol/disulfide exchange reactions or a simple oxidation process of free thiol groups. As a result, TCS can covalently anchor in the mucus layer²⁹⁻³⁰.

The PAS technique is a widely employed colorimetric assay for the demonstration of mucin. The periodic acid solution is used as the oxidant. The periodic acid oxidizes the hydroxyl (OH) groups in the monosaccharide units of mucin, thus generating Schiff reactive aldehyde groups. These free aldehyde groups then react with the Schiff reagent to give a bright red magenta color. In this study, low (0.2 mg /ml), medium (1 mg/ml), and high (2 mg/ml) concentration of mucin is selected, due to the fact that the amount of mucin changes in the female reproductive tract during the menstrual cycle, the daily production of cervix mucus in a healthy woman is around 20–60 mg, which increases up to 700 mg/day and becomes less viscous During the midcycle, the mucus compositional differences also exist among individuals¹³⁸. As shown in Fig. 6-7, the proportion of mucin adsorption of PEO/TCS-PLA NFs is similar to that of PEO/TCS NFs. The possible reason is that the thiolated groups exposed at the surface of the PEO/TCS-PLA NFs are no less than that exposed at the surface of the PEO/TCS NFs, since TCS forms discontinuous, large, or small beads while TCS-PLA blend forms continuous and uniform fiber shell. In contrast, little

mucin is adsorbed on PEO NFs. These results confirm that both PEO/TCS and PEO/TCS-PLA NFs have the ability to adsorb mucin and potentially enhance mucoadhesion *in vivo*.

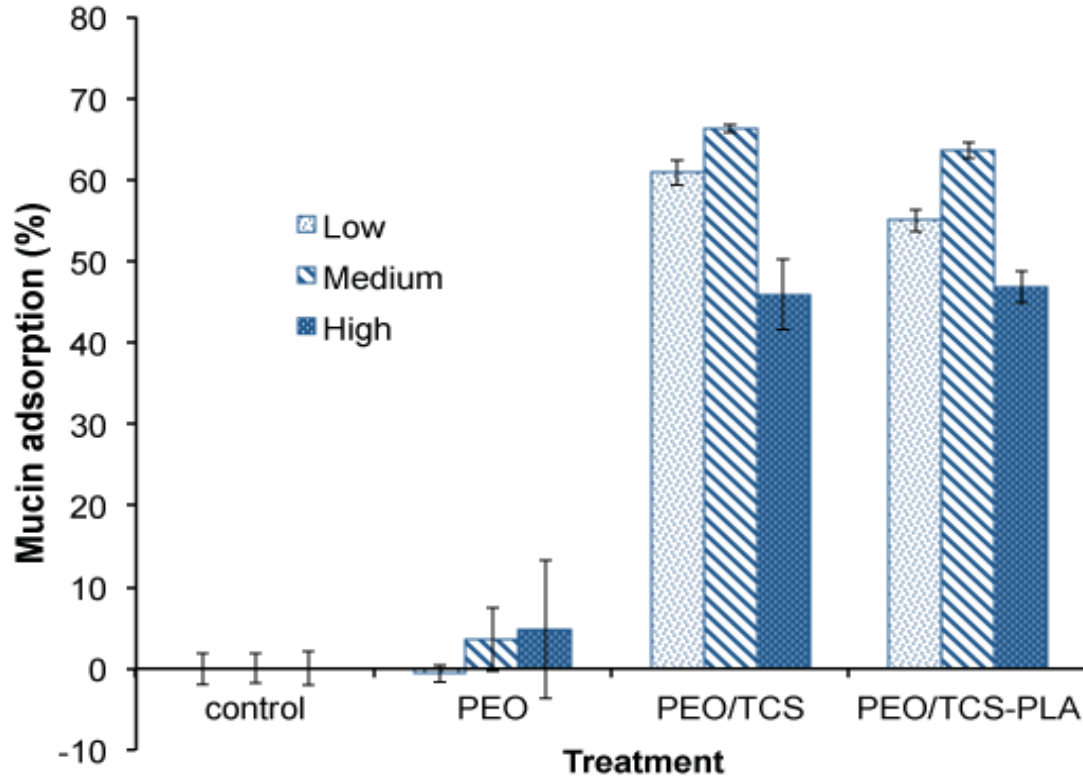


Fig. 6-7 Adsorption of mucin on PEO, PEO/TCS and PEO/TCS-PLA nanofibers (NFs).

The mucoadhesion of PEO/TCS and PEO/TCS-PLA NFs are assessed following the infusion procedure. As illustrated in Fig. 6-8, after rinsing using VFS, the fluorescence intensity of both NFs is not markedly reduced. Both NFs are spontaneously adsorbed to the surface of the porcine vaginal tissue, as a strong interaction exists between TCS and mucin. Moreover, the interconnected NFs inseparably associates with each other, and thus constituting a network, even if part of NFs is detached from the tissue the integrated network would not peel off. These results confirm that both PEO/TCS and PEO/TCS-PLA NFs are resistant to vaginal fluid and subsequently might increase the retention time *in vivo*.

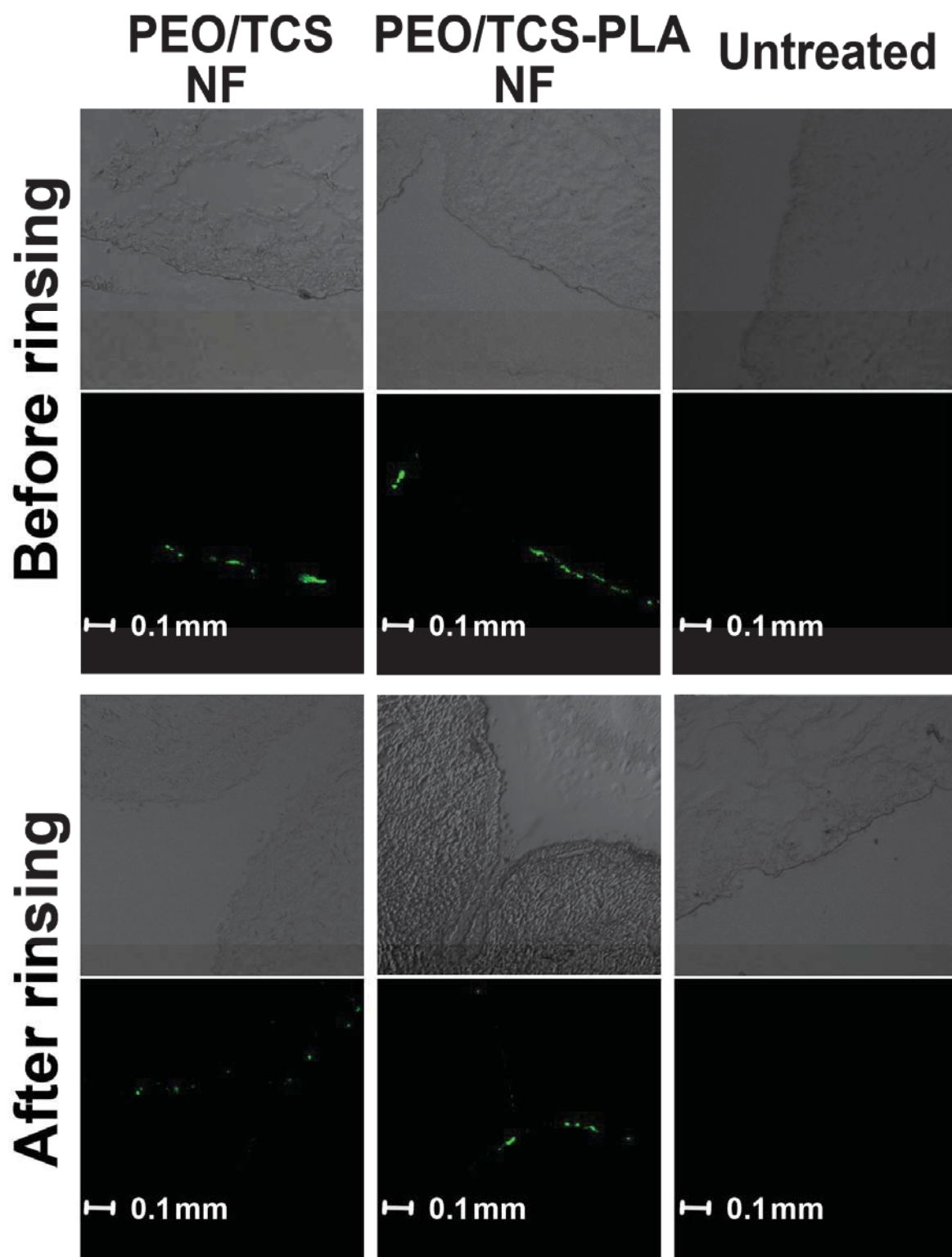


Fig. 6-8 Fluorescence microcopy of thin sections of porcine vaginal tissue treated with PEO/TCS nanofibers (NFs), PEO/TCS-PLA NFs, and VFS without NFs before (top row) and

after (bottom row) rinsing by vaginal fluid simulant buffer. Scale bar = 0.1 mm.

6.3.7 *In vivo* safety studies in C57Bl/6 mice.

In order to determine whether the exposure of the MPs results in inflammation and toxicity to the vaginal mucosa, the H & E stained vaginal sections of the mouse are evaluated. The PEO/TCS-PLA NFs contain the equivalent to approximately 65 mg/kg TFV, it has greatly exceeded the effective dose, 8 mg/kg, after conversion from the effective human dose (40 mg/person)^{23b} base on body surface area (BSA) normalization method¹⁶⁸. Fig. 6-9 shows the representative mice treated with NFs daily. Light microscopic examination indicates intact vaginal epithelium and lack of leukocyte influx in the representative vaginal sections from mouse treated with NFs daily for 1 day (Fig. 6-9 top row), and 7 days (Fig. 6-9 bottom row). In contrast, vaginal tissue sections following daily intravaginal administration of with 2% BZK (positive control), due to its well-known toxic effects on genital tracts, reveals extensive denudation of the epithelial cell layer and leukocyte infiltration (red arrows in Fig. 6-9)¹⁶⁹.

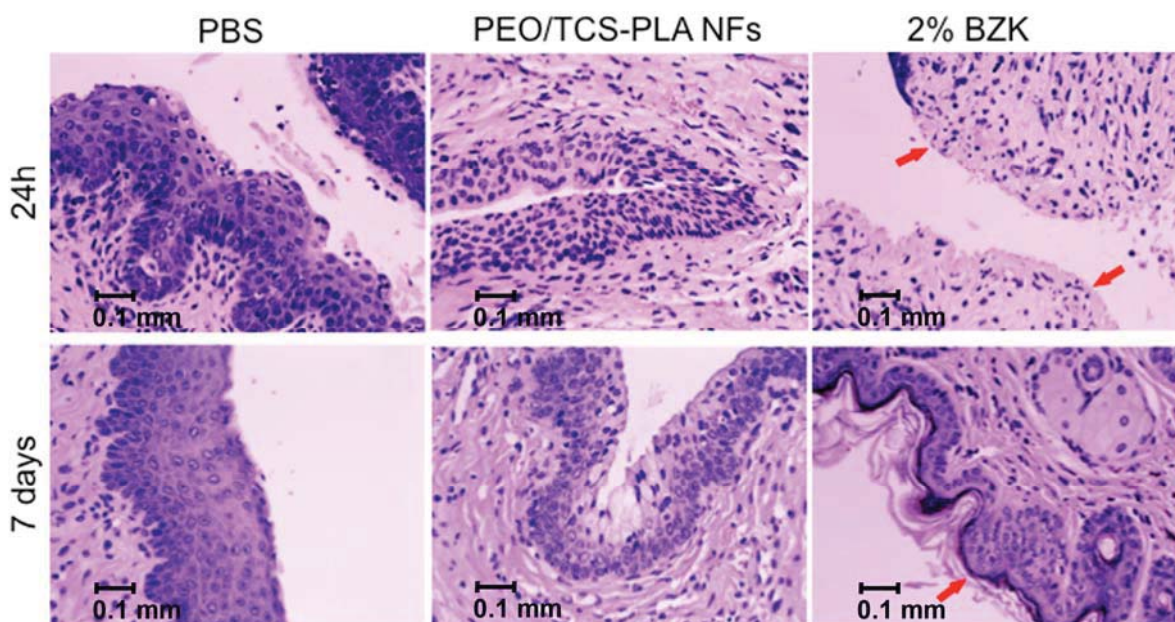


Fig. 6-9 H&E stain *in vivo* safety evaluation in C57BL/6 mice after 24 h (top row) and 7 days (bottom row) exposure with PBS, PEO/TCS-PLA nanofibers (NFs), and Benzalkonium chloride (BZK). Scale bar = 0.1 mm.

The CD45-associated protein is a lymphocyte-specific membrane protein. The increasing of the lymphocytes infiltration within the vagina epithelium indicates the vaginal inflammation¹³⁹. The CD45-positive cells distribution is studied using IHC analyses. In order to determine whether MPs treatment induced an infiltration of immune cells, After NFs application the distribution of CD45 positive cells in the vaginal tissue and the integrity of the vaginal epithelium is similar to that of PBS-treated (negative control) tissues, the number of the CD45-positive cells is elevated within the tissue treated by the 2% BZK as the red arrows shown in Fig. 6-10.

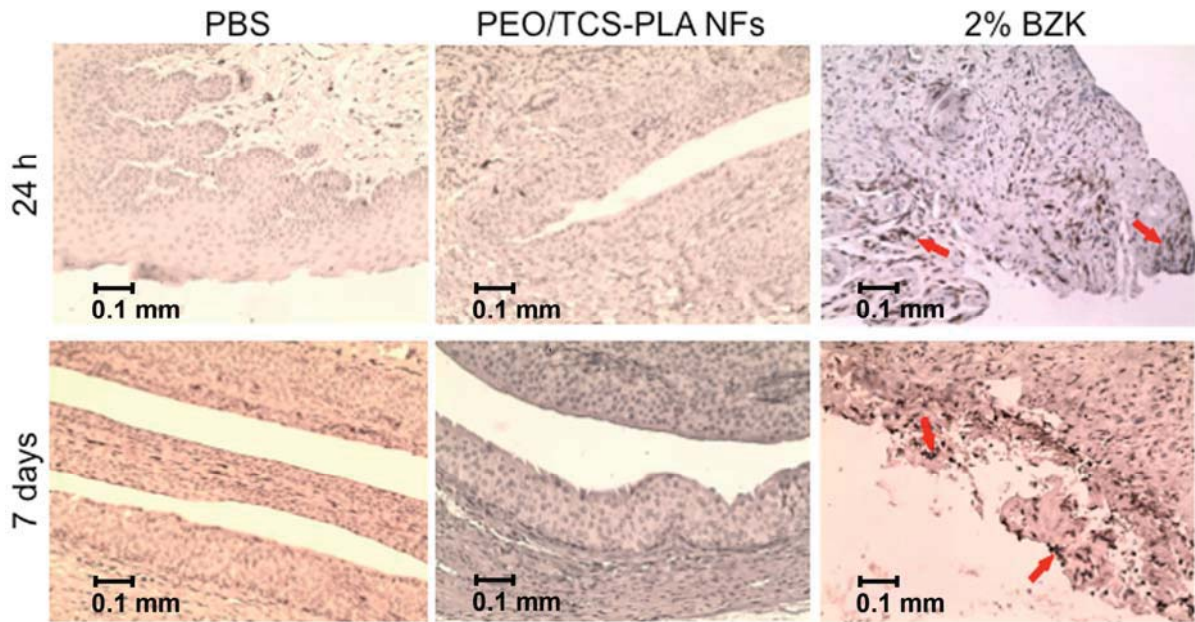


Fig. 6-10 Immunohistochemical stain *in vivo* safety evaluation in C57BL/6 mice after 24 h (top row) and 7 days (bottom row) exposure with PBS, PEO/TCS-PLA nanofibers (NFs), and Benzalkonium chloride (BZK). Scale bar = 0.1 mm.

6.4 Conclusion

In the previously reports, various TFV loaded nanomedicines are prepared with low EE% and drug loading due to the high hydrophilicity of TFV. In this study, the novel TFV loaded electrospun nanofibers are developed consisting PEO, TCS and PLA to enhance its EE%. The obtained NF can be considered as a core-shell structure, with 13% to 25% drug loading, sustained release, non-cytotoxic nature, and enhanced mucoadhesion. The *in vivo* toxicity studies indicates local non-physiological or toxicity effects.

Owning to these promising properties, TFV loaded NF can be considered as a good candidate for the delivery of water-soluble small-molecule drugs, and a promising vaginal delivery system for the prevention of HIV transmission.

CHAPTER 7

SUMMARY AND CONCLUSIONS

7.1 Summary

Women are more susceptible to HIV infection in comparison with men due to not only the human physiology, but also social, economic, and legal disadvantages. To protect women from HIV transmission, there is an urgent need to develop a formulation for the topical application of anti-HIV microbicides. The conventional vaginal formulations, such as gel, tablet, and suppository, are either lack the controlled release of drug substance or proper vaginal retention time. These limitations result in low acceptability and adherence of the patients to the dosage regime. However, these problems may be solved by novel nanomedicines. The aim of this dissertation is to test the hypothesis that a mucoadhesive polymer based nanomedicine can prolong the contact time with the vaginal tissue, provide the controlled release of the drug, and is safe *in vivo*. Various formulation and are investigated, their physicochemical properties, mucoadhesive properties, and safety are evaluated.

In Chapter 3, the size of chitosan (CS) nanoparticles (NPs) ranged from 168 nm to 277 nm. When 50% (v/v) ethanol is used as a solvent, the percent encapsulation efficiency (EE%) increases from 7% to 20%, the drug loading increased from 0.20% to 1.14% (w/w). However the size was also increased to 580 nm (n=3). It is shown that NPs are safe to both vaginal epithelial cell line and *Lactobacillus* over 48 hours. When the diameter of the NPs decreases from 900 nm to 188 nm, the mucoadhesion increases from 6% to 12%. Overall, the CS NPs are mucoadhesive and safe as a microbicide carrier, the drawback of the CS NPs is the low EE%.

In Chapter 4, the TFV loaded thiolated chitosan (TCS) NPs are prepared by ionic gelation. The particles are spherical with diameters ranged from 148 nm to 255 nm. The EE% and drug loading is 25% and 1.62% (w/w), respectively. The NPs provide a controlled release over of the drug following Higuchi model. The TCS NPs are not cytotoxic to both vaginal epithelial cell line and *Lactobacillus* over 48 h. The cellular uptake is time dependent. It is mainly occurred via caveolin mediated endocytosis. The mucoadhesive properties of TCS NPs is 5-fold higher than that of CS NPs. Compare to the CS NPs, the TCS NPs exhibit relatively higher EE%, drug loading, and mucoadhesion.

In Chapter 5, the microparticles (MPs) are successfully formulated with an average diameter ranges from 2 μm to 3 μm with a drug loading of 7-12% (w/w). The MPs show a controlled drug release in both vaginal and seminal fluid simulant buffers. The MPs are found to have a high mucoadhesion (~50 folds at a higher ratio, and ~20 folds at a lower ratio of mucin: MPs) compare to non-layered sodium alginate MPs in both vaginal fluid and semen fluid simulant buffers. The multilayer MPs are non-cytotoxic to vaginal and endocervical epithelial cells. Histological analysis of the female C57BL/6 mice genital tract and other organs shows no damage upon once-daily administration of MPs up to 24 h and 7 days. The drug loading of the TCS MPs is significantly enhanced (from 1.62% to 12.73%) compare to that of the TCS NPs. However, the mucoadhesion of the MPs is slightly lower than that of the NPs due to the larger particle size.

In chapter 6, the TCS core/shell nanofibers (NFs) are fabricated by a coaxial electrospinning technique. The drug loading is 13%-25% (w/w), the EE% is about 100% because no loss of material during the electrospinning process. The NFs exhibit smooth surface with average diameters in the range of 50 to 100 nm. The NFs are non-cytotoxic at

the concentration of 1 mg/ml. The core-shell NFs exhibit a release kinetic following Weibull model, and are 40-60 fold more bioadhesive than NFs made solely with PEO. H&E and immunohistochemical (CD45) staining analysis of genital tract indicates non-toxicity and non-inflammatory effects of the NFs daily treatment for up to 7 days. The TCS NFs exhibit both high drug loading and high mucoadhesion; these data highlight the potential of TCS NFs templates for the topical vaginal delivery of anti-HIV/AIDS microbicides.

7.2 Future perspective

The application of the nanomedicines to the vagina may be beneficial to patients by causing much less discomfort and reducing the frequency of the administration simultaneously. However, further in-depth studies of this drug delivery system are needed. Can these nanomedicines delivery other small molecular and biological microbicides, such as maraviroc and sifuvirtide? What is the effectiveness of the antiviral activity of the nanomedicines? What is the retention time of the TCS nanomedicines in the body of animals? What is the longer term effect of the formulations to vaginal tissue? There are numerous questions that are exigent to be answered.

REFERENCES

1. Hackley, V. A.; Ferraris, C. F., The use of nomenclature in dispersion science and technology. *NIST Recommended Practice Guide. Special Publication*. **2001**, 960, 76.
2. AIDS epidemic update. In UNAIDS (ed) (UNAIDS, ed),. *WHO Library Cataloguing-in-Publication Data* **2007**.
3. Krishnan, S.; Dunbar, M. S.; Minnis, A. M.; Medlin, C. A.; Gerdt, C. E.; Padian, N. S., Poverty, gender inequities, and women's risk of human immunodeficiency virus/AIDS. *Ann N Y Acad Sci* **2008**, 1136, 101-10.
4. UNAIDS. *Report on the Global AIDS Epidemic* **2006**.
5. Askew, I.; Berer, M., The contribution of sexual and reproductive health services to the fight against HIV/AIDS: a review. *Reprod Health Matters* **2003**, 11 (22), 51-73.
6. Weber, J.; Desai, K.; Darbyshire, J., The development of vaginal microbicides for the prevention of HIV transmission. *PLoS Med* **2005**, 2 (5), e142.
7. Ndesendo, V. M.; Pillay, V.; Choonara, Y. E.; Buchmann, E.; Bayever, D. N.; Meyer, L. C., A review of current intravaginal drug delivery approaches employed for the prophylaxis of HIV/AIDS and prevention of sexually transmitted infections. *AAPS PharmSciTech* **2008**, 9 (2), 505-20.
8. Mamo, T.; Moseman, E. A.; Kolishetti, N.; Salvador-Morales, C.; Shi, J.; Kuritzkes, D. R.; Langer, R.; von Andrian, U.; Farokhzad, O. C., Emerging nanotechnology approaches for HIV/AIDS treatment and prevention. *Nanomedicine (Lond)* **2010**, 5 (2), 269-85.
9. Sosnik, A., Nanotechnology contributions to the pharmacotherapy of pediatric HIV: a dual scientific and ethical challenge and a still pending agenda. *Nanomedicine (Lond)* **2010**, 5 (6), 833-7.

10. Wilks, M.; Wiggins, R.; Whiley, A.; Hennessy, E.; Warwick, S.; Porter, H.; Corfield, A.; Millar, M., Identification and H₂O₂ production of vaginal lactobacilli from pregnant women at high risk of preterm birth and relation with outcome. *J Clin Microbiol* **2004**, *42* (2), 713-7.
11. Stone, A., Microbicides: a new approach to preventing HIV and other sexually transmitted infections. *Nature reviews. Drug discovery* **2002**, *1* (12), 977-85.
12. (a) Cohen, C. R.; Lingappa, J. R.; Baeten, J. M.; Ngayo, M. O.; Spiegel, C. A.; Hong, T.; Donnell, D.; Celum, C.; Kapiga, S.; Delany, S.; Bukusi, E. A., Bacterial vaginosis associated with increased risk of female-to-male HIV-1 transmission: a prospective cohort analysis among African couples. *PLoS Med* **2012**, *9* (6), e1001251; (b) Low, N.; Chersich, M. F.; Schmidlin, K.; Egger, M.; Francis, S. C.; van de Wijgert, J. H.; Hayes, R. J.; Baeten, J. M.; Brown, J.; Delany-Moretlwe, S.; Kaul, R.; McGrath, N.; Morrison, C.; Myer, L.; Temmerman, M.; van der Straten, A.; Watson-Jones, D.; Zwahlen, M.; Hilber, A. M., Intravaginal practices, bacterial vaginosis, and HIV infection in women: individual participant data meta-analysis. *PLoS Med* **2011**, *8* (2), e1000416.
13. (a) Baleta, A., Concern voiced over "dry sex" practices in South Africa. *Lancet* **1998**, *352* (9136), 1292; (b) Padian, N. S.; Shiboski, S. C.; Jewell, N. P., The effect of number of exposures on the risk of heterosexual HIV transmission. *J Infect Dis* **1990**, *161* (5), 883-7; (c) Guimaraes, M. D.; Vlahov, D.; Castilho, E. A., Postcoital vaginal bleeding as a risk factor for transmission of the human immunodeficiency virus in a heterosexual partner study in Brazil. Rio de Janeiro Heterosexual Study Group. *Arch Intern Med* **1997**, *157* (12), 1362-8.
14. (a) Blish, C. A.; McClelland, R. S.; Richardson, B. A.; Jaoko, W.; Mandaliya, K.; Baeten, J. M.; Overbaugh, J., Genital Inflammation Predicts HIV-1 Shedding Independent of Plasma

Viral Load and Systemic Inflammation. *Journal of acquired immune deficiency syndromes* **2012**, *61* (4), 436-40; (b) Mayer, K. H.; Venkatesh, K. K., Interactions of HIV, other sexually transmitted diseases, and genital tract inflammation facilitating local pathogen transmission and acquisition. *Am J Reprod Immunol* **2011**, *65* (3), 308-16; (c) Morgan, D.; Mahe, C.; Okongo, J. M.; Mayanja, B.; Whitworth, J. A., Genital ulceration in rural Uganda: sexual activity, treatment-seeking behavior, and the implications for HIV control. *Sex Transm Dis* **2001**, *28* (8), 431-6; (d) O'Farrell, N., Transmission of HIV: genital ulceration, sexual behaviour, and circumcision. *Lancet* **1989**, *2* (8672), 1157.

15. (a) Laskey, S. B.; Siliciano, R. F., A mechanistic theory to explain the efficacy of antiretroviral therapy. *Nature reviews. Microbiology* **2014**, *12* (11), 772-80; (b) Engelman, A.; Cherepanov, P., The structural biology of HIV-1: mechanistic and therapeutic insights. *Nature reviews. Microbiology* **2012**, *10* (4), 279-90.

16. (a) das Neves, J.; Michiels, J.; Arien, K. K.; Vanham, G.; Amiji, M.; Bahia, M. F.; Sarmiento, B., Polymeric Nanoparticles Affect the Intracellular Delivery, Antiretroviral Activity and Cytotoxicity of the Microbicide Drug Candidate Dapivirine. *Pharm Res* **2011**; (b) Wan, L.; Pooyan, S.; Hu, P.; Leibowitz, M. J.; Stein, S.; Sinko, P. J., Peritoneal macrophage uptake, pharmacokinetics and biodistribution of macrophage-targeted PEG-fMLF (N-formyl-methionyl-leucyl-phenylalanine) nanocarriers for improving HIV drug delivery. *Pharm Res* **2007**, *24* (11), 2110-9; (c) Mbopi-Keou, F. X.; Trottier, S.; Omar, R. F.; Nkele, N. N.; Fokoua, S.; Mbu, E. R.; Domingo, M. C.; Giguere, J. F.; Piret, J.; Mwatha, A.; Masse, B.; Bergeron, M. G., A randomized, double-blind, placebo-controlled Phase II extended safety study of two Invisible Condom formulations in Cameroonian women. *Contraception* **2010**, *81* (1), 79-85; (d) McCormack, S.; Ramjee, G.; Kamali, A.; Rees, H.;

Crook, A. M.; Gafos, M.; Jentsch, U.; Pool, R.; Chisembe, M.; Kapiga, S.; Mutemwa, R.; Vallely, A.; Palanee, T.; Sookrajh, Y.; Lacey, C. J.; Darbyshire, J.; Grosskurth, H.; Profy, A.; Nunn, A.; Hayes, R.; Weber, J., PRO2000 vaginal gel for prevention of HIV-1 infection (Microbicides Development Programme 301): a phase 3, randomised, double-blind, parallel-group trial. *Lancet* **2010**, 376 (9749), 1329-37.

17. Sanchez-Rodriguez, J.; Vacas-Cordoba, E.; Gomez, R.; De La Mata, F. J.; Munoz-Fernandez, M. A., Nanotech-derived topical microbicides for HIV prevention: the road to clinical development. *Antiviral research* **2015**, 113, 33-48.

18. (a) Zhang, T.; Zhang, C.; Agrahari, V.; Murowchick, J. B.; Oyler, N. A.; Youan, B. B., Spray drying tenofovir loaded mucoadhesive and pH-sensitive microspheres intended for HIV prevention. *Antiviral research* **2013**, 97 (3), 334-46; (b) Date, A. A.; Destache, C. J., A review of nanotechnological approaches for the prophylaxis of HIV/AIDS. *Biomaterials* **2013**, 34 (26), 6202-28.

19. (a) Akanbi, M. O.; Scarsi, K. K.; Taiwo, B.; Murphy, R. L., Combination nucleoside/nucleotide reverse transcriptase inhibitors for treatment of HIV infection. *Expert opinion on pharmacotherapy* **2012**, 13 (1), 65-79; (b) Cihlar, T.; Ray, A. S., Nucleoside and nucleotide HIV reverse transcriptase inhibitors: 25 years after zidovudine. *Antiviral research* **2010**, 85 (1), 39-58; (c) De Clercq, E., Anti-HIV drugs: 25 compounds approved within 25 years after the discovery of HIV. *International journal of antimicrobial agents* **2009**, 33 (4), 307-20.

20. Grim, S. A.; Romanelli, F., Tenofovir disoproxil fumarate. *Ann Pharmacother* **2003**, 37 (6), 849-59.

21. (a) Abdool Karim, Q.; Abdool Karim, S. S.; Frohlich, J. A.; Grobler, A. C.; Baxter, C.;

Mansoor, L. E.; Kharsany, A. B.; Sibeko, S.; Mlisana, K. P.; Omar, Z.; Gengiah, T. N.; Maarschalk, S.; Arulappan, N.; Mlotshwa, M.; Morris, L.; Taylor, D., Effectiveness and safety of tenofovir gel, an antiretroviral microbicide, for the prevention of HIV infection in women. *Science* **2010**, 329 (5996), 1168-74; (b) Johnson, T. J.; Gupta, K. M.; Fabian, J.; Albright, T. H.; Kiser, P. F., Segmented polyurethane intravaginal rings for the sustained combined delivery of antiretroviral agents dapivirine and tenofovir. *Eur J Pharm Sci* **2010**, 39 (4), 203-12.

22. Antimisiaris, S. G.; Mourtas, S., Recent advances on anti-HIV vaginal delivery systems development. *Advanced drug delivery reviews* **2015**.

23. (a) Garg, S.; Goldman, D.; Krumme, M.; Rohan, L. C.; Smoot, S.; Friend, D. R., Advances in development, scale-up and manufacturing of microbicide gels, films, and tablets. *Antiviral Res* **2010**, 88 Suppl 1, S19-29; (b) Abdool Karim, Q.; Abdool Karim, S. S.; Frohlich, J. A.; Grobler, A. C.; Baxter, C.; Mansoor, L. E.; Kharsany, A. B.; Sibeko, S.; Mlisana, K. P.; Omar, Z.; Gengiah, T. N.; Maarschalk, S.; Arulappan, N.; Mlotshwa, M.; Morris, L.; Taylor, D.; Group, C. T., Effectiveness and safety of tenofovir gel, an antiretroviral microbicide, for the prevention of HIV infection in women. *Science* **2010**, 329 (5996), 1168-74; (c) Joglekar, N.; Joshi, S.; Kakde, M.; Fang, G.; Cianciola, M.; Reynolds, S.; Mehendale, S., Acceptability of PRO2000 vaginal gel among HIV un-infected women in Pune, India. *AIDS Care* **2007**, 19 (6), 817-21; (d) Mayer, K. H.; Maslankowski, L. A.; Gai, F.; El-Sadr, W. M.; Justman, J.; Kwiecien, A.; Masse, B.; Eshleman, S. H.; Hendrix, C.; Morrow, K.; Rooney, J. F.; Soto-Torres, L., Safety and tolerability of tenofovir vaginal gel in abstinent and sexually active HIV-infected and uninfected women. *AIDS* **2006**, 20 (4), 543-51; (e) Rosen, R. K.; Morrow, K. M.; Carballo-Diequez, A.; Mantell, J. E.; Hoffman, S.; Gai, F.; Maslankowski, L.;

El-Sadr, W. M.; Mayer, K. H., Acceptability of tenofovir gel as a vaginal microbicide among women in a phase I trial: a mixed-methods study. *J Womens Health (Larchmt)* **2008**, *17* (3), 383-92.

24. Karim, Q. A.; Karim, S. S.; Frohlich, J. A.; Grobler, A. C.; Baxter, C.; Mansoor, L. E.; Kharsany, A. B.; Sibeko, S.; Mlisana, K. P.; Omar, Z.; Gengiah, T. N.; Maarschalk, S.; Arulappan, N.; Mlotshwa, M.; Morris, L.; Taylor, D., Effectiveness and Safety of Tenofovir Gel, an Antiretroviral Microbicide, for the Prevention of HIV Infection in Women. *Science* **2010**.

25. Khutoryanskiy, V. V., Advances in mucoadhesion and mucoadhesive polymers. *Macromolecular bioscience* **2011**, *11* (6), 748-64.

26. Shaikh, R.; Raj Singh, T. R.; Garland, M. J.; Woolfson, A. D.; Donnelly, R. F., Mucoadhesive drug delivery systems. *Journal of pharmacy & bioallied sciences* **2011**, *3* (1), 89-100.

27. Hombach, J.; Bernkop-Schnurch, A., Mucoadhesive drug delivery systems. *Handbook of experimental pharmacology* **2010**, (197), 251-66.

28. Wang, X.; Iqbal, J.; Rahmat, D.; Bernkop-Schnurch, A., Preactivated thiomers: permeation enhancing properties. *International journal of pharmaceutics* **2012**, *438* (1-2), 217-24.

29. Bernkop-Schnurch, A., Thiomers: a new generation of mucoadhesive polymers. *Adv Drug Deliv Rev* **2005**, *57* (11), 1569-82.

30. Leitner, V. M.; Walker, G. F.; Bernkop-Schnurch, A., Thiolated polymers: evidence for the formation of disulphide bonds with mucus glycoproteins. *European journal of pharmaceutics and biopharmaceutics : official journal of Arbeitsgemeinschaft fur*

Pharmazeutische Verfahrenstechnik e.V **2003**, 56 (2), 207-14.

31. Duan, J.; Zhang, Y.; Han, S.; Chen, Y.; Li, B.; Liao, M.; Chen, W.; Deng, X.; Zhao, J.; Huang, B., Synthesis and in vitro/in vivo anti-cancer evaluation of curcumin-loaded chitosan/poly(butyl cyanoacrylate) nanoparticles. *Int J Pharm* **2010**.

32. (a) Hamidi, M.; Azadi, A.; Rafiei, P., Hydrogel nanoparticles in drug delivery. *Adv Drug Deliv Rev* **2008**, 60 (15), 1638-49; (b) Zhang, S.; Kawakami, K., One-step preparation of chitosan solid nanoparticles by electrospray deposition. *Int J Pharm* **2010**, 397 (1-2), 211-7.

33. Sun, W.; Mao, S.; Wang, Y.; Junyaprasert, V. B.; Zhang, T.; Na, L.; Wang, J., Bioadhesion and oral absorption of enoxaparin nanocomplexes. *Int J Pharm* **2010**, 386 (1-2), 275-81.

34. Nasti, A.; Zaki, N. M.; de Leonardis, P.; Ungphaiboon, S.; Sansongsak, P.; Rimoli, M. G.; Tirelli, N., Chitosan/TPP and chitosan/TPP-hyaluronic acid nanoparticles: systematic optimisation of the preparative process and preliminary biological evaluation. *Pharm Res* **2009**, 26 (8), 1918-30.

35. (a) Agnihotri, S. A.; Mallikarjuna, N. N.; Aminabhavi, T. M., Recent advances on chitosan-based micro- and nanoparticles in drug delivery. *Journal of controlled release : official journal of the Controlled Release Society* **2004**, 100 (1), 5-28; (b) Pandey, R.; Ahmad, Z.; Sharma, S.; Khuller, G. K., Nano-encapsulation of azole antifungals: potential applications to improve oral drug delivery. *Int J Pharm* **2005**, 301 (1-2), 268-76.

36. Plapied, L.; Vandermeulen, G.; Vroman, B.; Preat, V.; des Rieux, A., Bioadhesive nanoparticles of fungal chitosan for oral DNA delivery. *Int J Pharm* **2010**, 398 (1-2), 210-8.

37. Sayin, B.; Somavarapu, S.; Li, X. W.; Sesardic, D.; Senel, S.; Alpar, O. H., TMC-MCC (N-trimethyl chitosan-mono-N-carboxymethyl chitosan) nanocomplexes for mucosal

delivery of vaccines. *Eur J Pharm Sci* **2009**, 38 (4), 362-9.

38. Calvo, P.; Remunan-Lopez, C.; Vila-Jato, J. L.; Alonso, M. J., Chitosan and chitosan/ethylene oxide-propylene oxide block copolymer nanoparticles as novel carriers for proteins and vaccines. *Pharm Res* **1997**, 14 (10), 1431-6.

39. Mohammadpourounghi, N.; Behfar, A.; Ezabadi, A.; Zolfagharian, H.; Heydari, M., Preparation of chitosan nanoparticles containing Naja naja oxiana snake venom. *Nanomedicine* **2010**, 6 (1), 137-43.

40. Tiyaaboonchai, W.; Limpeanchob, N., Formulation and characterization of amphotericin B-chitosan-dextran sulfate nanoparticles. *Int J Pharm* **2007**, 329 (1-2), 142-9.

41. Park, J. H.; Saravanakumar, G.; Kim, K.; Kwon, I. C., Targeted delivery of low molecular drugs using chitosan and its derivatives. *Adv Drug Deliv Rev* **2010**, 62 (1), 28-41.

42. Bei, D.; Marszalek, J.; Youan, B. B., Formulation of dacarbazine-loaded cubosomes-part I: influence of formulation variables. *AAPS PharmSciTech* **2009**, 10 (3), 1032-9.

43. Fernandez-Urrusuno, R.; Calvo, P.; Remunan-Lopez, C.; Vila-Jato, J. L.; Alonso, M. J., Enhancement of nasal absorption of insulin using chitosan nanoparticles. *Pharm Res* **1999**, 16 (10), 1576-81.

44. Sano, M.; Hosoya, O.; Takao, S.; Seki, T.; Kawaguchi, T.; Sugibayashi, K.; Juni, K.; Morimoto, Y., Relationship between Solubility of Chitosan in Alcoholic Solution and Its Gelation. *Chemical and pharmaceutical bulletin* **1999**, 47 (7), 1044-1046.

45. Sassi, A. B.; Isaacs, C. E.; Moncla, B. J.; Gupta, P.; Hillier, S. L.; Rohan, L. C., Effects of physiological fluids on physical-chemical characteristics and activity of topical vaginal microbicide products. *J Pharm Sci* **2008**, 97 (8), 3123-39.

46. Owen, D. H.; Katz, D. F., A vaginal fluid simulant. *Contraception* **1999**, 59 (2), 91-5.

47. Lackman-Smith, C.; Osterling, C.; Luckenbaugh, K.; Mankowski, M.; Snyder, B.; Lewis, G.; Paull, J.; Profy, A.; Ptak, R. G.; Buckheit, R. W., Jr.; Watson, K. M.; Cummins, J. E., Jr.; Sanders-Beer, B. E., Development of a comprehensive human immunodeficiency virus type 1 screening algorithm for discovery and preclinical testing of topical microbicides. *Antimicrob Agents Chemother* **2008**, *52* (5), 1768-81.
48. (a) Klebanoff, S. J.; Coombs, R. W., Viricidal effect of *Lactobacillus acidophilus* on human immunodeficiency virus type 1: possible role in heterosexual transmission. *J Exp Med* **1991**, *174* (1), 289-92; (b) Quayle, A. J., The innate and early immune response to pathogen challenge in the female genital tract and the pivotal role of epithelial cells. *J Reprod Immunol* **2002**, *57* (1-2), 61-79.
49. Thongborisute, J.; Takeuchi, H.; Yamamoto, H.; Kawashima, Y., Visualization of the penetrative and mucoadhesive properties of chitosan and chitosan-coated liposomes through the rat intestine. *J Liposome Res* **2006**, *16* (2), 127-41.
50. Ma, Z.; Lim, L. Y., Uptake of chitosan and associated insulin in Caco-2 cell monolayers: a comparison between chitosan molecules and chitosan nanoparticles. *Pharm Res* **2003**, *20* (11), 1812-9.
51. Tobyna, M.; Johnsona, J.; Dettmar, P., Factors affecting in vitro gastric mucoadhesion IV. Influence of tablet excipients, surfactants and salts on the observed mucoadhesion of polymers. *European Journal of Pharmaceutics and Biopharmaceutics* **1997**, *43* (1), 65-71.
52. Jackson, S. J.; Perkins, A. C., In vitro assessment of the mucoadhesion of cholestyramine to porcine and human gastric mucosa. *Eur J Pharm Biopharm* **2001**, *52* (2), 121-7.
53. Grabovac, V.; Guggi, D.; Bernkop-Schnurch, A., Comparison of the mucoadhesive properties of various polymers. *Adv Drug Deliv Rev* **2005**, *57* (11), 1713-23.

54. Dudhania, A.; Kosaraju, S., Bioadhesive chitosan nanoparticles: Preparation and characterization. *Carbohydrate Polymers* **2010**, *81* 243–251.
55. Vander Heyden, Y.; Nijhuis, A.; Smeyers-Verbeke, J.; Vandeginste, B. G.; Massart, D. L., Guidance for robustness/ruggedness tests in method validation. *J Pharm Biomed Anal* **2001**, *24* (5-6), 723-53.
56. Miller, J. C.; Miller, J. N., Statistics for Analytical Chemistry. . 3 ed., New York: Ellis Horwood **1993**.
57. Bei, D.; Marszalek, J.; Youan, B. B., Formulation of dacarbazine-loaded Cubosomes--part II: influence of process parameters. *AAPS PharmSciTech* **2009**, *10* (3), 1040-7.
58. (a) Grayson, A. C.; Doody, A. M.; Putnam, D., Biophysical and structural characterization of polyethylenimine-mediated siRNA delivery in vitro. *Pharm Res* **2006**, *23* (8), 1868-76; (b) Woodrow, K. A.; Cu, Y.; Booth, C. J.; Saucier-Sawyer, J. K.; Wood, M. J.; Saltzman, W. M., Intravaginal gene silencing using biodegradable polymer nanoparticles densely loaded with small-interfering RNA. *Nat Mater* **2009**, *8* (6), 526-33.
59. Wu, Y.; Wang, Y.; Luo, G.; Dai, Y., In situ preparation of magnetic Fe₃O₄-chitosan nanoparticles for lipase immobilization by cross-linking and oxidation in aqueous solution. *Bioresour Technol* **2009**, *100* (14), 3459-64.
60. Hu, M.; Li, Y.; Decker, E. A.; Xiao, H.; McClements, D. J., Influence of tripolyphosphate cross-linking on the physical stability and lipase digestibility of chitosan-coated lipid droplets. *J Agric Food Chem* **2010**, *58* (2), 1283-9.
61. Van Gelder, J.; Witvrouw, M.; Pannecouque, C.; Henson, G.; Bridger, G.; Naesens, L.; De Clercq, E.; Annaert, P.; Shafiee, M.; Van den Mooter, G.; Kinget, R.; Augustijns, P.,

Evaluation of the potential of ion pair formation to improve the oral absorption of two potent antiviral compounds, AMD3100 and PMPA. *Int J Pharm* **1999**, *186* (2), 127-36.

62. Denkba, E. D.; Seyyalb, M.; Pikin, E., Implantable 5-fluorouracil loaded chitosan scaffolds prepared by wet spinning. *Journal of Membrane Science* **2000**, *172* (1-2,1), 33-38.

63. Yu, C. Y.; Cao, H.; Zhang, X. C.; Zhou, F. Z.; Cheng, S. X.; Zhang, X. Z.; Zhuo, R. X., Hybrid nanospheres and vesicles based on pectin as drug carriers. *Langmuir* **2009**, *25* (19), 11720-6.

64. Ma, L.; Liu, C., Preparation of chitosan microspheres by ionotropic gelation under a high voltage electrostatic field for protein delivery. *Colloids Surf B Biointerfaces* **2010**, *75* (2), 448-53.

65. Tadros, T.; Izquierdo, P.; Esquena, J.; Solans, C., Formation and stability of nano-emulsions. *Adv Colloid Interface Sci* **2004**, *108-109*, 303-18.

66. Lide, D. R., 2009-2010; p 8-52.

67. Costa, P.; Sousa Lobo, J. M., Modeling and comparison of dissolution profiles. *European journal of pharmaceutical sciences : official journal of the European Federation for Pharmaceutical Sciences* **2001**, *13* (2), 123-33.

68. Bhatt, D. C.; Dhake, A. S.; Khar, R. K.; Mishra, D. N., Development and in-vitro evaluation of transdermal matrix films of metoprolol tartrate. *Yakugaku Zasshi* **2008**, *128* (9), 1325-31.

69. (a) Wu, Y.; Yang, W.; Wang, C.; Hu, J.; Fu, S., Chitosan nanoparticles as a novel delivery system for ammonium glycyrrhizinate. *Int J Pharm* **2005**, *295* (1-2), 235-45; (b) Bao, H.; Li, L.; Zhang, H., Influence of cetyltrimethylammonium bromide on physicochemical properties and microstructures of chitosan-TPP nanoparticles in aqueous solutions. *J Colloid Interface*

Sci **2008**, 328 (2), 270-7.

70. Cordova, M.; Cheng, M.; Trejo, J.; Johnson, S. J.; Willhite, G. P.; Liang, J. T.; Berkland, C., Delayed HPAM gelation via transient sequestration of chromium in polyelectrolyte complex nanoparticles. *Macromolecules* **2008**, 41, 4398-4404.

71. Baloglu, E.; Senyigit, Z. A.; Karavana, S. Y.; Bernkop-Schnurch, A., Strategies to prolong the intravaginal residence time of drug delivery systems. *J Pharm Pharm Sci* **2009**, 12 (3), 312-36.

72. Balzarini, J.; Pannecouque, C.; De Clercq, E.; Aquaro, S.; Perno, C. F.; Egberink, H.; Holy, A., Antiretrovirus activity of a novel class of acyclic pyrimidine nucleoside phosphonates. *Antimicrob Agents Chemother* **2002**, 46 (7), 2185-93.

73. Squier, C. A.; Mantz, M. J.; Schlievert, P. M.; Davis, C. C., Porcine vagina ex vivo as a model for studying permeability and pathogenesis in mucosa. *J Pharm Sci* **2008**, 97 (1), 9-21.

74. (a) Bravo-Osuna, I.; Vauthier, C.; Farabollini, A.; Palmieri, G. F.; Ponchel, G., Mucoadhesion mechanism of chitosan and thiolated chitosan-poly(isobutyl cyanoacrylate) core-shell nanoparticles. *Biomaterials* **2007**, 28 (13), 2233-43; (b) De Campos, A. M.; Sanchez, A.; Gref, R.; Calvo, P.; Alonso, M. J., The effect of a PEG versus a chitosan coating on the interaction of drug colloidal carriers with the ocular mucosa. *Eur J Pharm Sci* **2003**, 20 (1), 73-81; (c) Ikinici, G.; Senel, S.; Akincibay, H.; Kas, S.; Ercis, S.; Wilson, C. G.; Hincal, A. A., Effect of chitosan on a periodontal pathogen *Porphyromonas gingivalis*. *Int J Pharm* **2002**, 235 (1-2), 121-7.

75. (a) Jung, T.; Kamm, W.; Breitenbach, A.; Kaiserling, E.; Xiao, J. X.; Kissel, T., Biodegradable nanoparticles for oral delivery of peptides: is there a role for polymers to affect mucosal uptake? *Eur J Pharm Biopharm* **2000**, 50 (1), 147-60; (b) Leane, M. M.;

Nankervis, R.; Smith, A.; Illum, L., Use of the ninhydrin assay to measure the release of chitosan from oral solid dosage forms. *Int J Pharm* **2004**, *271* (1-2), 241-9; (c) Vllasaliu, D.; Exposito-Harris, R.; Heras, A.; Casettari, L.; Garnett, M.; Illum, L.; Stolnik, S., Tight junction modulation by chitosan nanoparticles: Comparison with chitosan solution. *Int J Pharm* **2010**.

76. Ghaderi, R.; Carlfors, J., Biological activity of lysozyme after entrapment in poly(d,l-lactide-co-glycolide)-microspheres. *Pharm Res* **1997**, *14* (11), 1556-62.

77. Murugesu, A.; Astete, C.; Leonardi, C.; Morgan, T.; Sabliov, C. M., Chitosan/PLGA particles for controlled release of alpha-tocopherol in the GI tract via oral administration. *Nanomedicine (Lond)* **2011**.

78. Roldo, M.; Hornof, M.; Caliceti, P.; Bernkop-Schnurch, A., Mucoadhesive thiolated chitosans as platforms for oral controlled drug delivery: synthesis and in vitro evaluation. *Eur J Pharm Biopharm* **2004**, *57* (1), 115-21.

79. Meng, J.; Sturgis, T. F.; Youan, B. B., Engineering tenofovir loaded chitosan nanoparticles to maximize microbicide mucoadhesion. *Eur J Pharm Sci* **2011**, *44* (1-2), 57-67.

80. Jang, K. I.; Lee, H. G., Stability of chitosan nanoparticles for L-ascorbic acid during heat treatment in aqueous solution. *J Agric Food Chem* **2008**, *56* (6), 1936-41.

81. Kast, C. E.; Bernkop-Schnurch, A., Thiolated polymers--thiomers: development and in vitro evaluation of chitosan-thioglycolic acid conjugates. *Biomaterials* **2001**, *22* (17), 2345-52.

82. Kätzel, U.; Vorbau, M.; Stintz, M.; Gottschalk-Gaudig, T.; Barthel, H., Dynamic light scattering for the characterization of polydisperse fractal systems: II. Relation between

structure and DLS results. *Part Part Syst Charact* **2008**, 25, 19-30.

83. Don, T. M.; Hsu, S. H.; Chiu, W. Y., Structures and Thermal Properties of Chitosan-Modified Poly(methyl methacrylate). *J Polym Sci Part A: Polym Chem* **2001**, 39, 1646–1655.

84. Nayak, A. K.; Laha, B.; Sen, K. K., Development of hydroxyapatite-ciprofloxacin bone-implants using "Quality by design". *Acta Pharm* **2011**, 61 (1), 25-36.

85. Xie, J.; Wang, C. H., Self-assembled biodegradable nanoparticles developed by direct dialysis for the delivery of paclitaxel. *Pharm Res* **2005**, 22 (12), 2079-90.

86. Pifer, M. A.; Kibuule, L. K.; Maerz, T.; Studzinski, D. M.; Baker, K. C.; Herkowitz, H. N., In vitro response of human chondrocytes to a combination of growth factors and a proteinase inhibitor. *Orthopedics* **2012**, 35 (1), 35-42.

87. Douglas, K. L.; Piccirillo, C. A.; Tabrizian, M., Cell line-dependent internalization pathways and intracellular trafficking determine transfection efficiency of nanoparticle vectors. *Eur J Pharm Biopharm* **2008**, 68 (3), 676-87.

88. (a) Ranga Rao, K. V.; Buri, P., A novel in situ method to test polymers and coated microparticles for bioadhesion. *Endocr Rev* **1989**, 52 15 (13), 265-270; (b) Albrecht, K.; Zirm, E. J.; Palmberger, T. F.; Schlocker, W.; Bernkop-Schnurch, A., Preparation of thiomers microparticles and in vitro evaluation of parameters influencing their mucoadhesive properties. *Drug Dev Ind Pharm* **2006**, 32 (10), 1149-57.

89. Lopes, L. B.; Ferreira, D. A.; de Paula, D.; Garcia, M. T.; Thomazini, J. A.; Fantini, M. C.; Bentley, M. V., Reverse hexagonal phase nanodispersion of monoolein and oleic acid for topical delivery of peptides: in vitro and in vivo skin penetration of cyclosporin A. *Pharm Res* **2006**, 23 (6), 1332-42.

90. Montgomery, D., Response surface methods and design in design and analysis of experiments. *New York: John Wiley and sons* **1995, Inc.**, 405-458.
91. Ferreira, S. L.; Bruns, R. E.; da Silva, E. G.; Dos Santos, W. N.; Quintella, C. M.; David, J. M.; de Andrade, J. B.; Breitzkreitz, M. C.; Jardim, I. C.; Neto, B. B., Statistical designs and response surface techniques for the optimization of chromatographic systems. *J Chromatogr A* **2007**, *1158* (1-2), 2-14.
92. Nagarwal, R. C.; Singh, P. N.; Kant, S.; Maiti, P.; Pandit, J. K., Chitosan nanoparticles of 5-fluorouracil for ophthalmic delivery: characterization, in-vitro and in-vivo study. *Chem Pharm Bull (Tokyo)* **2011**, *59* (2), 272-8.
93. Choi, S. U.; Bui, T.; Ho, R. J., pH-dependent interactions of indinavir and lipids in nanoparticles and their ability to entrap a solute. *J Pharm Sci* **2008**, *97* (2), 931-43.
94. Cleland, W. W., Dithiothreitol, a New Protective Reagent for Sh Groups. *Biochemistry* **1964**, *3*, 480-2.
95. Hu, B.; Pan, C.; Sun, Y.; Hou, Z.; Ye, H.; Zeng, X., Optimization of fabrication parameters to produce chitosan-tripolyphosphate nanoparticles for delivery of tea catechins. *J Agric Food Chem* **2008**, *56* (16), 7451-8.
96. Merchant, H. A.; Shoaib, H. M.; Tazeen, J.; Yousuf, R., Once-daily tablet formulation and in vitro release evaluation of cefpodoxime using hydroxypropyl methylcellulose: a technical note. *AAPS PharmSciTech* **2006**, *7* (3), 78.
97. Lee, W. A.; He, G. X.; Eisenberg, E.; Cihlar, T.; Swaminathan, S.; Mulato, A.; Cundy, K. C., Selective intracellular activation of a novel prodrug of the human immunodeficiency virus reverse transcriptase inhibitor tenofovir leads to preferential distribution and accumulation in lymphatic tissue. *Antimicrob Agents Chemother* **2005**, *49* (5), 1898-906.

98. Ubaldi, C.; Bonacchi, D.; Lorenzi, G.; Hermanns, M. I.; Pohl, C.; Baldi, G.; Unger, R. E.; Kirkpatrick, C. J., Gold nanoparticles induce cytotoxicity in the alveolar type-II cell lines A549 and NCIH441. *Part Fibre Toxicol* **2009**, *6*, 18.
99. Au, C.; Mutkus, L.; Dobson, A.; Riffle, J.; Lalli, J.; Aschner, M., Effects of nanoparticles on the adhesion and cell viability on astrocytes. *Biol Trace Elem Res* **2007**, *120* (1-3), 248-56.
100. Verhelst, R.; Verstraelen, H.; Claeys, G.; Verschraegen, G.; Van Simaey, L.; De Ganck, C.; De Backer, E.; Temmerman, M.; Vanechoutte, M., Comparison between Gram stain and culture for the characterization of vaginal microflora: definition of a distinct grade that resembles grade I microflora and revised categorization of grade I microflora. *BMC Microbiol* **2005**, *5*, 61.
101. Casella, J. F.; Flanagan, M. D.; Lin, S., Cytochalasin D inhibits actin polymerization and induces depolymerization of actin filaments formed during platelet shape change. *Nature* **1981**, *293* (5830), 302-5.
102. Luxford, K. A.; Murphy, C. R., Cytoskeletal control of the apical surface transformation of rat uterine epithelium. *Biol Cell* **1993**, *79* (2), 111-6.
103. (a) Meng, H.; Yang, S.; Li, Z.; Xia, T.; Chen, J.; Ji, Z.; Zhang, H.; Wang, X.; Lin, S.; Huang, C.; Zhou, Z. H.; Zink, J. I.; Nel, A. E., Aspect Ratio Determines the Quantity of Mesoporous Silica Nanoparticle Uptake by a Small GTPase-Dependent Macropinocytosis Mechanism. *ACS Nano* **2011**; (b) Mercer, J.; Helenius, A., Virus entry by macropinocytosis. *Nat Cell Biol* **2009**, *11* (5), 510-20.
104. Perumal, O. P.; Inapagolla, R.; Kannan, S.; Kannan, R. M., The effect of surface functionality on cellular trafficking of dendrimers. *Biomaterials* **2008**, *29* (24-25), 3469-76.

105. Pho, M. T.; Ashok, A.; Atwood, W. J., JC virus enters human glial cells by clathrin-dependent receptor-mediated endocytosis. *J Virol* **2000**, 74 (5), 2288-92.
106. Benmerah, A.; Lamaze, C., Clathrin-coated pits: vive la difference? *Traffic* **2007**, 8 (8), 970-82.
107. Manes, S.; del Real, G.; Martinez, A. C., Pathogens: raft hijackers. *Nat Rev Immunol* **2003**, 3 (7), 557-68.
108. Rybin, V. O.; Grabham, P. W.; Elouardighi, H.; Steinberg, S. F., Caveolae-associated proteins in cardiomyocytes: caveolin-2 expression and interactions with caveolin-3. *Am J Physiol Heart Circ Physiol* **2003**, 285 (1), H325-32.
109. Georgieva, J. V.; Kalicharan, D.; Couraud, P. O.; Romero, I. A.; Weksler, B.; Hoekstra, D.; Zuhorn, I. S., Surface characteristics of nanoparticles determine their intracellular fate in and processing by human blood-brain barrier endothelial cells in vitro. *Mol Ther* **2011**, 19 (2), 318-25.
110. Rejman, J.; Oberle, V.; Zuhorn, I. S.; Hoekstra, D., Size-dependent internalization of particles via the pathways of clathrin- and caveolae-mediated endocytosis. *Biochem J* **2004**, 377 (Pt 1), 159-69.
111. Bathori, G.; Cervenak, L.; Karadi, I., Caveolae--an alternative endocytotic pathway for targeted drug delivery. *Crit Rev Ther Drug Carrier Syst* **2004**, 21 (2), 67-95.
112. Peng, S. F.; Tseng, M. T.; Ho, Y. C.; Wei, M. C.; Liao, Z. X.; Sung, H. W., Mechanisms of cellular uptake and intracellular trafficking with chitosan/DNA/poly(gamma-glutamic acid) complexes as a gene delivery vector. *Biomaterials* **2011**, 32 (1), 239-48.
113. Hammes, A.; Andreassen, T. K.; Spoelgen, R.; Raila, J.; Hubner, N.; Schulz, H.; Metzger, J.; Schweigert, F. J.; Lippa, P. B.; Nykjaer, A.; Willnow, T. E., Role of endocytosis in cellular

uptake of sex steroids. *Cell* **2005**, 122 (5), 751-62.

114.Dekker, J.; Rossen, J. W.; Buller, H. A.; Einerhand, A. W., The MUC family: an obituary. *Trends Biochem Sci* **2002**, 27 (3), 126-31.

115.Bernkop-Schnurch, A.; Schwarz, V.; Steininger, S., Polymers with thiol groups: a new generation of mucoadhesive polymers? *Pharm Res* **1999**, 16 (6), 876-81.

116.Nicolazzo, J. A.; Reed, B. L.; Finnin, B. C., The effect of various in vitro conditions on the permeability characteristics of the buccal mucosa. *J Pharm Sci* **2003**, 92 (12), 2399-410.

117.Lesch, C. A.; Squier, C. A.; Cruchley, A.; Williams, D. M.; Speight, P., The permeability of human oral mucosa and skin to water. *J Dent Res* **1989**, 68 (9), 1345-9.

118.Bernkop-Schnurch, A.; Hornof, M.; Guggi, D., Thiolated chitosans. *Eur J Pharm Biopharm* **2004**, 57 (1), 9-17.

119.Poelvoorde, N.; Verstraelen, H.; Verhelst, R.; Saerens, B.; De Backer, E.; dos Santos Santiago, G. L.; Vervaet, C.; Vaneechoutte, M.; De Boeck, F.; Van Bortel, L.; Temmerman, M.; Remon, J. P., In vivo evaluation of the vaginal distribution and retention of a multi-particulate pellet formulation. *European journal of pharmaceutics and biopharmaceutics : official journal of Arbeitsgemeinschaft fur Pharmazeutische Verfahrenstechnik e.V* **2009**, 73 (2), 280-4.

120. (a) Alukda, D.; Sturgis, T.; Youan, B. B., Formulation of tenofovir-loaded functionalized solid lipid nanoparticles intended for HIV prevention. *Journal of pharmaceutical sciences* **2011**, 100 (8), 3345-56; (b) Agrahari, V.; Zhang, C.; Zhang, T.; Li, W.; Gounev, T. K.; Oyler, N. A.; Youan, B. B., Hyaluronidase-sensitive nanoparticle templates for triggered release of HIV/AIDS microbicide in vitro. *The AAPS journal* **2014**, 16 (2), 181-93; (c) Meng, J.; Zhang, T.; Agrahari, V.; Ezoulin, M. J.; Youan, B. B.,

Comparative biophysical properties of tenofovir-loaded, thiolated and nonthiolated chitosan nanoparticles intended for HIV prevention. *Nanomedicine* **2014**, *9* (11), 1595-612.

121. Bilancetti, L.; Poncelet, D.; Loisel, C.; Mazzitelli, S.; Nastruzzi, C., A statistical approach to optimize the spray drying of starch particles: application to dry powder coating. *AAPS PharmSciTech* **2010**, *11* (3), 1257-67.

122. (a) Li, X.; Anton, N.; Arpagaus, C.; Belleteix, F.; Vandamme, T. F., Nanoparticles by spray drying using innovative new technology: the Buchi nano spray dryer B-90. *J Control Release* **2010**, *147* (2), 304-10; (b) Peltonen, L.; Valo, H.; Kolakovic, R.; Laaksonen, T.; Hirvonen, J., Electrospraying, spray drying and related techniques for production and formulation of drug nanoparticles. *Expert Opin Drug Deliv* **2010**, *7* (6), 705-19.

123. Li, X.; Kong, X.; Shi, S.; Zheng, X.; Guo, G.; Wei, Y.; Qian, Z., Preparation of alginate coated chitosan microparticles for vaccine delivery. *BMC biotechnology* **2008**, *8*, 89.

124. Shinde, U. A.; Nagarsenker, M. S., Characterization of gelatin-sodium alginate complex coacervation system. *Indian journal of pharmaceutical sciences* **2009**, *71* (3), 313-7.

125. D'Souza, S. S.; DeLuca, P. P., Development of a dialysis in vitro release method for biodegradable microspheres. *AAPS PharmSciTech* **2005**, *6* (2), E323-8.

126. Zhang, Y.; Huo, M.; Zhou, J.; Zou, A.; Li, W.; Yao, C.; Xie, S., DDSolver: an add-in program for modeling and comparison of drug dissolution profiles. *The AAPS journal* **2010**, *12* (3), 263-71.

127. Han, H. K.; Shin, H. J.; Ha, D. H., Improved oral bioavailability of alendronate via the mucoadhesive liposomal delivery system. *Eur J Pharm Sci* **2012**, *46* (5), 500-7.

128. Heng, P. W.; Chan, L. W.; Tang, E. S., Use of swirling airflow to enhance coating

performance of bottom spray fluid bed coaters. *International journal of pharmaceutics* **2006**, 327 (1-2), 26-35.

129. Masters, K., Spray-Air contact, particle formation and drying. In *Spray Drying in Practice*, SprayDryConsult Ubtl. ApS: Denmark, 2002; pp 129-191.

130. Maury, M.; Murphy, K.; Kumar, S.; Shi, L.; Lee, G., Effects of process variables on the powder yield of spray-dried trehalose on a laboratory spray-dryer. *European journal of pharmaceutics and biopharmaceutics : official journal of Arbeitsgemeinschaft fur Pharmazeutische Verfahrenstechnik e.V* **2005**, 59 (3), 565-73.

131. Chapter 6. Viscosity. In *Introduction to Physical Polymer Science*, 4 th ed.; Sperling, L. H., Ed. 2006; pp 77-87.

132. (a) Hamdy, S.; Haddadi, A.; Ghotbi, Z.; Hung, R. W.; Lavasanifar, A., Part I: targeted particles for cancer immunotherapy. *Current drug delivery* **2011**, 8 (3), 261-73; (b) Hung, R. W.; Hamdy, S.; Haddadi, A.; Ghotbi, Z.; Lavasanifar, A., Part II: targeted particles for imaging of anticancer immune responses. *Current drug delivery* **2011**, 8 (3), 274-81.

133. Singh, S. K.; Banala, V. T.; Gupta, G. K.; Verma, A.; Shukla, R.; Pawar, V. K.; Tripathi, P.; Mishra, P. R., Development of docetaxel nanocapsules for improving in vitro cytotoxicity and cellular uptake in MCF-7 cells. *Drug development and industrial pharmacy* **2015**, 1-10.

134. Fang, Y.; Al-Assaf, S.; Phillips, G. O.; Nishinari, K.; Funami, T.; Williams, P. A.; Li, L., Multiple steps and critical behaviors of the binding of calcium to alginate. *The journal of physical chemistry. B* **2007**, 111 (10), 2456-62.

135. Chantler, E.; Debruyne, E., Factors regulating the changes in cervical mucus in different hormonal states. *Advances in experimental medicine and biology* **1977**, 89, 131-41.

136. Gipson, I. K.; Ho, S. B.; Spurr-Michaud, S. J.; Tisdale, A. S.; Zhan, Q.; Torlakovic, E.; Pudney, J.; Anderson, D. J.; Toribara, N. W.; Hill, J. A., 3rd, Mucin genes expressed by human female reproductive tract epithelia. *Biol Reprod* **1997**, *56* (4), 999-1011.
137. Clift, A. F., Early studies on the rheology of cervical mucus. *American journal of obstetrics and gynecology* **1979**, *134* (7), 829-32.
138. Godley, M. J., Quantitation of vaginal discharge in healthy volunteers. *British journal of obstetrics and gynaecology* **1985**, *92* (7), 739-42.
139. Catalone, B. J.; Kish-Catalone, T. M.; Budgeon, L. R.; Neely, E. B.; Ferguson, M.; Krebs, F. C.; Howett, M. K.; Labib, M.; Rando, R.; Wigdahl, B., Mouse model of cervicovaginal toxicity and inflammation for preclinical evaluation of topical vaginal microbicides. *Antimicrobial agents and chemotherapy* **2004**, *48* (5), 1837-47.
140. Dendukuri, D.; Tsoi, K.; Hatton, T. A.; Doyle, P. S., Controlled synthesis of nonspherical microparticles using microfluidics. *Langmuir : the ACS journal of surfaces and colloids* **2005**, *21* (6), 2113-6.
141. Bhardwaj, N.; Kundu, S. C., Electrospinning: a fascinating fiber fabrication technique. *Biotechnol Adv* **2010**, *28* (3), 325-47.
142. Yoshimoto, H.; Shin, Y. M.; Terai, H.; Vacanti, J. P., A biodegradable nanofiber scaffold by electrospinning and its potential for bone tissue engineering. *Biomaterials* **2003**, *24* (12), 2077-82.
143. Jiang, H.; Wang, L.; Zhu, K., Coaxial electrospinning for encapsulation and controlled release of fragile water-soluble bioactive agents. *Journal of controlled release : official journal of the Controlled Release Society* **2014**, *193*, 296-303.
144. Nawalakhe,, R. G.; Hudson,, S. M.; Seyam,, A.-F. M.; Waly,, A. I.; Abou-Zeid,, N.

Y.; Ibrahim, H. M., Development of Electrospun Iminochitosan for Improved Wound Healing Application *Journal of Engineered Fibers and Fabrics* **2012**, 7 (2), 9.

145. Albrecht, K.; Bernkop-Schnurch, A., Thiomers: forms, functions and applications to nanomedicine. *Nanomedicine* **2007**, 2 (1), 41-50.

146. Makhlof, A.; Werle, M.; Tozuka, Y.; Takeuchi, H., A mucoadhesive nanoparticulate system for the simultaneous delivery of macromolecules and permeation enhancers to the intestinal mucosa. *Journal of controlled release : official journal of the Controlled Release Society* **2011**, 149 (1), 81-8.

147. Jiang, H.; Hu, Y.; Li, Y.; Zhao, P.; Zhu, K.; Chen, W., A facile technique to prepare biodegradable coaxial electrospun nanofibers for controlled release of bioactive agents. *Journal of controlled release : official journal of the Controlled Release Society* **2005**, 108 (2-3), 237-43.

148. Valenta, C.; Kast, C. E.; Harich, I.; Bernkop-Schnurch, A., Development and in vitro evaluation of a mucoadhesive vaginal delivery system for progesterone. *Journal of controlled release : official journal of the Controlled Release Society* **2001**, 77 (3), 323-32.

149. Li, G.; Chen, Y.; Hu, J.; Wu, X.; He, X.; Li, J.; Zhao, Z.; Chen, Z.; Li, Y.; Hu, H.; Lan, P., A 5-fluorouracil-loaded polydioxanone weft-knitted stent for the treatment of colorectal cancer. *Biomaterials* **2013**, 34 (37), 9451-61.

150. Agrahari, V.; Youan, B. B., Sensitive and rapid HPLC quantification of tenofovir from hyaluronic acid-based nanomedicine. *AAPS PharmSciTech* **2012**, 13 (1), 202-10.

151. (a) Liang, D.; Hsiao, B. S.; Chu, B., Functional electrospun nanofibrous scaffolds for biomedical applications. *Adv Drug Deliv Rev* **2007**, 59 (14), 1392-412; (b) Zeugolis, D. I.; Khew, S. T.; Yew, E. S.; Ekaputra, A. K.; Tong, Y. W.; Yung, L. Y.; Huttmacher, D. W.;

Sheppard, C.; Raghunath, M., Electro-spinning of pure collagen nano-fibres - just an expensive way to make gelatin? *Biomaterials* **2008**, 29 (15), 2293-305; (c) Ghasemi-Mobarakeh, L.; Prabhakaran, M. P.; Morshed, M.; Nasr-Esfahani, M. H.; Ramakrishna, S., Electrospun poly(epsilon-caprolactone)/gelatin nanofibrous scaffolds for nerve tissue engineering. *Biomaterials* **2008**, 29 (34), 4532-9.

152. Mckee, M. G.; Wilkes, G. L.; Colby, R. H.; Long, T. E., Correlations of Solution Rheology with Electrospun Fiber Formation of Linear and Branched Polyesters. *Macromolecules* **2004**, 37 (5), 7.

153. Mina, B.-M.; Leeb, S. W.; Limb, J. N.; Youb, Y.; Leeb, T. S.; Kang, P. H.; Park, W. H., Chitin and chitosan nanofibers: electrospinning of chitin and deacetylation of chitin nanofibers. *Polymer* **2004**, 45, 6.

154. (a) Liu, X.; Ma, P. X., The nanofibrous architecture of poly(L-lactic acid)-based functional copolymers. *Biomaterials* **2010**, 31 (2), 259-69; (b) Liu, W.; Wei, J.; Chen, Y.; Huo, P.; Wei, Y., Electrospinning of poly(L-lactide) nanofibers encapsulated with water-soluble fullerenes for bioimaging application. *ACS Appl Mater Interfaces* **2013**, 5 (3), 680-5.

155. (a) Li, Y.; Chen, F.; Nie, J.; Yang, D., Electrospun poly(lactic acid)/chitosan core-shell structure nanofibers from homogeneous solution. *Carbohydr Polym* **2012**, 90 (4), 1445-51; (b) Ignatova, M.; Manolova, N.; Markova, N.; Rashkov, I., Electrospun non-woven nanofibrous hybrid mats based on chitosan and PLA for wound-dressing applications. *Macromolecular bioscience* **2009**, 9 (1), 102-11.

156. (a) Beukenkamp, J.; Rieman, W.; Lindenbaum, S., Behavior of Condensed Phosphates in Anion-Exchange Chromatography. *Analytical Chemistry* **1954**, 26 (3), 505-512; (b) Watters, J. I.; Loughran, E. D.; Lambert, S. M., The acidity of triphosphoric acid. *Journal*

of the American Chemical Society **1956**, 78 (19), 4855–4858.

157. Homayoni, H.; Ravandi, S. A. H.; Valizadeh, H., Electrospinning of chitosan nanofibers: Processing optimization. *Carbohydrate Polymers* **2009**, 77, 6.

158. El-hefian, E. A.; Yahaya, A. H.; Misran, M., Characterisation of chitosan solubilised in aqueous formic and acetic acids. *Maejo International Journal of Science and Technology* **2009**, 3 (03), 415-425.

159. D'ISOZZA, R.; TEJAA, A. S., Effective carbon number molecular weight carbon number Pressure Temperature. *Chemical Engineering Communications* **1987**, 61 (1-6), 13-22.

160. Pakravan, M.; Heuzey, M. C.; Ajji, A., Core-shell structured PEO-chitosan nanofibers by coaxial electrospinning. *Biomacromolecules* **2012**, 13 (2), 412-21.

161. Fuertges, F.; Abuchowski, A., The clinical efficacy of poly(ethylene glycol)-modified proteins. *Journal of Controlled Release* **1990**, 11 (1-3), 10.

162. Alvarez, E., Surface Tension of Organic Acids + Water Binary Mixtures from 20 °C to 50 °C. *Journal of Chemical & Engineering Data* **1997**, 42, 957-960.

163. Yu, J. H.; Fridrikh, S. V.; Rutledge, G. C., Production of Submicrometer Diameter Fibers by Two-Fluid Electrospinning. *Advanced Materials* **2004**, 16 (17), 5.

164. Jin, Y.; Jia, C.; Huang, S. W.; O'Donnell, M.; Gao, X., Multifunctional nanoparticles as coupled contrast agents. *Nature communications* **2010**, 1, 41.

165. Zivanovic, S.; Li, J.; Davidson, P. M.; Kit, K., Physical, mechanical, and antibacterial properties of chitosan/PEO blend films. *Biomacromolecules* **2007**, 8 (5), 1505-10.

166. Dash, S.; Murthy, P. N.; Nath, L.; Chowdhury, P., Kinetic modeling on drug release

from controlled drug delivery systems. *Acta poloniae pharmaceutica* **2010**, 67 (3), 217-23.

167. Lederman, M. M.; Offord, R. E.; Hartley, O., Microbicides and other topical strategies to prevent vaginal transmission of HIV. *Nature reviews. Immunology* **2006**, 6 (5), 371-82.

168. Reagan-Shaw, S.; Nihal, M.; Ahmad, N., Dose translation from animal to human studies revisited. *FASEB journal : official publication of the Federation of American Societies for Experimental Biology* **2008**, 22 (3), 659-61.

169. Doncel, G. F.; Chandra, N.; Fichorova, R. N., Preclinical assessment of the proinflammatory potential of microbicide candidates. *Journal of acquired immune deficiency syndromes* **2004**, 37 Suppl 3, S174-80.

VITA

Jianing Meng was born on November 26, 1985 in Nanjing, China. In 2004, she received his high school Diploma from Changping First High School High in Beijing, China. Thereafter, she received her Bachelor's degree in Pharmaceutics from China Pharmaceutical University (Nanjing, China) in the summer of 2008.

After graduating with a Bachelor's degree, She was accepted into the interdisciplinary Ph.D. program with Pharmaceutical Sciences and Chemistry as his disciplines. Jianing Meng is a member of American Association of Pharmaceutical Sciences (AAPS). She also authored and co-authored several peer reviewed publications in renowned international journals and has presented his work in various annual scientific meetings.